Russian Chemical Reviews **77** (6) 487 – 520 (2008) © 2008 Russian Academy of Sciences and Turpion Ltd

DOI 10.1070/RC2008v077n06ABEH003782

Pulsed electron – electron double resonance (PELDOR) as EPR spectroscopy in nanometre range

Yu D Tsvetkov, A D Milov, A G Maryasov

Contents

I.	Introduction	487
II.	Theoretical foundations of the PELDOR technique	489
III.	Methodological features of the PELDOR technique	493
IV.	Applications of the PELDOR technique	495
V.	Conclusion	517

Abstract. The results of development of pulsed electron – electron double resonance (PELDOR) method and its applications in structural studies are generalised and described systematically. The foundations of the theory of the method are outlined, some methodological features and applications are considered, in particular, determination of the distances between spin labels in the nanometre range for iminoxyl biradicals, spin-labelled biomacromolecules, radical ion pairs and peptide – membrane complexes. The attention is focussed on radical systems that form upon self-assembly of nanosized complexes (in particular, peptide complexes), spatial effects, and radical pairs in photolysis and photosynthesis. The position of PELDOR among other structural EPR techniques is analysed. The bibliography includes 157 references.

I. Introduction

One of the key problems in structural chemistry is to measure interatomic distances or distances between atomic groups in molecules as well as intermolecular distances in various molecular systems. X-Ray crystallography is the main classical method for these investigations. However, growth of crystals and structure determination from X-ray analysis data is still a complicated task. In addition, single crystals of biomacromolecules and their complexes may not either exhibit catalytic properties or be biologically active. Therefore, NMR and EPR spectroscopies or other spectroscopic methods of investigation of disordered samples are more useful for obtaining structural information in the liquid phase or in frozen solutions, *i.e.*, under the conditions that are more appropriate for simulation of biological systems rather than single crystals. Valuable information on the structure and behaviour of nucleic acids, proteins and protein complexes can be obtained using recently developed computational methods of classical molecular dynamics (MD). An important step forward that offers new prospects for structural studies by EPR spectroscopy was made using pulsed methods, in particular, the pulsed electron – electron double resonance (PELDOR) technique. This review generalises on a systematic basis the results obtained in PELDOR studies of some structural problems.

Continuous wave EPR spectroscopy is widely used in studies of the structure and dynamics of paramagnetic centres, especially, spin labels in various biomacromolecules. However, there are significant limitations on the studies of weak magnetic dipolar interactions. Nevertheless, research on just these interactions can give structural information on the systems containing paramagnetic particles arranged at distances (r) of the order of 1 nm and longer. The dipolar interactions are proportional to $1/r^3$, which makes a contribution of about 0.3 mT to the EPR linewidth at a distance of 2 nm. This contribution to the EPR linewidth in randomly oriented samples is much smaller than the contributions from other inhomogeneous line broadenings, *e.g.*, anisotropic hyperfine broadening or the g-factor anisotropy. Obtaining reliable data on dipolar interactions at distances $r \geqslant 1.5$ nm against the background from other sources of line broadening using continuous wave EPR spectroscopy is a very complicated task. Therefore, at present dipolar interactions are studied using pulsed EPR methods that allow one to exclude the inhomogeneous broadening due to all other mechanisms except the dipolar interactions. The electron spin echo (ESE) technique[1] makes it possible to obtain information on dipolar interactions by studying the kinetics of ESE signal decay at variable time delays between microwave pulses. This pulsed method was developed and successfully used in the 1970 – 1990s for distance determination and investigations of the spatial distribution of radicals in irradiated substances and other systems.[2–4]

However, some limitations exist on the ESE technique. The minimum measurable interparticle distance is about 3 nm (or the maximum spin concentration is about 10^{19} cm^{-3}), being determined by the minimum measurable phase relaxation time $(T_f)_{min}$, which is in turn related to the dead time of a pulsed

Yu D Tsvetkov, A D Milov, A G Maryasov Institute of Chemical Kinetics and Combustion, Siberian Branch of the Russian Academy of Sciences, ul. Institutskaya 3, 630090 Novosibirsk, Russian Federation.
Fax (7-383) 330 73 50,
tel. (7-383) 333 21 92, e-mail: tsvetkov@kinetics.nsc.ru (Yu D Tsvetkov),
tel. (7-383) 333 13 77, e-mail: milov@kinetics.nsc.ru (A D Milov),
maryasov@kinetics.nsc.ru (A G Maryasov)

Received 11 February 2008
Uspekhi Khimii **77** (6) 515 – 550 (2008); translated by A M Raevskiy

EPR spectrometer. If the nearest environment of the particle includes magnetic nuclei, the ESE signal decay is modulated at the frequency of anisotropic hyperfine coupling with these nuclei (so-called Electron Spin Echo Envelope Modulation effects, or ESEEM).[5] This modulation complicates the analysis of the decay kinetics because now the parameters (frequencies) of dipolar interaction cannot unambiguously be determined. Often it appears that these limitations preclude extraction of reliable information on dipolar interaction using the simplest pulsed ESE technique to almost the same extent as in the case of continuous wave EPR spectroscopy.

These problems were eliminated after the development,[6] by researchers from the Institute of Chemical Kinetics and Combustion, Siberian Branch of the Russian Academy of Sciences (Novosibirsk, Russain Federation), of two-frequency pulsed ESE version for the determination of distances between paramagnetic centres based on the data on magnetic spin – spin dipole interactions.[7] This pulsed method was called PELDOR by analogy with the commonly accepted abbreviation ELDOR (Electron Double Resonance) for two-frequency continuous wave EPR spectroscopy. Some researchers prefer the abbreviation DEER (Double Electron Electron Resonance), but in this case some problems arise due to difficulties in operation with computer search systems. The PELDOR pulse sequence is shown in Fig. 1.

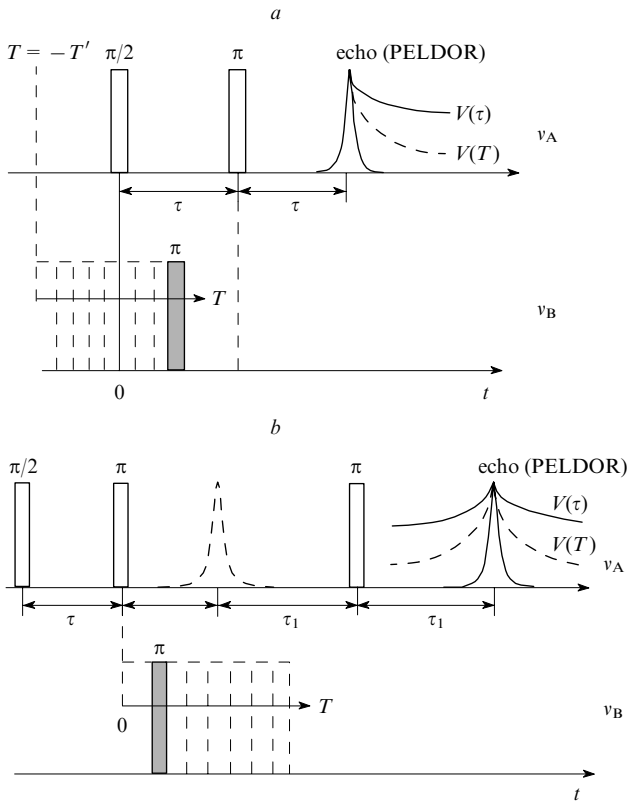


Figure 1. Pulse sequences used in PELDOR method.
(*a*) Three-pulse PELDOR technique. The spin echo signal $V(\tau)$ appears after application of the $\pi/2$ and π pulses at the frequency ν_A. The pumping π-pulse applied at instant T at the frequency ν_B changes the echo signal amplitude. These changes are detected as the PELDOR signal $V(T)$. (*b*) Four-pulse PELDOR technique. The echo signal is induced by applying three pulses ($\pi/2$, π, π) at the frequency ν_A. Changes in the echo signal (PELDOR effect) appear after application of the pumping π pulse at the frequency ν_B during the time interval from τ to $\tau + \tau_1$.

Theoretical analysis of pulsed EPR experiments is performed using two types of spins called the A- and B-spins (Fig. 2 *a*). In conventional ESE spectroscopy only the A-spins (at echo signal frequency ν_A) change their orientation upon application of the $\pi/2$ and π pulses that are responsible for the appearance of the echo signal. In the two-frequency method the B-spins are affected by the π pump pulses applied at the frequency ν_B at instant $t = T$ during the time interval τ between the first and second pulses applied at the detection frequency ν_A (see Fig. 1 *a*).

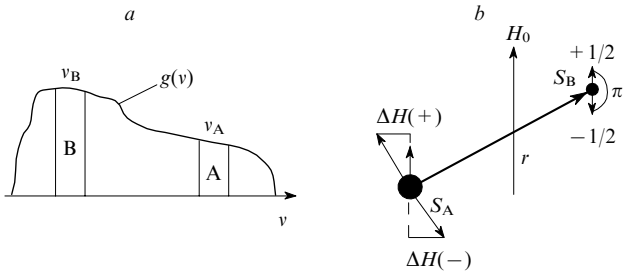


Figure 2. EPR spectrum the shape of which is described by the function $g(\nu)$, and dipolar interaction between spins A and B.
Spectral regions excited by the pulses A and B (spins A and B, respectively) (*a*). The local field at the spin A site changes from $\Delta H(+)$ to $\Delta H(-)$ as the spin B changes its orientation upon application of the pumping π pulse at the frequency ν_B (*b*).

The pulse acting on the B-spins changes their z-projection and, as a result, the local magnetic field at the A-spins (Fig. 2 *b*). The magnitude of these changes is determined by magnetic dipolar interaction between the A- and B-spins. As a result, the change in the local magnetic field at the A-spins leads to additional defocussing of the A-spins when the magnetisation vector precesses in the xy plane after application of the first $\pi/2$ pulse. This in turn changes the amplitude of the echo signal $V(\tau)$ compared to its amplitude in the absence of the pulsed pump of the B-spins. The effect depends on the time delay (T) of the pump pulse after the first $\pi/2$ pulse at the frequency ν_A (see Fig. 1 *a*). Experiments are carried out at constant interval $\tau = \tau_0$. The two-frequency pulsed technique is suitable for studying the decay kinetics of the ESE signal amplitude normalised to the signal amplitude in the absence of pumping

$$V(T) = \frac{V(T, \tau_0)}{V(\tau_0)},$$

as function of the time interval T. Since the time interval τ between the $\pi/2$ and π pulses has a constant duration, it is possible to eliminate the masking effects of dynamic and relaxation processes typical of the kinetics $V(\tau)$ in conventional two-pulse ESE from the decay kinetics of the echo signal and to obtain the changes in the echo signal due to dipolar interactions only. It should be emphasised that, in contrast to conventional ESE spectroscopy, the PELDOR technique has a zero dead time and the minimum T value is only determined by the duration of the pump pulse (this pulse can be applied prior to applying the first pulse at the frequency ν_A at instant $t = -T'$, see Fig. 1 *a*). Note that NMR spectroscopy uses a similar method of investigation of dipolar nuclear interactions.[8,9]

A PELDOR version [10] with three excitation pulses applied at the frequency ν_A (see Fig. 1 *b*) is also available. In this case

(four-pulse PELDOR) the first two pulses form the echo signal at the instant 2τ and the additional (third) pulse applied at the instant $2\tau + \tau_1$ refocusses the magnetisation, thus creating the echo signal at the instant $2\tau + 2\tau_1$. The pump pulse at the frequency ν_B is applied between the second and third pulses that are applied at the frequency ν_A (see Fig. 1 *b*). The dependence of the amplitude of the refocussed echo $V(T)$ on the position of the pump pulse on the time scale in the interval from τ to $\tau + \tau_1$ is measured. Similarly to the three-pulse PELDOR version, information on dipolar interaction can be extracted by analysing the decay kinetics $V(T)$, which can be detected as a function symmetrical with respect to the instant $t = 2\tau + 2\tau_1$. The four-pulse PELDOR technique is characterised by zero dead time.

Early PELDOR studies were followed by elaboration of efficient single-frequency, zero-dead-time pulsed EPR techniques.[11,12] A so-called (2 + 1) ESE technique[13] whose experimental design is similar to that of the PELDOR experiments should be pointed out. However, the (2 + 1) ESE approach is of limited use owing to the need for applying an additional (+ 1) microwave pulse at the operating frequency of the spectrometer; this pulse is incoherent with the two main pulses that form the ESE signal. The single-frequency methods have their advantages and drawbacks compared to the PELDOR technique. Detailed consideration of these issues goes beyond the scope of this review, although we will dwell on some points in the text below. Undoubtedly, the PELDOR technique is the simplest method of applied research and analysis of results obtained. Researchers face difficulties only in practical implementation of the design of spectrometers with two sources of microwave radiation. Recently, these problems have been successfully solved in commercially available Bruker E 580 and E 680 EPR spectrometers (Germany) which become more and more popular instruments.

A number of reviews of the pioneering PELDOR studies are available.[14–20] The authors of more recent reviews either briefly outline the PELDOR among the bunch of other EPR techniques[21,22] or put emphasis on particular methodological issues and applications.[23,24]

The PELDOR technique is a version of high-resolution pulsed EPR spectroscopy. The theory of the phenomenon and the experimental design have been elaborated quite well and the necessary equipment is now commercially available. Therefore, the PELDOR finds an increasing number of applications in chemistry, biology and related fields of research. In this review we generalise the results obtained in this field of chemical radiospectroscopy up to the end of the year 2007.

II. Theoretical foundations of the PELDOR technique

In this Section we will consider some theoretical results that are necessary when analysing the kinetics of PELDOR signal decays using various models of spatial organisation of spin systems.

Since the available spectrometers permit efficient investigations of spin pairs only with interparticle distances of at least 1 – 1.5 nm, theoretical analysis is usually performed assuming that the magnetic dipole interaction between A-spins and B-spins is much weaker that the frequency difference between the corresponding pulses $\Delta\nu_{AB}$. This interaction is also assumed to be weak compared to the amplitude of microwave pulses and therefore it is thought that both components of the dipolar doublet are excited to the same extent. The amplitudes and durations of microwave pulses are such that the effect of the excitation pulses on the B-spins and that of the pump pulse on the A-spins can be ignored. These assumptions are valid in most cases of theoretical analysis of PELDOR experiments.

1. Spatially oriented pairs

It is assumed that the spin – lattice relaxation time T_1 of the spin system is much longer than the phase relaxation time T_f and that the interval τ between pulses is much shorter than T_f. In this case both spin – lattice and phase relaxation of the spins of paramagnetic centres can be ignored and the PELDOR signal has the form[6,7]

$$V(T) = V(0)[1 - p_b(1 - \cos(DT))], \tag{1}$$

where $V(0)$ is the echo signal in the absence of pumping and p_b is the probability of changes in the orientation of the B spin under the action of the pumping pulse or the extent of excitation of the spectrum at the frequency ν_B,

$$D = \omega_D(1 - 3\cos^2\theta) + J, \tag{2a}$$

$$\omega_D = 2\pi\nu_D = \frac{\gamma^2\hbar}{r_{AB}^3}. \tag{2b}$$

Here θ is the angle between the direction of external magnetic field and the vector $\boldsymbol{r}$, J is the constant of exchange interaction, γ is the gyromagnetic ratio for electron spin, $\hbar$ is the Planck constant and r_{AB} is the distance between the A-spins and B-spins. The lower limit of D measurements is determined by the rate of phase relaxation $1/T_f$. Since $V(0) \sim \exp(-2\tau/T_f)$ and $T \leqslant \tau$, the minimum experimentally measurable value D_{min} is $D_{min} \approx 1/T_f$. Relationship (1) contains information necessary for analysis of the PELDOR data for the simplest oriented systems, *e.g.*, pairs of paramagnetic centres in single crystals.[1,5] The decay kinetics of the signal $V(T)$ for polyoriented systems can be derived by appropriately averaging expression (1).

2. Randomly distributed paramagnetic centres

In this case the PELDOR signal decay can be calculated using the Markov method[6,14,25,26] assuming the all B-spins act on the A-spins independently. Then the decay $V(T)$ is given by

$$V(T) = V(0)\left\langle \prod_j \left(1 - p_b\left[1 - \cos(D_j T)\right]\right)\right\rangle_{r,\theta}, \tag{3}$$

where the subscript j refers to the B-spins and the angular brackets denote the averaging over the angle and over the distances between spins of the centres under study. In this case we assume a random particle distribution over the whole volume. The averaging using expression (3) gives an exponential decay $V(T)$ in the form

$$V(T) = V(0)\exp\left(-\frac{8\pi^2}{9\sqrt{3}}\gamma^2\hbar p_b C T\right) = \tag{4}$$

$$= V(0)\exp\left(-2p_b\Delta\omega_{1/2}T\right),$$

where $\Delta\omega_{1/2} = 8.2 \times 10^{13} C\ \mathrm{cm}^3\ \mathrm{s}^{-1}$ is the dipolar linewidth and C is the concentration of paramagnetic centres. This result for PELDOR is in exact correspondence with the expression for the ESE signal decay due to dipolar interaction in the case of randomly distributed particles.[1,3]

3. Randomly oriented pairs

If the interacting centres in pairs are at the same distance (r = const), the function describing the kinetics of PELDOR signal decay can be derived with ease by averaging expression (1) over the angle θ only. The result is as follows:[7, 14, 15]

$$V(T) = V(0)\{1 - p_b[1 - \Phi(T)]\}, \tag{5}$$

$$\Phi(T) = \left[\frac{\pi(c^2 + s^2)}{6\omega_D T}\right]^{1/2} \cos\left[(\omega_D + J)T - \operatorname{arctg}\left(\frac{s}{c}\right)\right], \tag{6}$$

where c and s are the Fresnel integrals

$$c = \int_0^v \cos\left(\frac{\pi}{2}x^2\right)\mathrm{d}x,$$

$$s = \int_0^v \sin\left(\frac{\pi}{2}x^2\right)\mathrm{d}x, \tag{7}$$

$$v = \left(\frac{6\omega_D T}{\pi}\right)^{1/2}.$$

Relation (5) shows oscillations of the PELDOR signal decay at the frequency $\omega_D + J$ (Fig. 3 *a*) due to the dipolar and exchange ($J > 0$) interactions in randomly oriented systems. Note that in the case of negative exchange interaction ($J < 0$) the time dependence of the signal is significantly distorted compared to the case $J > 0$ (Fig. 3 *b*). For instance, at $J = -\omega_D$, oscillations are observed at the frequency $\sim 3\,\omega_D$. One should keep in mind that the kinetics of the PELDOR signal decay $V(T)$ can directly be analysed only at $J > 0$, because calculations showed that at $J < 0$ the function $V(T)$ has a number of harmonics depending on the J/ω_D ratio (see Fig. 3 *b*). This means that analysis of the signal in the time domain can only lead to significant errors when estimating the distances in the presence of nonzero exchange interaction.

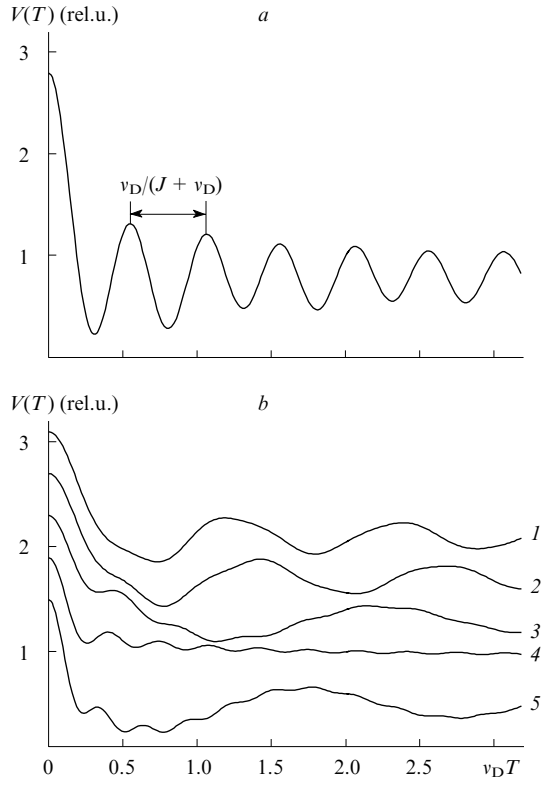


Figure 3. PELDOR signal decay oscillations due to dipole–dipole and exchange interactions for randomly oriented pairs at constant spin–spin distance: $J > 0$ (*a*), $J < 0$ at J/ν_D ratio of -0.1 (*1*), -0.2 (*2*), -0.5 (*3*), -1.0 (*4*) and -1.5 (*5*) (*b*).

Generally, Fourier analysis of the kinetics $V(T)$ (*i.e.*, the frequency spectrum in the form of the so-called dipolar Pake doublet) makes it possible to extract information not only on the magnitude of the parameters ω_D and J, but also on the sign of J.[27] Indeed, with allowance for axial anisotropy of dipolar interaction the dipolar splitting of the lines in the doublet corresponds to the frequencies

$$\omega_{\parallel} = |2\omega_D - J|,$$

$$\omega_{\perp} = |\omega_D + J|.$$

Note that in most cases the Fourier analysis is to a great extent simplified because the PELDOR technique permits distance measurements at $r > 1.5-2.0$ nm (see below), where, with rare exception, the exchange interaction is weak,[28] $J \approx 0$ and the dipolar spectrum allows one to obtain $\omega_{\parallel} = 2\omega_D$ and $\omega_{\perp} = \omega_D$ (Fig. 4) immediately.

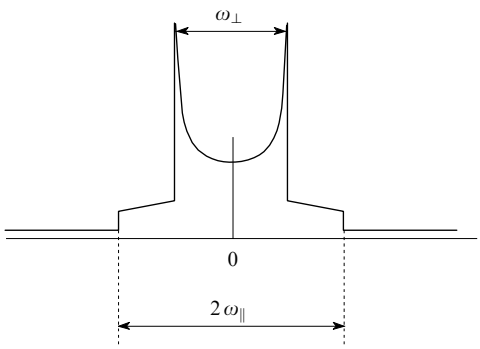


Figure 4. Dipolar Pake doublet at $J = 0$.

From Eqn (6) it follows that the amplitude of the PELDOR signal oscillations in polyoriented systems decreases with an increase in T and dipolar frequency ω_D. An important reason for damping of oscillations also consists in spread of the distances r_{AB} between paramagnetic centres. Figure 5 shows that even small spread $\delta r_{AB}/r_{AB} \approx 0.1$ leads to strong damping of oscillations (they almost disappear at $\delta r_{AB}/r_{AB} = 0.25$). Thus, a simple Fourier analysis of the signal $V(T)$ in order to determine the r and J values is incomplete. In the text below we will return to the analysis of the decay kinetics of the PELDOR signal, which also contains important information on the distance distribution function in pairs.

A nonparametric method of determination of the average distance between spins in a pair of paramagnetic centres with a broad distance distribution was also proposed.[29] It is based on determination of position of the first minimum of the derivative of the PELDOR signal with respect to time T. The method requires a relatively high accuracy of signal measurements and provides the possibility of fast evaluation of the average distance without imposing any limitations on the distribution function.

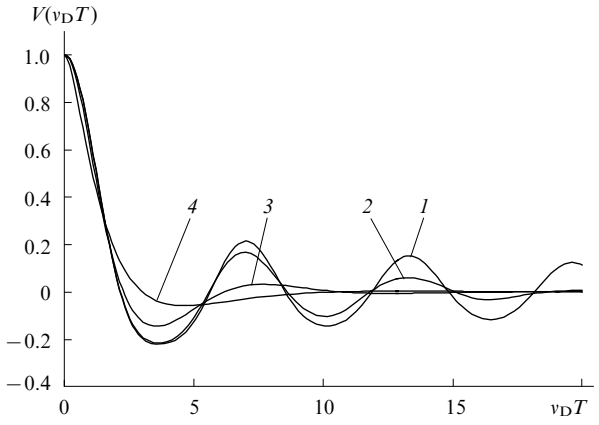


Figure 5. Effect of the spread of spin–spin distances ($\delta r_{AB}/r_{AB}$) on PELDOR signal decay.
$\delta r_{AB}/r_{AB}$ = 0 (*1*), 0.1 (*2*), 0.15 (*3*), 0.25 (*4*).

4. Intramolecular and intermolecular dipolar interactions

In complex real systems, such as samples containing radical pairs, clusters or aggregates of paramagnetic particles, there are two types of dipolar interactions. There are the interaction between paramagnetic centres within the same element and the interaction between paramagnetic centres localised within different elements. Assuming that these interactions are independent and denoting the PELDOR signal decays due to these contributions as $V(T)_{intra}$ and $V(T)_{inter}$, respectively, the overall function describing the decay of the signal $V(T)$ has the form

$$V(T) = V(T)_{intra} V(T)_{inter}.$$

This makes it possible to separate the dipolar contributions in complex systems. For instance, in the case of frozen solutions of biradicals the intra-pair dipolar contribution $V(T)_{intra}$ is described by expressions (5)–(7), while the inter-pair interaction, $V(T)_{inter}$, is described by relation (4). The contributions can be separated by measuring the signal $V(T)$ at different concentrations of radical pairs, aggregates or clusters.[18, 30] Taking into account expression (4), a simple extraction of the exponential component, as is most often done, seems to be quite dangerous procedure. Here, one should know with certainty that there are no spatial inhomogeneity effects (see below) or other complicating factors (*e.g.*, the shortest distance between the A- and B-spins [31]), which cannot be described by the simple exponential expression (4). In this case, problems (namely, the appearance of false maxima) can also arise in reconstructing the pair distribution function from $V(T)$.

5. PELDOR signal decay for groups comprising N spins

It is not infrequent that the interparticle distances in a group of particles are much shorter than the distances between groups as in, *e.g.*, radical pairs formed during photolysis or radiolysis of solids. In these cases analysis of the PELDOR signal decay enables evaluation of the geometric parameters of such groups and the number of paramagnetic centres in the group.[14, 15, 32] In the simplest case we can assume that the system under study consists of identical groups containing N particles each. Ignoring possible positional and orientational correlations of particles in the groups, the PELDOR signal decay due to dipolar interactions within the group is given by

$$V(T)_{intra} = V(0)[1 - p_b\langle 1 - \cos(DT)\rangle_{r,\theta}]^{N-1}, \quad (8)$$

where $\langle ... \rangle_{r,\theta}$ denotes the averaging over the angle and spin–spin distances in the group.

The averaging (8) leads to a fast decay $V(T)_{intra}$ at short times $T \leqslant T^*$ corresponding to dipole spin–spin interaction with the effective spin–spin separation (r_{eff}) in the group, where

$$T^* = \frac{r_{eff}^3}{\gamma^2 \hbar}. \quad (9)$$

From expression (8) it follows that the function $V(T)_{intra}$ tends to its limiting value V_p at times $T \geqslant T^*$ (Fig. 6 *a*); here to a good approximation one has $\langle \cos(DT)\rangle = 0$. The limiting value V_p equals [32]

$$V_p = \left(1 - p_b\right)^{N-1} \approx 1 - (N-1)p_b. \quad (10)$$

The approximate equality on the right side is valid at $Np_b < 1$. From expression (10) it follows that if the V_p and p_b values are known from the experiment, one can estimate the number, N, of spins in the group (Fig. 6 *b*).

If there exists a distribution over the number (N) of particles in groups, which is described by the function $F(N)$, the PELDOR technique makes it possible to evaluate the moments of the distribution function over the number of particles or to determine the effective N value, N_{eff}, in the group.[32] In this case, not only the dependence $V_p(p_b)$, but also the dependence $V_p(p_a)$ or $N = N(p_a)$ is studied, where p_a is the probability of spin excitation at the frequency ν_A. Specific methods for analysis of PELDOR experimental data for evaluating the moments of the distribution function $F(N)$ were elaborated.[33, 34]

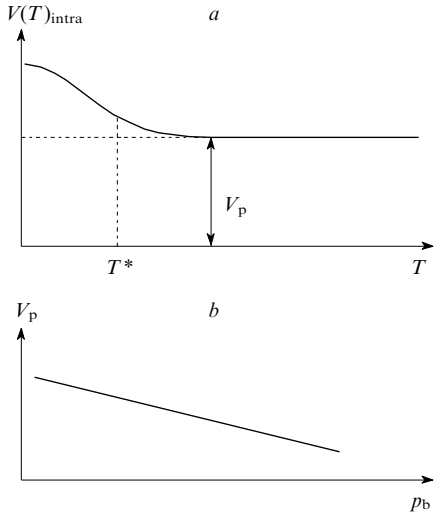


Figure 6. *N*-Spin PELDOR signal decay for randomly oriented pairs (distances in pairs are not fixed) assuming no correlations between spin–spin distances in pairs (*a*) and the dependence of the limiting decay value (V_p) on the excitation probability p_b (*b*).

6. Interparticle distance distribution function for paramagnetic species

Methods of calculations of the distance distribution function in radical pairs from PELDOR data have been elaborated quite recently [29, 35–38] and immediately found wide application in

practice. Now we will consider one method in more detail. The problem, in essence, is to solve an inverse ill-posed problem using Tikhonov's regularisation techniques.[39] One should keep in mind that the instability of the solution to the inverse problem is retained.

The distribution function over distances between spin labels in groups (aggregates) is determined using the decay $V_{\text{intra}}(T)$. We will denote the distance distribution function of spin labels as $F(r) = \mathrm{d}n(r)/\mathrm{d}r$, where $\mathrm{d}n(r)$ is the proportion of pairs of spin labels in the aggregate, for which the distance between labels in the pair is in the range from r to $r + \mathrm{d}r$. The form of the function $F(r)$ will be determined by comparing the experimental dependences of V_{intra} with the dependences calculated for aggregates containing N spin labels (V_{calc}). We will use the known dependence of the PELDOR signal for randomly oriented pairs of spin labels [Eqns (5)–(7)] assuming that at most one pair of labels in each aggregate contributes to the signal. This approach is valid at rather small amplitudes of the pump pulse p_{b}, when the pulse excites only a small proportion of N spin labels and the excitation probability of two or more spin labels can be neglected. The relation for the normalised PELDOR signal averaged over the angle θ ($J = 0$) in expression (8) has the form

$$V(T) = 1 - (N-1)p_{\text{b}}[1 - \langle f(r,T)\rangle_r], \tag{11}$$

where

$$f(r,T) = \left\langle \cos\left\{\frac{\gamma^2\hbar}{r^3}\left[1 - 3\cos^2(\theta)\right]T\right\}\right\rangle_\theta . \tag{12}$$

The function $\langle f(r,T)\rangle$ in expression (11) has the meaning of distance-averaged relation (12). For a continuous distance distribution between spin labels in aggregates the decay kinetics (11) can be written as follows:

$$V(T) = V_{\text{p}} + (1 - V_{\text{p}})\int_{r_1}^{r_2} F(r)f(r,T)\mathrm{d}r, \tag{13}$$

where

$$V_{\text{p}} = 1-(N-1)p_{\text{b}},$$

and $F(r)$ is the distance distribution function between spin labels in aggregates. The integration limits r_1 and r_2 in relation (13) confine the physically reasonable range of distances between spin labels. By dividing the interval from r_1 to r_2 into a series of discrete values r_k and replacing the integral in expression (13) by the sum, we get the equation for the experimental set of T_z values

$$V(T_z) = V_{\text{p}} + (1-V_{\text{p}})\sum_k F(r_k)\mathrm{d}r_k\left[\int_{r_k}^{r_k+\mathrm{d}r_k} f(r,T_z)\frac{\mathrm{d}r}{\mathrm{d}r_k}\right]. \tag{14}$$

From relation (14) one can determine the distribution function $F(r_k)$ and the V_{p} value by comparing the experimental dependence of V_{intra} with the calculated dependence $V(T_z)$. To solve this problem, it is convenient to re-write relation (14) as follows:

$$V_{\text{calc}} = 1 - \frac{V_z}{V_0} = \sum_k F(r_k)(1-V_{\text{p}})\left[1 - \int_{r_k}^{r_k+\mathrm{d}r_k} f(r,T_z)\frac{\mathrm{d}r}{\mathrm{d}r_k}\right]\mathrm{d}r_k =$$

$$= \sum_k X_k\left[1 - \int_{r_k}^{r_k+\mathrm{d}r_k} f(r,T_z)\frac{\mathrm{d}r}{\mathrm{d}r_k}\right], \tag{15}$$

where

$$X_k = (1-V_{\text{p}})F(r_k)\mathrm{d}r_k .$$

Now expression (15) represents a system of linear equations with the unknown parameters X_k. The values

$$\int_{r_k}^{r_k+\mathrm{d}r_k} f(r,T_z)\frac{\mathrm{d}r}{\mathrm{d}r_k}$$

can be numerically calculated using relation (12) for a set of experimental values T_z. In accordance with expression (15) now the V_{calc} value should be compared with the experimental value $V_{\text{e}} = 1 - V_{\text{intra}}$. The X_k values thus obtained allow one to determine both the form of the function $F(r)$ and the V_{p} value, *i.e.*, the number N, because from the normalisation of the function $F(r)$ to unity one has

$$\sum_k X_k = 1 - V_{\text{p}} .$$

The distribution function was determined using Tikhonov's regularisation technique for ill-posed problems [39] whose applicability to analysis of the PELDOR data was studied recently.[38] The procedure included variation of the X_k values under constraint condition $X_k \geqslant 0$ and numerical minimisation of the functional M:

$$M = R - \lambda\Omega,$$

$$R = \sum_{z=1}^{n}\left[V(T_z)_{\text{calc}} - V(T_z)_{\text{e}}\right]^2,$$

$$\Omega = \sum_{k=1}^{m} X_k^2 .$$

Here n is the number of experimental time points T_z, m is the number of distance points r_k and $\lambda \geqslant 0$ is Tikhonov's regularisation parameter.[39] The regularisation parameter λ affects the extent of smoothness of the resultant dependence $F(r)$. At small λ, the solution is unstable towards small deviations of the experimental values V_{intra}, *i.e.*, the function $F(r)$ executes random large-amplitude oscillations with respect to the stable solution. At large λ, the solution becomes too smooth and there is a risk of losing characteristic details of the distribution; besides, here one gets a poorer description of the experimental data. Having determined the function $F(r)$ using the methods listed above, one should make sure whether it correctly describes the experimental PELDOR signal decays.

The aforesaid is a brief outline of the approach to determination of the function $F(r)$, which was used in our recent studies.[36,40–45] Programs for reconstruction of the function $F(r)$ from PELDOR data (for detailed description, see Ref. 46) are also popular. We believe that solution to the ill-posed inverse problem requires particularly critical evaluation of possible systematic and random errors in the experiment.

7. Orientation selectivity in the PELDOR technique

The pulses A and B act in different narrow frequency intervals of the EPR spectrum. The relatively large anisotropy of magnetic-resonance parameters of EPR of iminoxyl radicals causes excitation of only that region of the EPR spectrum, which corresponds to radicals with particular orientation relative to external magnetic field. Now we are concerned with orientation selectivity in PELDOR spectroscopy. Radicals with different spatial orientations are to different extent

excited by the pulses responsible for the formation of the spin echo signal and by the pumping pulse.

If radical pairs have a particular orientation relative to one another, there exists a correlation between the values of the parameters $V(0)$, p_b and D in Eqn (1), which should correctly be taken into account.[14,47] If the geometry of a pair of paramagnetic centres is fixed but the whole sample is disordered, the values being averaged are unambiguously determined by the orientation of external magnetic field in the system of coordinates related to the pair.[14] Such a frame of reference can be specified using six parameters, namely, three Euler angles (they describe rotation from the molecular axes of one spin label to the molecular axes of the other label) and three components of the vector r_{AB} connecting these labels. The PELDOR signal given by relation (1) is averaged over all possible orientations of external magnetic field $\boldsymbol{H}_0$ in this molecular system of coordinates. Here, it is convenient to use the difference between the echo signal amplitudes without the pumping pulse, $V(0)$, and with the pumping pulse, $V(T)$

$$V_d(T) = \langle V(0) - V(T) \rangle_{\Omega, g(\nu)},$$

where Ω and $g(\nu)$ denote the averaging of $V_d(T)$ over the orientations of external magnetic field and over the inhomogeneous contour of the EPR line of each radical in the pair. The result of such averaging [27] is as follows:

$$V_d(T) = A \int_0^1 \xi(\cos\theta)\left(1 - \cos\left\{\left[\omega_D\left(1 - 3\cos^2\theta\right) + J\right]T\right\}\right) d\cos\theta,$$

where A is the normalising factor and θ is the angle between the direction of external magnetic field and the vector connecting the spins in the pair. Compared to expressions (5)–(7), all information on the mutual orientation of radicals is contained in the function $\xi(\cos\theta)$, which was called the geometric form-factor.[27] This function also depends on the parameters of the microwave pulses.

The corresponding analytical expression and examples of the form-factor calculations for iminoxyl radicals in the X-band can be found in Ref. 27.

The results obtained in Ref. 27 were extended [48] to the case of microwave pulses of finite amplitude, where the dipolar splitting in the spectrum can be comparable in magnitude or even be higher than alternating magnetic fields affecting the system. It was shown that obtaining a rather large amplitude of PELDOR signal modulation requires that the pumping pulse should excite both components of the Pake doublet for the B spin.

Orientation selectivity in PELDOR technique was first reported in an X-band study of iminoxyl radical pairs (see biradical **2** in Table 1 in Section IV.1).[47] However, it should be noted that orientation selectivity is weak in the X-band. High-frequency (high-field) studies offer new great prospects for experimental investigations of mutual orientation of paramagnetic centres. In this case a high resolution of the EPR spectrum with respect to the g-factor enables PELDOR measurements by exciting EPR lines with preset values g_{xx}, g_{yy}, g_{zz} by applying pulses at the frequencies ν_A and ν_B and obtaining reliable data on mutual orientation of radicals in pairs. Detailed information on orientation selectivity was recently obtained in the 95 (W-band),[49–51] 180 (Refs 52–54) and 360 GHz.[49] These new experimental results favoured further development of the theory and methods of analysis of orientation selectivity in PELDOR.[50,51]

At the end of this Section, we will formulate the following order of analysis of PELDOR experimental data based on the available theoretical concepts.

1. Separation of the contributions $V(T)_{inter}$ and $V(T)_{intra}$ from the initial decay kinetics of the signal $V(T)$.

2. Drawing conclusions on specific features of spatial distribution of paramagnetic particles based on the $V(T)_{inter}$ pattern.

3. The kinetics $V(T)_{intra}$ permit identification of aggregates, determination of the number of particles in the aggregates or specific features of the statistics of particles in groups, evaluation of distances from the Fourier analysis of $V(T)_{intra}$ and calculations of the distance distribution function $F(r)$.

Usually these data serve as a basis for conclusions about the structure of radical pairs or aggregates. Reliability of the results obtained can be checked using quantum chemical computational methods, *e.g.*, the molecular dynamics methods.

III. Methodological features of the PELDOR technique

1. EPR spectrometer for PELDOR experiments

We do our PELDOR investigations using a pulsed EPR spectrometer described in detail elsewhere.[55] The spectrometer operates in the frequency range 8–10 GHz at a pulse power of ~1 kW and a minimum pulse duration of 20 ns. The pump source is a magnetron operating on the self-excitation mode at a fixed frequency of 9400 MHz. The maximum output microwave power is 5 kW at pulse durations between 15 and 40 ns. The pulse sequence, pulse durations, intervals between the pulses and the repetition frequency are specified by a programmer.

At present, X-band (8–10 GHz) PELDOR spectrometers are most widely used, although spectrometers operating at record high frequencies to 360 GHz have been designed recently.[49] With allowance for increasing popularity of PELDOR technique the company Bruker BioSpin MRI GmbH (Germany) produced a series of pulsed EPR spectrometers equipped with accessories for PELDOR spectroscopy and operating in the X-, Q- and W-bands.[56–58] A model E 580 X-band spectrometer for four-pulse PELDOR experiments uses almost 1 kW (amplified) microwave pulses of duration to 8 ns and the possible frequency difference is $\Delta\nu = \nu_A - \nu_B = 800$ MHz. The sensitivity and temporal resolution of the instrument can be illustrated by the fact that a 10^{-9} W signal can be detected 10^{-8} s after application of microwave power of several kW in a single pulse.

The pulsed EPR spectrometer for PELDOR measurements operates at two frequencies (ν_A and ν_B) applied to the sample under study. Two types of cavities are used, a monomodal cavity with low Q-factor, which allows simultaneous two-frequency excitation, and a bimodal cavity with two compartments that can be separately excited at the frequencies ν_A and ν_B. In this case the sample to be studied is placed in the common fragment of the cavity.

The design of the cavity for PELDOR spectroscopy should allow for production of rather large microwave field strength (H_1) in the sample to rotate the magnetisation vector and to excite as large region of the EPR spectrum as possible (rotation after application of a 10-ns $\pi/2$ pulse requires the amplitude $H_1 = 1$ mT). This is achieved by using specific cavity design that allows the field H_1 to be concentrated in the sample at relatively low Q-factor. A review of various versions of cavity design is available in the literature.[59] In our studies we use a

bimodal cavity, which is schematically shown along with a Dewar vessel and a sample in Fig. 7. In this cavity two TE_{102} modes are overlapped at a right angle; the design of the cavity is similar to that proposed for double resonance experiments in continuous wave EPR spectroscopy.[60] Both cavities are tuned using quartz or Teflon rods introduced into the corresponding compartment. Frequency isolation between the cavities operating at the frequencies ν_A and ν_B is 20 dB at $\nu_A = 9.4$ GHz, $\nu_A - \nu_B = 100$ MHz, and Q-factors $Q_A = 220$ and $Q_B = 150$. To carry out variable-temperature experiments, the Dewar vessel can be replaced by a gas stream tube.

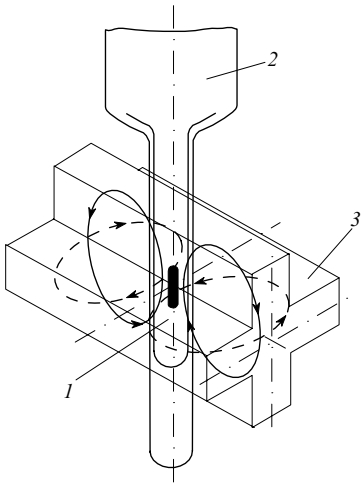


Figure 7. Measuring cell in PELDOR experiments.
Sample (*1*), quartz Dewar vessel (*2*), and TE_{102} bimodal cavity tuned to the frequencies ν_A and ν_B (*3*).

The concentration sensitivity of the PELDOR spectrometers matches that of pulsed EPR spectrometers. Compared to the continuous wave spectrometers (sensitivity of Brücker c.w. EPR spectrometers is $10^{10}-10^{11}$ spins per sample), the sensitivity of the PELDOR spectrometers is 1–2 orders of magnitude lower, especially for broad EPR spectra, where pulses excite only a certain region of the spectrum under study. At the same time one should keep in mind that the PELDOR effect is proportional to the extent of excitation of the spectrum by the B pulse, *i.e.*, to the p_b value.

PELDOR measurements are limited to the time interval $0-\tau$. In this interval, the echo signal decay due to phase relaxation should not be large. The loss of the echo signal intensity due to phase relaxation limits the initial amplitude of the PELDOR signal. There is a number of methods for partial compensation of these losses. The sensitivity can be improved by reducing, *e.g.*, phase relaxation by decreasing the concentration of paramagnetic centres (C_R), because $T_f \sim 1/C_R$. Yet another approach is based on reduction of the phase relaxation by reduction of the nuclear spin diffusion. This is achieved by replacing protons by deuterons and by using solvents containing no mobile rotating groups (*e.g.*, CH_3) to shorten the phase relaxation.[61] Owing to spectral diffusion the phase relaxation can be temperature dependent, especially for type T_1 samples.[1,3] Therefore, usually the most reliable method of extension of T_f is to carry out measurements at maximum possible low (cryogenic) temperatures. The sensitivity can also be improved using the temporal factor, namely, elongation of the signal acquisition time, but in this case the situation is governed by the stability of the spectrometer over time.

The sensitivity is to some extent improved in four-pulse PELDOR experiments where the change in the interval T occurs at a constant value of the time interval between the pumping pulse and the third π observer pulse (see Fig. 1 *b*).[62]

2. Determination of the parameter p_b

Analysis of the kinetics of PELDOR signal decays requires determination of the parameter p_b, which is related to the angle of rotation of the B-spin magnetisation after application of the pumping pulse. If the linewidth is small compared to the pumping pulse amplitude (H_1), all spins rotate by the same angle and the p_b value is given by

$$p_b = \sin^2 \frac{\gamma H_1 \tau_p}{2}, \tag{16}$$

where τ_p is the duration of the pumping pulse (experimental parameter). For a broad EPR line relation (16) should be averaged over the line form-factor $g(\nu)$. The parameter p_b for a rectangular pulse can be calculated as follows:[1,63]

$$p_b = \int_{-\infty}^{+\infty} \frac{\omega_1^2 g(\nu)}{\omega_1^2 + 4\pi^2(\nu_B - \nu)^2} \sin^2 \left[\frac{\tau_p}{2} \sqrt{\omega_1^2 + 4\pi^2(\nu_B - \nu)^2} \right] d\nu, \tag{17}$$

where $\omega_1 = \gamma H_1$ and ν_B is the frequency at which the pumping pulse is applied. Thus, the parameter p_b can be calculated with known experimental parameters.

However, an experimental method of determination of the parameter p_b seems to be more reliable. For instance, this can be done using the experimental exponential decay $V(T)$ for uniformly distributed particles if their concentration is known [see relation (4)]. This is particularly convenient in the case of solutions of stable radicals. The p_b value can also be determined using relation (10) for radical pairs with $N = 2$. In some experiments one should also know the parameter p_a, which is calculated or experimentally determined by the same methods as those employed to determine the parameter p_b.

3. Range of distances measured by the PELDOR technique

We can evaluate the range of distances r to be measured from PELDOR signal decay oscillations. The lowest dipolar frequency (ω_D) is determined by the longest time interval τ_{max} between the echo excitation pulses applied at the frequency ν_A, at which the signal can still be detected by the two-pulse ESE technique. This time matches the phase relaxation time (T_f) and is determined by the concentrations of electron and nuclear spins, the temperature and by other properties of the spin system. For organic matrices an unavoidable reason for phase relaxation (even at liquid helium temperature) is spectral diffusion in the system of electron spins, which is due to spin diffusion in the system of nuclear spins (protons of the matrix);[1] in this case the decay of the spin echo signal obeys the law $\exp[-(\tau/T_f)^3]$. Usually, for organic matrices one has $T_f \approx \tau_{max} \approx 5$ μs. Assuming that detection of one half-period of oscillations of the $V(T)$ decay requires that condition $\omega_D \tau_{max} = \pi$ be valid, we get for r_{max} from relations (2)

$$r_{max} = \left(\frac{\gamma^2 \hbar}{\pi} \tau_{max} \right)^{1/3}.$$

The estimate of the upper bound of distances thus obtained is $r_{max} \approx 8$ nm at $\tau_{max} \approx 5$ μs.

If the bandwidth of the receiving channel is rather broad, the minimum value (r_{min}) or the maximum dipole width is

determined by the amplitude of the microwave field (H_1) at the sample at the frequency ν_B. This amplitude should be sufficiently large to excite both lines of the Pake dipolar doublet with a splitting of $2\omega_D$ (see Fig. 4). In this case one has $2\omega_D = \gamma H_1$ and for the pumping π pulse one gets $\gamma H_1 \tau_p = \pi$, where τ_p is the duration of the pulse applied at the frequency ν_B. For r_{min}, one gets

$$r_{min} = \left(2\frac{\gamma^2\hbar}{\pi}\tau_p\right)^{1/3},$$

which gives $r_{min} \approx 1.8$ nm at $\tau_p \approx 30$ ns. Thus, the range of distances to be measured using the PELDOR signal decay oscillations spans from 1.8 to 8 nm. Experiments and more detailed calculations with allowance for pulse durations shift the lower bound to $\sim$1.5 nm and the upper bound to 7.0 – 7.5 nm.[40, 48]

Limitations in two-frequency (ν_A and ν_B) PELDOR spectroscopy are due to the EPR linewidth, the frequency difference $\Delta\nu_{AB}$ and the duration, τ_p, of microwave pulses. In the frequency domain rectangular pulses should not overlap (this means that $\Delta\nu_{AB} < \Delta$ and $\Delta\nu_{AB}\tau_p \gg 1$, where Δ is the effective width of the EPR spectrum). For iminoxyl radicals one has $\Delta \approx 300$ MHz and if experiments are carried out at $\Delta\nu_{AB} \approx 100$ MHz and $\tau_p \approx 40$ ns, the conditions mentioned above are met. However, this imposes significant limitations on the investigations of narrow EPR spectra and on the short-pulse PELDOR studies. Useful tips concerning PELDOR experimental design and processing of results obtained are available from reviews.[23, 24]

IV. Applications of the PELDOR technique

1. Iminoxyl biradicals and polyradicals

Iminoxyl biradicals appeared to be convenient model systems for experimental check of most theoretical concepts developed for the PELDOR technique. Usually, experiments were carried out using linear molecular structures containing two piperidine, pyrrolidine, pyrroline or 3-imidazoline terminal radical fragments. Detailed consideration of the molecular structures and properties of this type of biradicals determined by continuous wave EPR spectroscopy were reported in monographs.[28, 64, 65] In the text below we will present the results obtained in PELDOR studies of these compounds. The structure of the iminoxyl biradicals studied by the PELDOR technique and the results of measurements of the distances (R) between the >NO fragments in these systems are listed in Table 1.

Modulation of PELDOR signal decay by dipolar interactions was first detected in the experiments with frozen glassy solutions of type **1** iminoxyl biradicals (see Table 1, Fig. 8).[7] The distance between the unpaired electrons was determined either by direct measurement of the modulation period of the PELDOR signal decay or from its Fourier-transformed spectrum. The biradical with R = H was chosen as test system in the pioneering field-step PELDOR study.[66]

Calculations of the pair distribution functions of the biradicals **1** and **16** (Fig. 9) were reported.[40] In contrast to conventional techniques, the functions $F(r)$ were calculated with allowance for the pulse durations in the PELDOR experiments. This improved the reliability of the determination of the distribution function $F(r)$ and allowed the numerical value and sign of the exchange integral J to be calculated for the biradicals in which the >NO fragments are separated by less

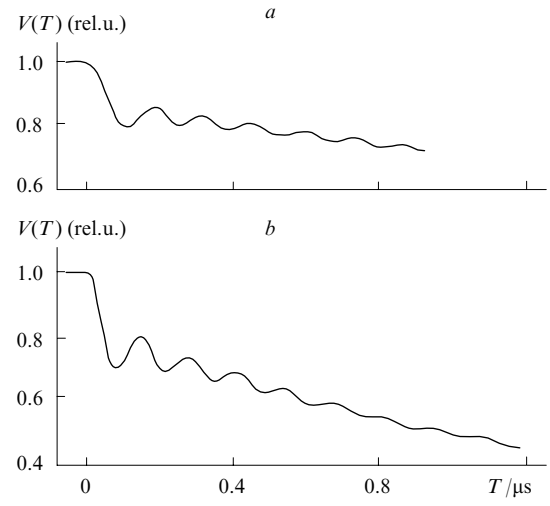


Figure 8. PELDOR signal decays for biradicals **1** (see Table 1).[8] R = H (*a*), Me (*b*).

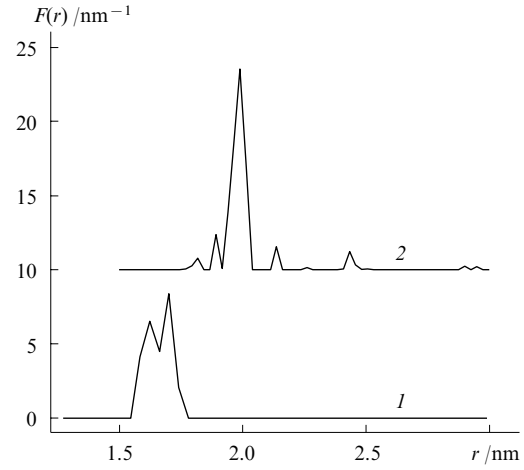


Figure 9. Distance distribution function $F(r)$ of biradicals **16** (*1*) and **1** (R = H) (*2*).[40]
Curve *2* is shifted by 10 nm^{-1}.

than 2 nm (see Table 1). Two conformations of biradical **16** with similar distances (1.62 and 1.70 nm) were found. Note that earlier the exchange integral (J = 11.0 MHz) was determined with certainty only for biradical **15** with effective conjugation in the bridge.[67] Probably, biradicals **5** and **9** are also characterised by nonzero exchange integral, but no data on exchange in these systems are available at the moment. Seemingly, the ester groups in the structure of many iminoxyl biradicals preclude effective exchange interaction.

Iminoxyl biradical **2** appeared to be the most popular. The distance between the >NO fragments was determined from the Fourier-transformed spectra of three-pulse[47, 68] and four-pulse[10] PELDOR data. (Note that in the latter case biradical **2** was used to test the first proposed four-pulse PELDOR technique.) The average distance measured by different authors is 1.97 ± 0.07 nm (see Table 1), being consistent with the results of calculations using molecular models.[68] It is assumed that biradical **2** adopts a certain possible conformation, which is then stabilised under the experimental conditions

Table 1. Iminoxyl biradicals and polyradicals studied by the PELDOR method.

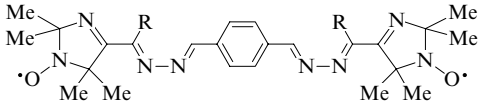
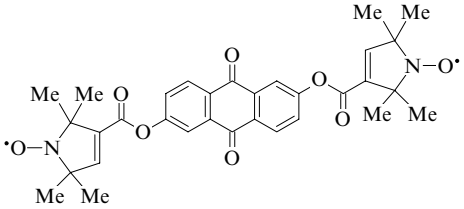
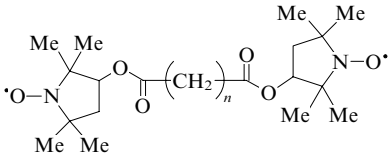
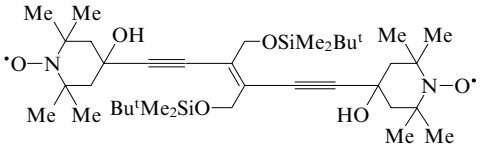
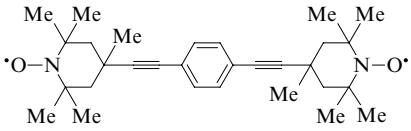
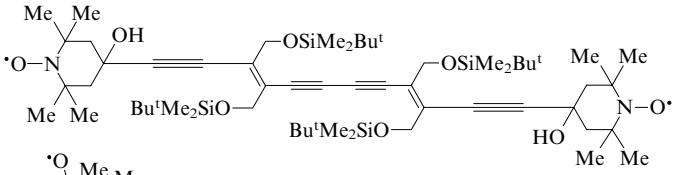
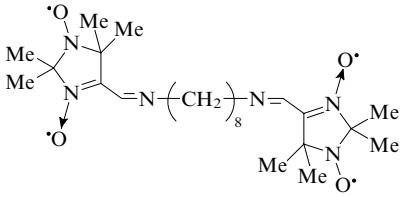
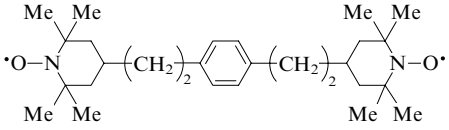
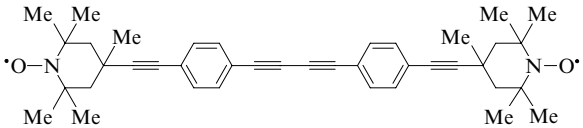
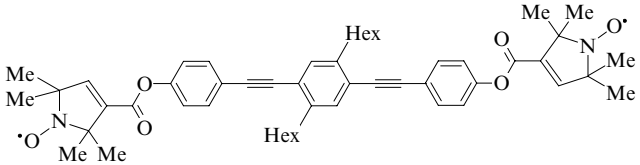
Radical	Structure		R /nm (J /MHz)	Ref.
1	 R = H, Me.		1.9 ± 0.16 1.94 ± 0.02 1.99 ± 0.06 (0.7 ± 0.4)	7 66 40
2			1.97 1.97 ± 0.03 1.94 ± 0.05 1.98 ± 0.07	47 67 10 68
3		$n = 8$ $n = 12$ $n = 14$ $n = 20$	2.04 ± 0.07 2.48 ± 0.13 2.71 ± 0.19 3.28 ± 0.44	68 68 68 68
4			1.54 ± 0.02	69
5			1.72 ± 0.03	69
6			2.20 ± 0.07	69
7			see [a]	32
8			see [a]	32
9			2.57 ± 0.14	69
10			2.83 ± 0.05 2.92 ± 0.04	12 67

Table 1 (continued).

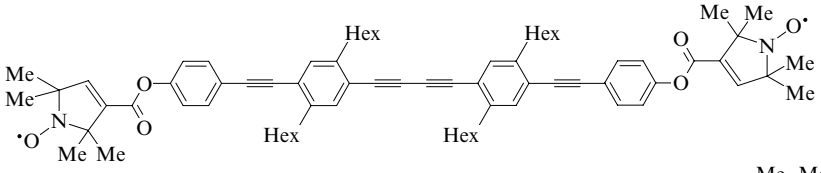
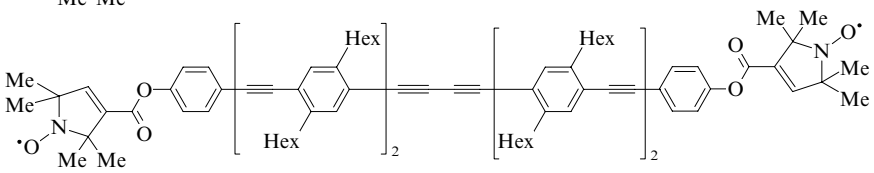
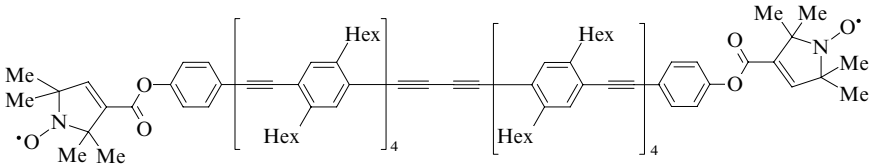
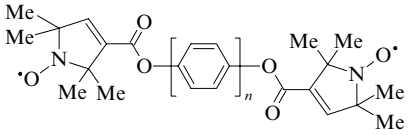
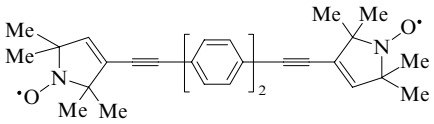
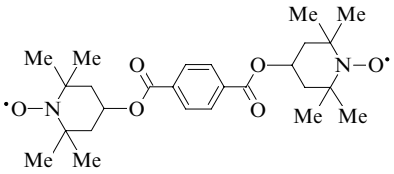
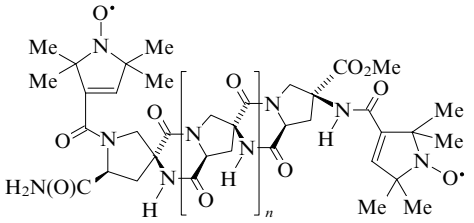
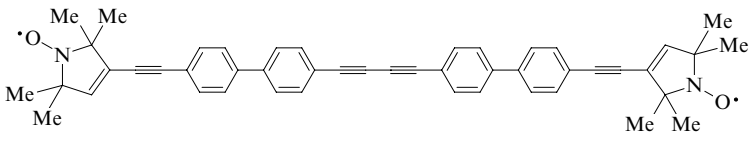
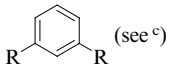
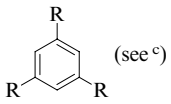
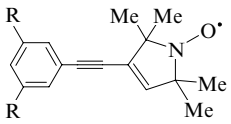
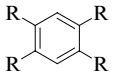
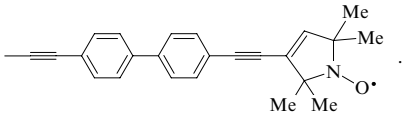
Radical	Structure		R /nm (J /MHz)	Ref.
11			3.63 ± 0.10	12
12			4.92 ± 0.20 5.00 ± 0.40	12 62
13			7.44 ± 0.82	62
14		$n = 1$ $n = 2$	1.54 ± 0.03 1.97 ± 0.03	67 67
15			2.40 ± 0.04 (11.0 ± 0.3)	67
16			1.62 ± 0.04 1.70 ± 0.04 (1.4 ± 0.5)	40 40
17		$n = 2$ $n = 3$ $n = 4$ $n = 5$ $n = 6$	2.37 ± 0.10 2.67 ± 0.17 2.94 ± 0.10 3.23 ± 0.14 3.45 ± 0.11	70 70 70 70 70
18			3.40 (1.0) [b]	71
19	 (see [c])		3.30 (4.0) [b]	71
20	 (see [c])		3.30 (4.0) [b]	71

Table 1 (continued).

Radical	Structure	R/nm (J/MHz)	Ref.
21	 (see [c])	2.50 (4.0) [b] 3.40 (4.0) [b]	71
22	 (see [c])	2.20 (5.0) [b] (*ortho*) 3.30 (4.0) [b] (*meta*) 3.80 (3.0) [b] (*para*)	71

Note. Hex stands for n-hexyl. [a] Broad conformational distribution. [b] The half-witdth of the distance distribution function is given in parentheses.

[c] R =  .

(glassy matrix, 80 K), because the lines in the Fourier-transformed spectrum were rather narrow ($\sim 3-4$ MHz).

In studies [67, 68] iminoxyl radicals were used as a 'ruler' for comparing the PELDOR-measured and calculated distances between spin labels and for evaluating the limiting distances that can be determined by the PELDOR technique based on experimental data. The distances were varied by varying the size of the bridging group linking the radical fragments. For instance, biradicals **3** with $(CH_2)_n$ aliphatic bridges were studied.[68] Measurements were carried out at 80 K with the biradical samples dissolved in polystyrene matrix. Despite the fact that the experimental Fourier-transformed spectra were rather broad, their maxima were successively shifted towards the low-frequency region with an increase in the chain length. The distances thus determined varied from 2.04 nm ($n = 8$) to 3.28 nm ($n = 20$).[68] Chain elongation by one CH_2 unit causes the distance between the >NO fragments in biradical **3** to increase by about 0.1 nm. In these experiments the linewidths in the Fourier-transformed spectra were determined by the set of conformations of the aliphatic polymer chain. It was established that the distances determined in study [68] with inclusion of conformational statistics assuming a fully stretched conformation of the aliphatic chain are in agreement with the results of force-field calculations. Note that biradical **3** seems to be an exception, because no modulation beats in the PELDOR signal decay were detected for structurally similar biradicals **7** and **8**.[32] We believe this is due to a broad set of conformations (enhanced flexibility) of the aliphatic bridge in these two biradicals.

In more recent studies the linker between the >NO fragments was chosen to be as conformationally rigid as possible. For instance, iminoxyl biradicals **14** and **15** were thoroughly studied in frozen deuterated toluene solutions by the X- and S-band PELDOR techniques (at 9.7 and 2.1 GHz, respectively).[67] This enabled unambiguous assignment of the lines in the Fourier-transformed spectrum to dipolar or hyperfine coupling whose signals are detected in the same frequency region. Lines at the frequencies corresponding to $\nu_\perp$ and $\nu_\parallel$ were detected in the X- and S-bands for all biradicals, but only for biradical **14** it was found that $\nu_\perp \neq 2\nu_\parallel$. Calculations for this biradical allowed the numerical value and sign of the exchange integral to be determined ($J = +11.0$ MHz).

Noteworthy is yet another result obtained in the study.[67] No modulation of the PELDOR signal decay was detected in both the X- and S-bands for a biradical that is structurally similar to radical **15** but has one benzene ring in the bridging group. The authors believed that the reason is strong exchange interaction in this biradical (evaluation of the exchange integral from the EPR spectral data gives $|J| = 73$ MHz), which leads to a spin state of the system that is described by two bound states (triplet and singlet) rather than two weakly interacting doublet states, as is typical of biradicals with weak exchange ($J \approx 0$) that contribute to PELDOR.

Attempts to determine the upper bound of distances that can be measured by the PELDOR technique were reported in studies [12, 62] of biradicals with a rigid structure specified by sequences of triple bonds and benzene rings (biradicals **9**–**13**). The longest distance (7.44 ± 0.82 nm) between the unpaired electrons was determined [62] for solutions of biradical **13** in deutero-*o*-terphenyl at 50 K. The distance in biradical **12** was determined [12, 62] with a high accuracy; it equals 5.0 ± 0.4 nm. The inter-spin distance in this radical (5.10 ± 0.12 nm) was also determined using yet another pulsed method, namely, the single frequency technique for refocusing (SIFTER).[12] Theoretical calculations for biradical **12** gave the distance 5.23–5.15 nm. Note that correlations between the results of MD calculations of linear conjugated structure and the PELDOR-measured distances between the >NO fragments of terminal radicals were also found for other shorter but 'rigid' biradicals **4**–**6**, **9**, **10** (see Refs 12, 67, 69).

The distance distribution function $F(r)$ contains valuable information on the set of possible conformations of the biradical under study; these are the spin-label conformations including those of the chains connecting the iminoxyl radical to the molecular skeleton, conformations of the iminoxyl radical itself and conformations of the molecular chain. Evaluation of the actual size and flexibility of the molecular skeleton of the biradical requires that the possible values of all these conformational contributions be preliminarily estimated by the MD method and compared with the data of PELDOR measurements. This was done for biradicals **10**–**13** that simulate *p*-phenylenethynylene [72] oligomers and for a series of bispeptide biradicals **17**.[70] Both types of 'rigid' molecular systems can be used as 'building blocks' for various nanostructures. The

authors of study [72] believe that the computational technique they have proposed can be used for estimating the flexibility of molecules and oligomers used in the design of molecular nanostructures with preset properties.

Molecular stranded-helical blocks built of bispeptide monomers labelled with pyrroline radicals at both ends were studied.[70] The number of monomers can sequentially be increased using a specific synthetic procedure. The structures of such spin-labelled blocks **17** with $n = 4-8$ are presented in Table 1. In contrast to other biradicals listed in Table 1, which, as rule, are soluble only in organic solvents, biradicals **17** are water soluble. Aqueous solutions of biradicals **17** were studied at 80 K in a buffer containing glycerol added for the glass transition to occur. The decay kinetics of four-pulse PELDOR signals were analysed using the Fourier-transformed spectra and calculations of the distance distribution function. The distances between >NO fragments in these compounds and the corresponding distribution functions $F(r)$ (Fig. 10) were determined. The average distance increases from 2.37 nm ($n = 4$) to 3.46 nm ($n = 8$), *i.e.*, each additional unit in the structure of the linker connecting two radicals makes a contribution of 0.27 nm to the average distance. Noteworthy is that the scatter of distances (standard deviation) increases as the chain length increases from 0.18 nm ($n = 4$) to 0.58 nm ($n = 8$). This parameter characterises the molecular flexibility of a given structure. The results obtained are by and large in agreement with the results of MD calculations.

An example of broad distributions over conformations and mutual spatial orientations is provided by spin-labelled [2]catenanes **23**.[73] Structurally, these supramolecular systems represent threaded rings. The rings are rather large; they are built of molecular groups that almost do not interact with one another. Once spin labels are introduced, the problem of mutual orientation of the rings becomes equivalent to the problem of determination of the distance distribution function for pair of labels, which can be solved using the PELDOR technique.

Calculations of a model function $F(r)$ that allows for equiprobable mutual arrangement of spin labels in a model chain comprised of two rings with the effective radius r_{eff} were reported.[73] The calculated function $F(r)$ was then compared with the PELDOR experimental data obtained in frozen solutions of [2]catenanes in three solvents (chloroform, *o*-terphenyl and 2-methyltetrahydrofuran) at 15 K. Correspondence between the experimental function $F(r)$ and the results obtained using the theoretical model proposed was found only for the data obtained in chloroform.[73] In other solvents the authors observed either aggregation of [2]catenanes (in 2-methyltetrahydrofuran) or a significant ring geometry distortion, which is likely due to the nonlinear conformation of the alkyl fragment of the macrochain in *o*-terphenyl. The calculated r_{eff} values are similar to the experimental data for the solutions in chloroform, *i.e.*, for this solvent all relative positions of spin labels are possible and, therefore, the rings freely move relative to each other. The simplest model used by the authors of Ref. 73 gives a quite correct description of the properties of molecules a few nanometre in size and can also be useful for analysis of large supramolecular systems.

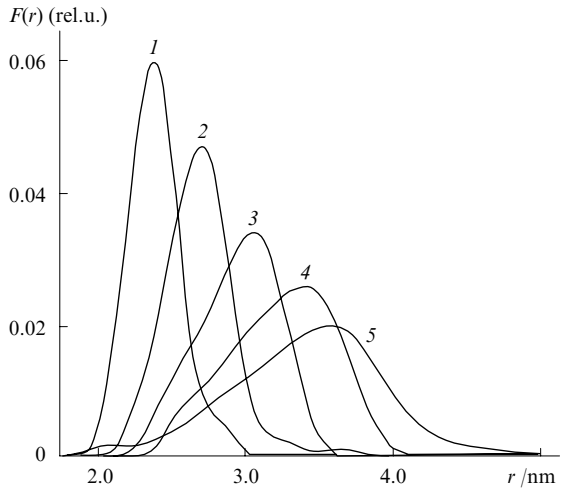
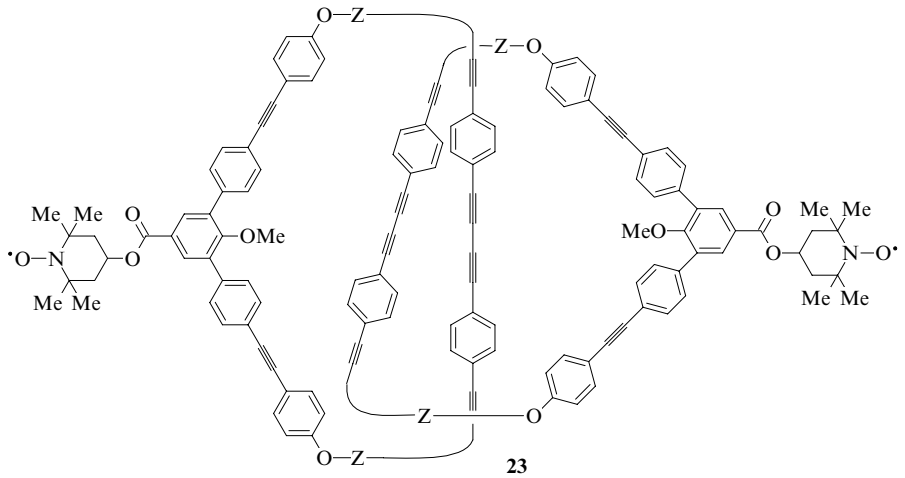


Figure 10. Distance distribution function $F(r)$ of biradicals **17**.[70] $n = 4$ (*1*), 5 (*2*), 6 (*3*), 7 (*4*), 8 (*5*).

As mentioned above, the number, N, of particles in a group of spins is an important parameter which can be determined by the PELDOR technique. Here the term 'groups' covers molecular aggregates, clusters and other spatially localised systems in which the distances between paramagnetic particles do not



23

$Z = (CH_2)_{11}$, $(CH_2)_{23}$, $(CH_2)_{23}$ — Me, $O(CH_2)_{23}$, Me.

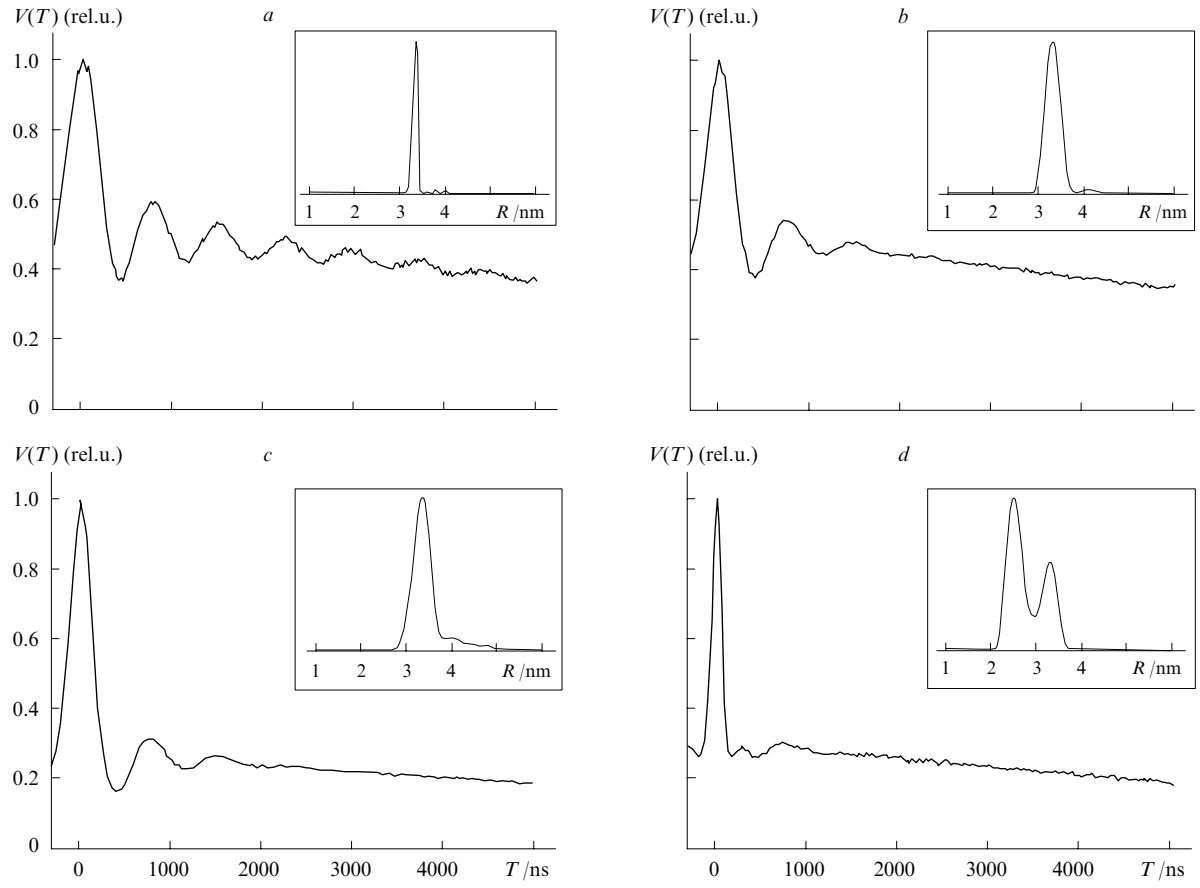


Figure 11. Four-pulse PELDOR signal decays and corresponding pair distribution functions calculated from these decays (see insets) for biradicals **18** (*a*) and **19** (*b*) and triradicals **20** (*c*) and **21** (*d*) (see Table 1).[71]

vary or vary only slightly. In the simplest case these are dimers, trimers, tetramers and other molecular aggregates that are typical of complex biological structures. Most often, structural studies of such systems involve not only distance measurements, but also determination of the number of particles in aggregates.

Aggregates with identical structure can be characterised by a number of preferred distances. The kinetics of the PELDOR signal decay are sensitive to the total number N of radical centres in the aggregate or, generally, to the distribution functions $F(N)$ over the number of particles in the aggregate.[32–34] The number of particles in aggregates has been determined since the pioneering PELDOR studies. The pair distribution ($N = 2$) was determined[32] for radicals that are formed as a result of sensitised photoionisation of frozen naphthalene solutions in decalin. Even if the distance distribution for pairs of paramagnetic centres is rather broad, as in this case, the pair distribution can be determined with certainty from the characteristic fast PELDOR signal decay at short times T; this distinguishes this situation from the exponential decay observed for radicals with random spatial distribution.

The most definite results were obtained recently in a PELDOR study of model iminoxyl polyradicals (specially synthesised bi-, tri- and tetraradicals).[71] The aim of that study was to experimentally evaluate the method with respect to accuracy of theoretical calculations that serve the basis for the determination of the number of particles in a group of spins for $N = 2$, 3 and 4 and to determine the pair distribution functions for these polyradicals. The structures of the compounds investigated are shown in Table 1 (structures **18**–**22**). Modulated four-pulse PELDOR decays (Fig. 11) were studied. Two decay parameters were determined experimentally; these are the limiting signal amplitude V_p after normalisation to the exponential decay due to dipolar intermolecular interactions and the probability of excitation of the spectrum by the pumping pulse p_b. The last-mentioned parameter ($p_b = 0.43$ and 0.12 for the pumping pulse durations of 12 and 92 ns, respectively) was determined from the PELDOR signal decay for the model biradicals **2**, **14** and **15** assuming $N = 2$. The parameter N was calculated using relation (10). With an accuracy of about 5% the experimental N values were found to be 2.1 for biradicals **18** and **19**, 3.0 for triradicals **20** and **21** and 3.9 for tetraradical **22** (see Table 1); this is in excellent agreement with the expected N values for these polyradicals. Experimental p_b values can depend on the mutual orientation of iminoxyl labels in polyradicals (orientation selectivity); therefore, this will affect the N values determined from relation (10). Calculations[71] of the excitation probabilities p_b using the signal decay data for biradical **19** and triradical **20** showed no or very weak dependence; therefore, one can to a first approximation consider that there is no spatial correlation between the orientations of spin labels.

The distance distribution for polyradicals has some specific features. If the functions $F(r)$ of biradicals **18** and **19** and symmetric triradical **20** have only one maximum each, the spectrum of distances obtained for triradical **21** (see Fig. 11 *d*)

exhibits two lines with a 2 : 1 intensity ratio owing to non-equivalent positions of spin labels. The function $F(r)$ of tetraradical **22** has three maxima corresponding to three possible distances in a rectangle whose vertices are occupied by spin labels. The distances in these polyradicals and the results of molecular modelling (figures in parentheses, shown for comparison) are listed in Table 1.

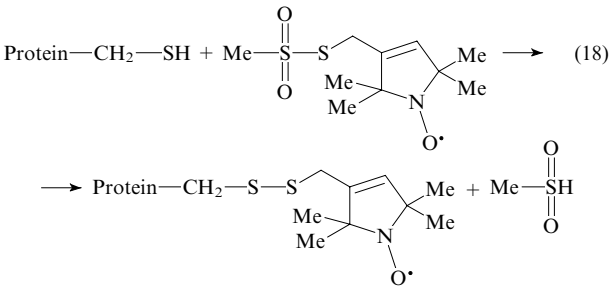
The orientation selectivity in biradical **11** and triradical **20** (see Table 1) was studied by W-band four-pulse PELDOR technique.[50] The PELDOR spectra and the modulation depth were studied at six points of the EPR spectrum, which corresponded to the hyperfine coupling constants (HFC) $A_\perp$ and $A_\parallel$ of anisotropic iminoxyl triplet. The corresponding lines are resolved in the W-band. Experiments involved measurements of the frequencies ν_A and ν_B and variation of the constant magnetic field H_0. The results obtained showed that the spin labels have no fixed relative orientations owing to hindered rotation, but their motion is correlated. These conclusions were confirmed by MD calculations.

2. Spin-labelled biomacromolecules and systems

Elaboration of site-directed spin labelling (SDSL) methods offered a new field of application of EPR spectroscopy in biochemistry and biophysics. The case in point is the determination of elements of the secondary and tertiary structure of membrane proteins (including the effect of the medium on their fragments), investigation of the orientations and motion of particular fragments of protein molecules under physiological conditions, determination of conformational transitions in the course of functioning of protein – membrane systems and many other applications.

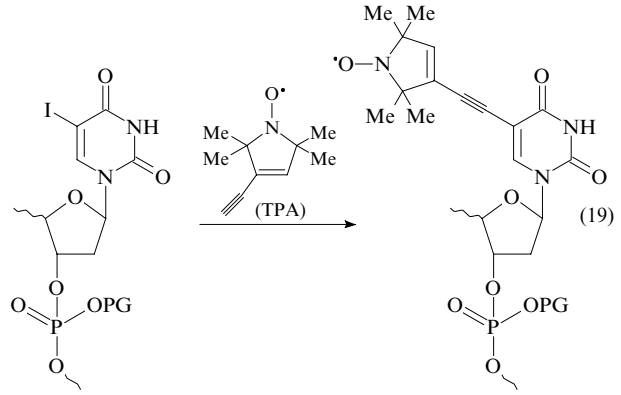
As rule, these investigations are carried out by conventional continuous wave EPR spectroscopy. They are systematically reviewed in a book series *Biological Magnetic Resonance* edited by L Berliner (a total of 22 issues were published to the year 2007). In the text below we will only dwell on the studies concerned with applications of the PELDOR technique. Pioneering studies in this field were reviewed in Volumes 14 and 21 of this book series.[74, 75]

Elaboration of efficient methods of SDSL for biologically valuable compounds was the key step, which in essence predetermined the possibility of setting and carrying out these investigations. Methods to solution of this problem for nucleic acids and oligonucleotides were considered in a review.[74] Among the most popular methods, mention may be made of a widely used spin labelling (using radical-substituted thiosulfonate) *via* the sulfhydryl group of cysteine residue of the protein molecule following reaction (18).[76 – 79]

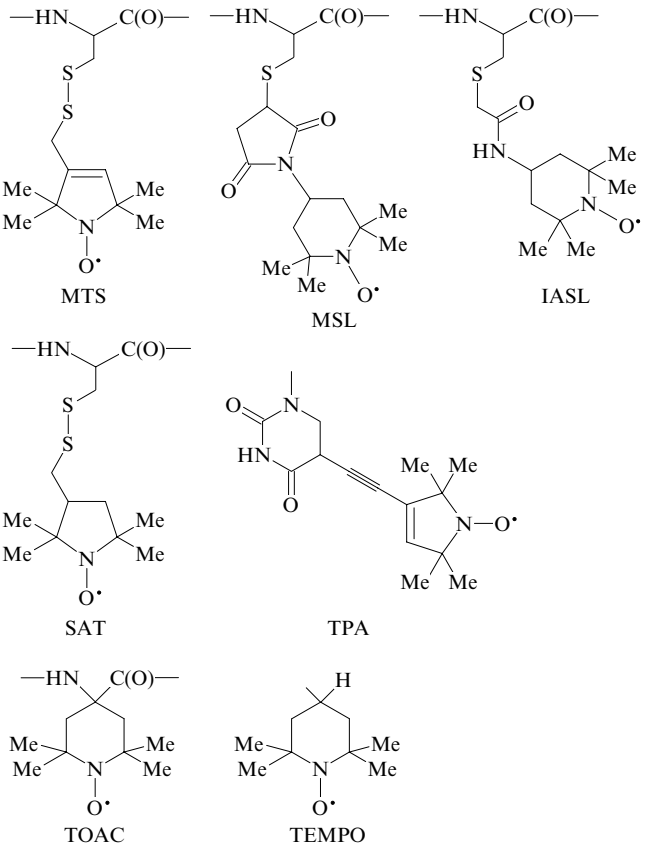


The synthesis is carried out either by introducing a label into the known position of cysteine in the protein or upon replacement of a particular base in the oligonucleotide structure by cysteine.

Yet another widely used SDSL method is to carry out a Sonogashira reaction in the course of automated solid-phase [on a porous glass (PG)] synthesis of oligonucleotides; here the iodine atom in the uridine fragment of nucleotide is replaced by a radical containing a triple bond [*e.g.*, using 2,2,5,5-tetramethylpyrrolin-1-yloxy-3-acetylene, TPA) (reaction (19)].[80]



This label has a restricted conformational mobility, which improves the accuracy of distance determination by the PELDOR technique. In most cases, the labels add to either the β-C atom of the peptide chain through the $C_\beta - S$ bond or to the uridine residue of the oligonucleotide (examples follow). (It should be noted that sometimes the labels are denoted by the same abbreviations as the reactants used to attach the labels, *i.e.*, TPA, TEMPO, *etc.*, but in some cases these abbreviations are followed by the 'suffix' 'SL', which stands for 'spin labelling'.)



In these cases the $\rangle N-O$ group and the amino acid or nucleotide residue of the biomolecule under study are sepa-

rated by at least 5–7 bonds (labels MTS, MSL, IASL, SAT, TPA), which significantly influences the interpretation of the results of distance measurements by EPR spectroscopic methods. The exceptions are two labels, namely, TOAC (it replaces the Aib residue in the peptide chain) and TEMPO (it adds to N- or C-terminal groups of the protein).

Conformational flexibity of the linker connecting the protein and label makes the design of molecular structures based on EPR measurements more ambiguous. The problem becomes particularly severe when interpreting data for short distances (1.0–2.0 nm) comparable with the size of the linker. An attempt to allow for conformational and structural effects in distance calculations from the data on dipolar interactions obtained by continuous wave and pulsed EPR spectroscopy was reported.[81] The most widely used computational approach involves measurements of distances between the C_β-atoms using molecular models of spin-labelled proteins (C_α are atoms of the protein chain). However, in this case the difference between the results of theoretical calculations and experimental data can be as high as 0.6 nm. It was shown that the best correlation ($R^2 = 0.8$) between the EPR measured distances and their calculated values (deviation of about 0.3 nm) is attained if the initial determination of possible conformational space for the labels in the model calculations (Monte Carlo simulations) is followed by MD calculations of the lowest-lying conformers.[81] It is these conformers for which the distance between spin labels is calculated. Yet another advantage of this approach consists in evaluation of possible spectrum of distances, which appears due to the scatter of conformers with respect to distances and dynamic mobility.

a. Nucleic acids

Structural information on DNA and RNA is necessary to gain a better insight into the mechanism of transfer of genetic information and on the catalytic properties of these key biomacromolecules. The use of the PELDOR technique for structural studies is based on the known SDSL procedures for particular nucleotide residues.[76–80] A detailed description of application of the Sonogashira method for preparation of labelled DNA and RNA was reported recently.[82]

One of the pioneering studies[83] concerned a self-complementary RNA1 containing the IASL labels introduced into uridine residues (**U**) of the duplex:

5′GCUGA**U**AUCAGC3′

3′CGACUA**U**AGUCG5′.

Measurements in frozen RNA1 aqueous solutions at 20 K gave a distance between spin labels of 3.5 ± 0.2 nm. No modulation of PELDOR signal decay by spin-labelled RNA2 was detected, which was attributed to aggregation of RNA2 duplexes.

DNA[84] and RNA[85] duplexes were studied in more detail. The distances between the TPA spin labels introduced into 2′-deoxyuridine (U′) fragments of DNA duplex helices following reaction (19) were determined by four-pulse PELDOR technique. The labels were introduced into the U′ residues localised in five different positions of the duplex oligonucleotides in such a fashion that the shortest distance corresponded to the DNA(1) sequence while the longest distance corresponded to the DNA(5) sequence (spin-labelled residues U′ are given in bold):

DNA(1) 3′GCGA**U**′ACATGCG5′

5′CGCTA**U**′GTACGC3′,

DNA(5) 3′GC**U**′GACTATATAGTCAGC5′

5′CGACTGATATATCAG**U**′CG3′.

Experiments were carried out with frozen (35 K) aqueous buffer solutions of duplexes containing 20% of ethylene glycol for the glass transition to occur. The distances between spin labels (1.92, 2.33, 3.47, 4.48 and 5.25 nm) were determined from the frequencies of Fourier-transformed spectra derived from corresponding PELDOR signal decays with an accuracy of 5%. Molecular dynamics calculations of various conformers of the duplex gave the following best approximation of the same distances: 1.96, 2.14, 3.30, 4.33 and 5.24 nm, respectively; this was treated as substantiation of the B-conformation of the helix for the duplexes frozen in aqueous solutions.

Six RNA duplexes containing TPA-labelled adenosine, uridine and cytidine residues were studied.[86] Deep modulation of the PELDOR signal decays enabled highly accurate determination of the distances in the duplexes, which vary from 1.93 ± 0.12 to 3.87 ± 0.13 nm depending on the number of base pairs between the labels. Comparison of the results obtained in study[86] with the data of distance measurements in DNA[84] showed that at the same number of base pairs between spin labels in DNA and RNA the distances between helices in the duplex are different. For instance, at 10 base pairs the distance in DNA was 4.48 ± 0.5 nm[84] (*cf.* 3.87 ± 0.13 nm in RNA[86]). The difference lying beyond the error of measurements was attributed to two various conformations, namely, type-A helix for RNA and a more stretched type-B helix for DNA. The results obtained were in good agreement with the results of MD distance calculations (correlation coefficient is 0.976, Fig. 12).[86] The authors of study[86] believed that the DNA and RNA duplexes retain their conformations in frozen (40 K) aqueous-phosphate buffer solutions with ethylene glycol additive (20%).

An original method of introduction of spin labels into polynucleotides was proposed.[87] MTS-Type labels were introduced into phosphothioate groups introduced into specified (fixed) positions between nucleotides of the DNA or RNA duplex chains rather than the desired nucleotide. In this case the label can be attached to any position of the modified

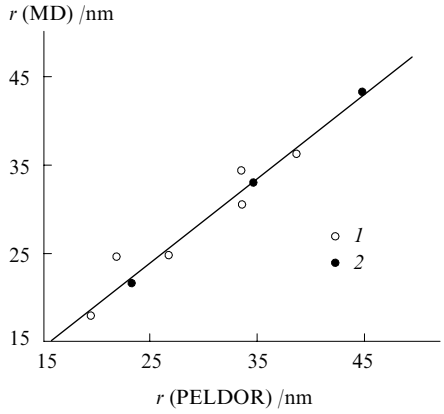


Figure 12. Correlation between spin label (TPA–TPA) distances in the RNA and DNA duplexes measured by the PELDOR method and obtained from molecular dynamics calculations.[86]
The base pair number was varied from 1 to 10; data for RNA (*1*) and DNA (*2*).

polynucleotide in order to carry out distance measurements. After formation of duplexes from polynucleotides labelled at different positions one can determine the distances for a broad spectrum of radical pairs. Using the samples thus prepared (measurements were carried out at 50 K using frozen aqueous solutions of DNA duplexes), eight distances between spin labels were determined by the PELDOR method from the positions of maxima of the pair distribution function. The minimum and maximum distances are respectively 2.56 and 3.88 nm for the DNA with the CS nucleotide sequence. Comparison [87] of the results of distance measurements with those of calculations performed using the NMR spectroscopy data that allow for possible conformations of the DNA in question revealed an excellent correlation ($R^2 = 0.98$) between them. It was suggested that this procedure for introduction of spin labels can be widely used in structural studies of DNA and RNA complexes with proteins.

TEMPO spin labels were successively introduced [88] into uridine residues of DNA duplexes in such a fashion that the labels were separated by 9, 12, 15, 18 or 21 pairs of bases:

5′GCU CGU CAU GGU CCU CAT TGT ACT AGC

CGA GCA GTA CCA GGA GTA ACA TGA UCG 5′.

Five doubly spin-labelled duplexes were synthesised and frozen (77 K). DNA solutions in D_2O and deuterated ethylene glycol were studied. Samples prepared in optimum manner for the X-band spectrometer (sufficiently high signal-to-noise ratio, long relaxation time $T_f \approx 8$ μs) contained the DNA duplex (12.5×10^{-6} mol litre^{-1}) in 50% solution of deuterated ethylene glycol in D_2O.

Detection of the PELDOR signal decay was followed by analysing the distance distribution function $F(r)$ calculated usng Tikhonov's regularisation method. Six distances between the spin labels in the range 2.8 – 6.8 nm were determined. The most interesting were the results obtained for mixtures of the spin-labelled duplexes (Fig. 13). It was established [88] that for a mixture of two different duplexes deconvolution of the complex function $F(r)$ using a Gaussian distribution function for each duplex allows one to quite accurately determine the average distance in each duplex and the concentration of each duplex in the mixture. However, analysis of the functions $F(r)$ of mixtures containing a larger number of duplexes becomes difficult, which is due to both errors and ambiguity in the solution to the ill-posed problem of reconstruction of $F(r)$ from the kinetics $V(T)$ and to possible transformations occurring under the action of, *e.g.*, stacking interactions in a complex mixture that change the spatial arrangement of DNA duplexes. Nevertheless, this study first demonstrates an analytical approach involving the PELDOR technique.

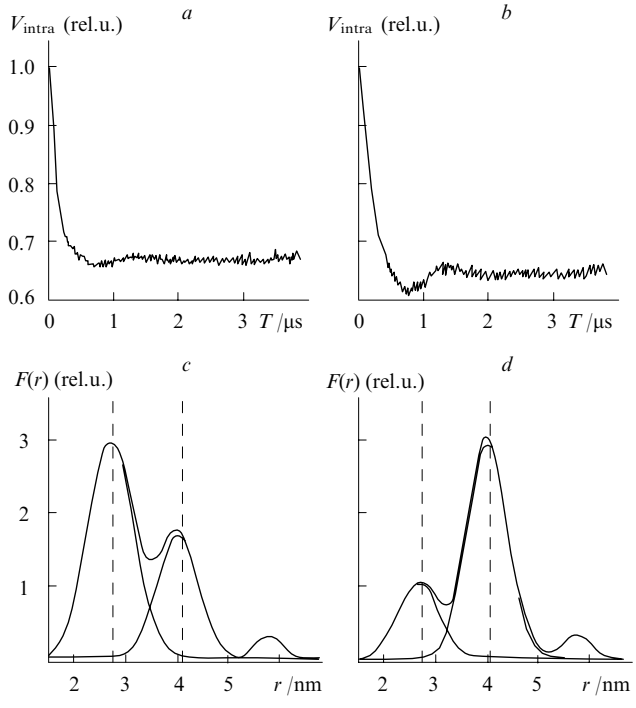


Figure 13. Results of investigations of spin-labelled duplex mixtures.[88] PELDOR signal decay kinetics for a mixture of duplexes with distances 2.8 and 4.1 nm taken in a 3 : 1 ratio (*a*) and for the same duplexes taken in a 1 : 3 ratio (*b*); distance distribution functions $F(r)$ for these mixtures and corresponding Gaussian curves simulating the distance distribution (*c*, *d*).

b. Peptides

Structural properties of peptides provide valuable information for understanding of biophysical functions of peptide – membrane systems. An important type of peptides are peptaibols, which exhibit antibiotic activity. They form ion channels in bacterial membranes, which causes degradation of membranes and eventually the death of cell structures. Information on the structure and properties of peptaibols and their aggregates is necessary for the design of efficient antibiotics.

Methods of synthesis of spin-labelled peptaibols were developed at the laboratories headed by C Toniolo (Padova, Italy) and T Ovchinnikova (Moscow, Russia). Spin-labelled peptaibols trichogin (T, 11 amino acid residues in the chain; $n = 11$), trichogin dimer (DT, $n = 22$), alamethicin (A, $n = 19$) and zervamicin (Z, $n = 15$) used in our studies were synthesised in these laboratories. [All glutamine residues of native alamethicin were replaced by methyl glutamate residues, Glu(OMe).] These peptides are built of amino acid residues, among which an important role is played by the α-aminoisobutyric acid (Aib) residue, and have chains of different length n and different N- and C-terminal groups. In contrast to trichogin and alamethicin that were labelled with TOAC in chain (instead of Aib residue), zervamicin was labelled with TEMPO at the N- and C-terminal atoms (TZT):

$$\text{Fmoc}\overset{1}{\textbf{Aib}}\text{GlyLeu}\overset{4}{\textbf{Aib}}\text{GlyGlyLeu}\overset{8}{\textbf{Aib}}\text{GlyIleLeuOMe} \quad \text{(TF)}$$

$$\text{Oct}\textbf{Aib}\text{GlyLeu}\textbf{Aib}\text{GlyGlyLeu}\textbf{Aib}\text{GlyIleLeuOMe} \quad \text{(TO)}$$

$$\text{TEMPO} - \text{TrpIleGln}\textbf{Aib}\text{IleThr}\textbf{Aib}\text{Leu}\textbf{Aib}\text{HypGln}. \quad \text{(TZT)}$$

$$.\textbf{Aib}\text{Hyp}\textbf{Aib}\text{Pro} - \text{TEMPO}$$

$$\text{Ac}\overset{1}{\textbf{Aib}}\text{Pro}\textbf{Aib}\text{Ala}\textbf{Aib}\text{AlaGlu(OMe)}\overset{8}{\textbf{Aib}}\text{Val}\textbf{Aib}\text{Gly}. \quad \text{(A)}$$

$$.\text{Leu}\textbf{Aib}\text{Pro Val}\overset{16}{\textbf{Aib}}\text{AibGlu(OMe)Glu(OMe)Phl}$$

$$\text{Ac}\overset{1}{\textbf{Aib}}\text{GlyLeu}\textbf{Aib}\text{GlyGlyLeu}\textbf{Aib}\text{GluIleLeu}\textbf{Aib}\text{Gly}. \quad \text{(DT)}$$

$$.\text{Leu}\textbf{Aib}\text{GlyGlyLeu}\overset{19}{\textbf{Aib}}\text{GlyIleLeuOMe}$$

Glassy frozen polar and nonpolar solutions were investigated by X-band EPR spectroscopy at 77 K. It is convenient to study peptide conformations in dilute solutions in polar solvents (alcohols, *etc.*) where the peptides are in free monomolecular state. In nonpolar solvents (toluene, decalin, *etc.*), self-aggregation of peptides occurs usually; this offers prospects for investigations of the structure and properties of peptide supramolecular aggregates, which is important for

undestanding of their biological activity. Of course, this problem can be solved using X-ray analysis data for peptide crystals, but the approach involving studies of peptides in media, which simulate the hydrophobic part of the cell bilayer, seems to be more interesting. Unlike crystals, the molecular environment and packing of peptide molecules in supramolecular aggregates will be governed by solvent molecules rather than the peptide molecules themselves.

Trichogin. In polar solvents both continuous wave EPR spectra and data on the kinetics of PELDOR signal decay indicate a statistically uniform distribution of trichogin molecules in frozen glassy solutions. A $V_{intra}(T)$ decay component modulated by dipolar interaction was detected for doubly labelled peptides. The distance between spin labels in the doubly labelled trichogins TF-1,8 and TO-1,8 in $CHCl_3$–DMSO mixture determined from the modulation period is 1.97 nm. This distance is sensitive to solvent polarity and for TO-1,8 it varied from 1.97 to 2.18 nm upon transition from methanol to ethanol (Refs 18, 30, 89). The proportion of molecules in this conformation (helix type 2_7 or 3_{10}) is about 30%. Other molecules show a broad distribution of distances between spin labels. Unfortunately, the distance distribution function was not calculated in the early studies.[30, 89] The assignment of the TOAC- labelled peptides to a particular conformation was based on the distances between labels calculated in Refs 30, 45, 90 and 91.

The type of the helix depends on many structural factors including geometric parameters of the amino acid residues in peptide, intra- and intermolecular hydrogen bonds and the medium polarity. All singly labelled trichogins in polar solvents showed exponential PELDOR signal decays, which indicated a uniform distribution of spin labels. Transition to nonpolar solvents qualitatively changes the situation, the change being related to peptide aggregation in the nonpolar medium.[92]

In nonpolar media a fast PELDOR signal decay in the initial period is followed by a slow decay modulated by dipolar interaction (Fig. 14, curves *1*, *2*). The addition of a polar solvent (ethanol) to the samples (solutions of TF-4 and TO-1 in chloroform–toluene mixture) causes qualitative changes in the signal decay, which becomes exponential (Fig. 14, curves *3* and *4*), thus indicating decomposition of aggregates. Having

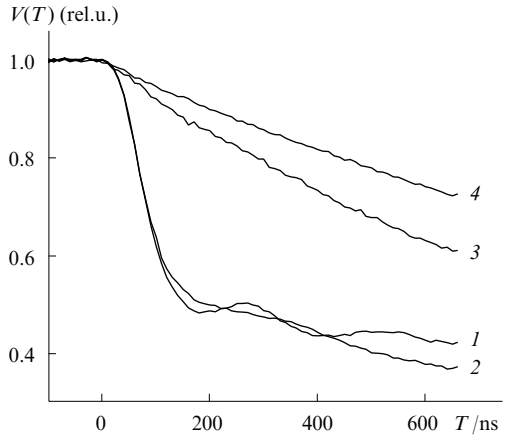


Figure 14. PELDOR signal decay obtained for spin-labelled trichogins TF-4 and TO-1 dissolved in a chloroform–toluene mixture (*1*, *2*), and changes in the decays obtained for the same mixture upon the addition of ethanol (*3*, *4*).[92]
Measured in the X-band at 77 K.

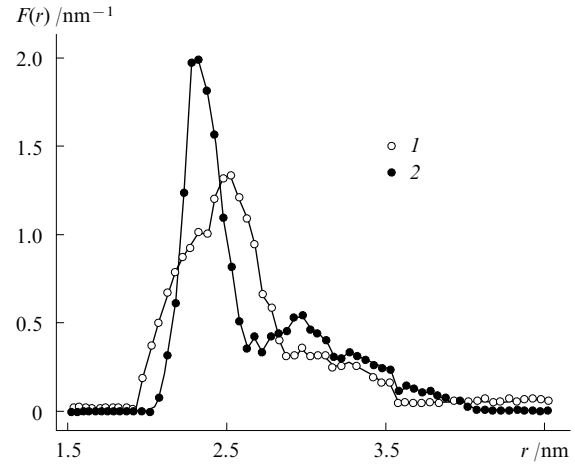


Figure 15. Distance distribution functions $F(r)$ of TO-1 (*1*) and TF-4 (*2*) trichogin aggregates formed in nonpolar media.

selected V_{intra} from the overall decay $V(T)$ and determined the V_p value for these samples, it was found that the number of spin labels in the aggregate is $N = 4 \pm 0.3$. The distribution function, $F(r)$, of distance between spin labels gives the value $r = 2.35$ nm for aggregates in the singly spin-labelled peptides TF-4 and $r = 2.60$ nm for TO-1 (Fig. 15).

The possible conformation of trichogins in these aggregates was studied[93] using aggregates formed from unlabelled peptide to which doubly labelled TO-1,8 (10%) was added in a chloroform–toluene mixture. This made it possible to select intramolecular dipole interaction in a single aggregate. The intramolecular distance between spin labels determined from experimentally detected PELDOR signal oscillations is $r = 1.57$ nm, which corresponds to the 3_{10}-helical conformation. The results obtained appeared to be consistent with the molecular model of an aggregate (Fig. 16). Helical peptide molecules in the 3_{10}-conformation form tetrameric structures

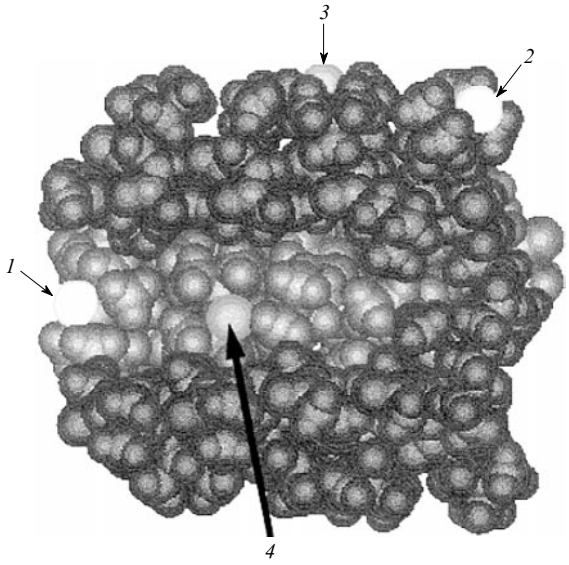


Figure 16. Structure of trichogin aggregates formed in nonpolar media.[92] The trichogin molecules in the 3_{10}-conformation form a tetramer. Arrows denote the spin labels in the peptide positions 1 (arrows *1*, *2*) and 4 (arrows *3*, *4*).

with polar groups oriented towards the centre of aggregates. The positions of the TOAC spin labels are shown in Fig. 16 by arrows. These results demonstrated for the first time the potential of the PELDOR technique in structural studies of biopolymer aggregates.

Aggregation of singly and doubly labelled trichogins in various solvents of low polarity was studied [94] and the aggregation mechanism was investigated [95] by continuous wave EPR spectroscopy. The EPR spectra of monomers and aggregates of the doubly labelled peptide TO-1,8 (solutions in chloroform at 20 °C) were separated and the dependence of the proportion of monomeric peptide molecules on the peptide concentration in the solution in the range 5×10^{-6}–7×10^{-4} mol litre^{-1} was obtained. A kinetic scheme of aggregation was proposed, which includes two stages, namely, dimerisation of peptide molecules and subsequent aggregation of dimers into tetramers. The equilibrium constants for both reaction stages were evaluated and it was shown that at peptide concentrations higher than 10^{-5} mol litre^{-1} most peptide molecules are present in solution in the aggregated forms.

The concentration dependence of parameters of dipole – dipole interactions between spin labels in frozen glassy solutions of aggregates formed from singly labelled trichogin analogues was studied [95] by the PELDOR technique. It was shown that the number of molecules in aggregates and the frequency and amplitude of the PELDOR signal oscillations due to dipole interactions between spin labels in aggregates are independent of the peptide concentration in the range 5×10^{-4}–8×10^{-3} mol litre^{-1}. Aggregation of spin-labelled trichogins in solutions of different polarity at room temperature was thoroughly studied by analysing dipole line broadening in continuous wave EPR spectra.[96]

Trichogin dimer. Changes in the distance distribution function obtained for the doubly spin-labelled peptide DT-1,19 in a methanol – toluene mixture (Fig. 17) can serve as an example of the effect of the medium polarity on the monomer – aggregate transition.[36, 97] In pure methanol, oscillations of the PELDOR signal decay were weak and a poorly resolved doublet function $F(r)$ had the total width of nearly 2 nm. The addition of toluene was followed by an increase in the amplitude of oscillations and the function $F(r)$ had two pronounced maxima corresponding to the distances 2.8 and 3.2 nm (α- and 3_{10}-conformations). In pure toluene the PELDOR signal decay is strongly modulated and the main maximum corresponds to the α-conformation, which indicates the formation of trichogin aggregates.

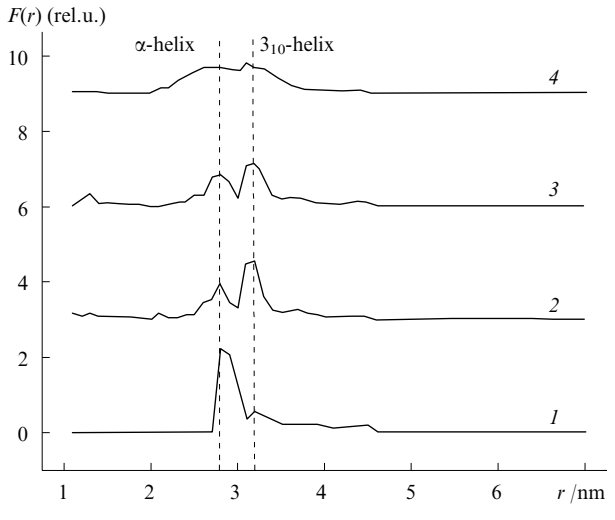


Figure 17. Changes in the distance distribution function $F(r)$ of doubly spin-labelled peptide DT-1,19 upon a change in the medium polarity.[36, 97] Toluene (*1*); toluene – methanol mixtures containing 10% (*2*) and 20% (*3*) of MeOH and neat methanol (*4*).

The study [36] of aggregation of singly spin-labelled peptides DT-1 showed, based on the V_p value, that $N \approx 2$ and the distance between the spin labels is 3.4 nm; this implies an antiparallel orientation of molecules in the aggregate. When constructing a model, one should take into attention the dipole moment of the peptide helix. In particular, the estimated total dipole moment of the α-helix in DT-1 equals 77.0 D and aligned to the helix axis. The distance between α-helices (0.8 nm) is determined by steric factors only. The structural model for DT-1 peptide aggregates is shown in Fig. 18.

The study [36] seems to be one of the first attempts to detect the effect of selectivity in relative orientation of spin labels in the biradical structure. The function $F(r)$ was calculated for different mutual orientations of >NO fragments in the peptide DT-1,19. Comparison with experimental data showed the lack of correlation between the orientations. Drawing definite conclusions requires investigations in the high-frequency region, because it is still unclear to which extent is the function $F(r)$ sensitive to orientation selectivity effects in the X-band.

Zervamicin. Aggregation of singly labelled zervamicin ZT in toluene – methanol mixtures was studied in detail.[98] As for other peptaibols, an increase in the content of methanol in the mixture causes decomposition of aggregates present in solution in pure toluene. Unlike trichogin the PELDOR signal decays V_{intra} of zervamicin in the mixtures containing 8.5% – 16% of methanol show no oscillations, but a fast decay followed by attainment of a constant limiting value V_p is detected in the initial portion (at 50 – 200 ns). These decay kinetics are characteristic of spin groups characterised by some types of distribution over distance and over the number of particles in the group. In this case one can estimate the distance between spins in the group from the initial decay using relation (11). It was found that this distance depends on the composition of the mixture and varies between 2.5 and 3.5 nm. The N value calculated from relation (12) also depends on the composition of the mixture. Analysis showed that, depending on the composition of the mixture, the aggregated state with $N_{max} = 2$ contains at least 44% – 67% of ZT molecules. Thus, at present there is lack of structural information for constructing a particular molecular model for this aggregate.

The distance distribution function for doubly labelled peptide TZT (Fig. 19) in frozen methanol solutions and in frozen methanol – toluene and methanol – chloroform mixtures was obtained.[45] The main maximum of the function $F(r)$ is at $r = 3.3$ nm, the position being only slightly dependent on the composition of the mixture. The halfwidth of the function $F(r)$ decreases from 0.3 for pure methanol to 0.15 nm for the mixtures. This can be explained by a decrease in the number of possible conformations of terminal groups of the TEMPO-labelled peptide TZT in the mixtures of low polarity compared to methanol. Molecular dynamics calculations showed that the main conformation of TZT molecule is a mixed $\alpha/3_{10}$-helical conformation, which is in agreement with NMR spectroscopy data. As the hydrophobicity of the medium is increased by adding toluene or chloroform to the methanol solution, the distribution function $F(r)$ shows the appearance of weak additional lines corresponding to the distance 4.2 nm and a more stretched 2_7-conformation of the TZT helix.

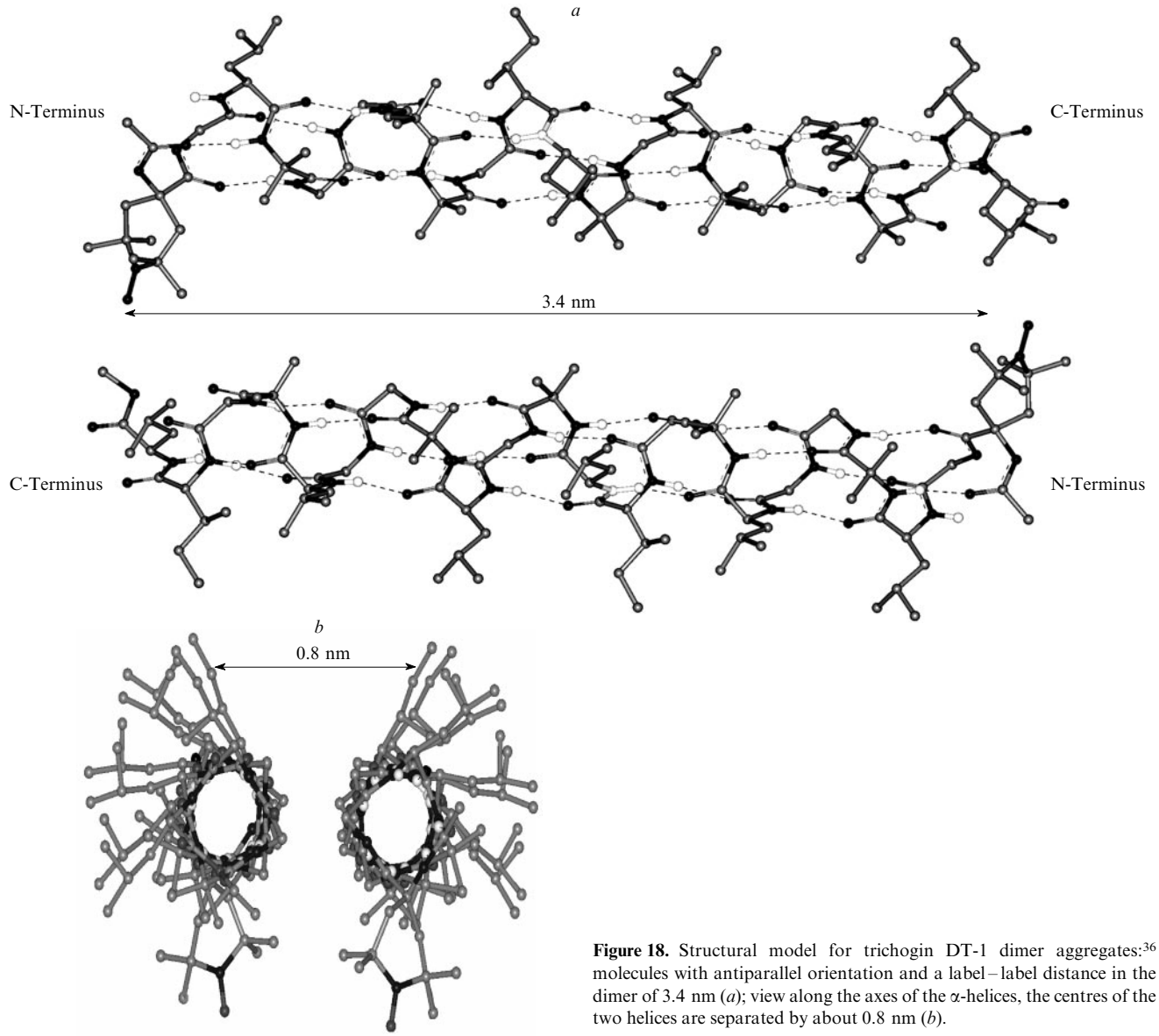


Figure 18. Structural model for trichogin DT-1 dimer aggregates:[36] molecules with antiparallel orientation and a label–label distance in the dimer of 3.4 nm (*a*); view along the axes of the α-helices, the centres of the two helices are separated by about 0.8 nm (*b*).

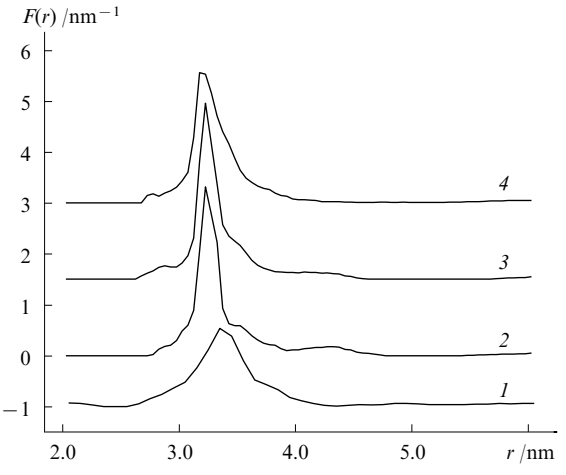


Figure 19. The distance distribution function $F(r)$ of doubly spin-labelled zervamicin in different media.[45]
Methanol (*1*), methanol–toluene (1 : 1) (*2*), methanol–toluene (3 : 7) (*3*) and methanol–chloroform (1 : 1) (*4*).

Alamethicin. Despite the fact that alamethicin seems to be the best studied peptide among peptaibols that form cell channels, detailed studies of the (i) mechanism of self-aggregation in membrane media and (ii) structure of membrane channels have not been reported for this compound as yet.

Spin-labelled alamethicins A-1, A-8, A-16 were investigated[42,44] by continuous wave EPR spectroscopy and PELDOR technique, alamethicin A-16 being studied in most detail. PELDOR spectroscopy data for solutions in chloroform–methanol (1 : 1) mixture at different peptide concentrations (10^{-3}–10^{-4} mol litre^{-1}) showed that the equilibrium is completely shifted towards free alamethicin molecules (exponential PELDOR signal decay was observed). Solutions of the same concentrations in the chloroform–toluene mixture showed decays typical of peptide aggregation, that is, a fast initial decay to $T \approx 200$ ns and a long oscillating 'tail' at $200 \leqslant T \leqslant 1500$ ns. The V_{intra} decay kinetics for all three spin-labelled peptides are shown in Fig. 20 *a*; in Fig. 20 *b* we present the pair distribution functions $F(r)$ for these peptides. Calculations of these functions with allowance for the duration of the microwave pulses[40,48] led to quite unexpected results. All three functions have similar shapes and nearly the same

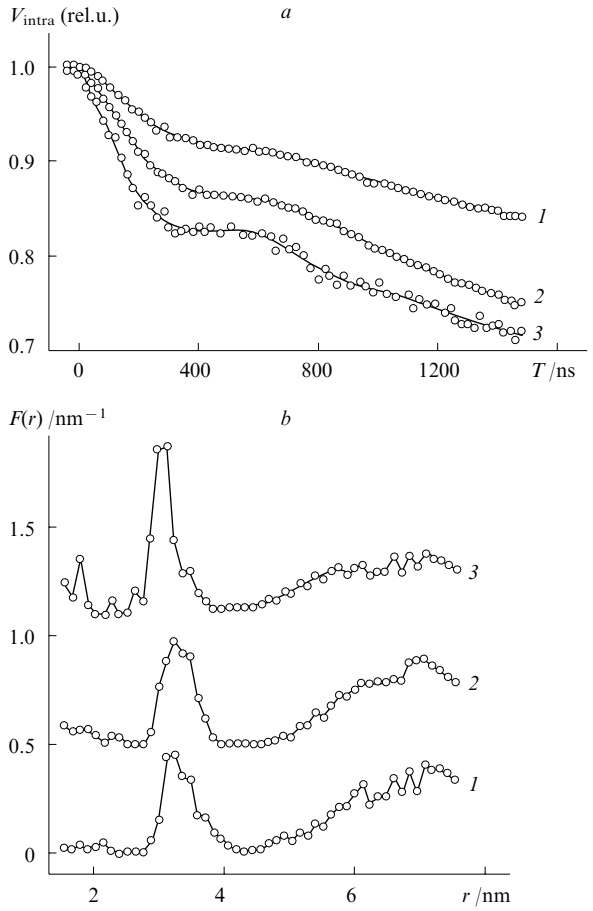


Figure 20. Normalised PELDOR signal decays for glassy frozen solutions of spin-labelled alamethicins A-1, A-8, A-16 in a chloroform – toluene (1 : 1) mixture at 77 K (*a*) and the respective distance distribution functions $F(r)$ calculated from these data (*b*).[44]
Alamethicin A-1 (*1*), alamethicin A-8 (*2*) and alamethicin A-16 (*3*).

parameters, namely, the main sharp maximum of the distribution is at 3.18 (A-1), 3.24 (A-8) and 3.06 nm (A-16), the broad maximum being in the region 7 nm. About 30% of the spin labels are at the short distances and the remaining species (70%) are in the region 7 nm. From analysis of the function $F(r)$ it follows that $N \geqslant 6$. Noteworthy is that the kinetics of the PELDOR signal decay calculated using the functions $F(r)$ for $N = 6$ and $N = 8$ almost coincide.

To obtain a more reliable N value, the EPR lineshapes of these peptides in chloroform – toluene mixture were studied at room temperature.[44] The parameter N can be determined from the correlation times of rotational mobility by approximating the rotational motion of a radical by the motion of a spherical particle in a liquid of known viscosity.[99] The N value thus estimated is $N \approx 6.8 \pm 2.5$. Thus, one can state that the system under study is characterised by $6 \leqslant N \leqslant 9$.

ESEEM experiments also showed that the observed modulation of the PELDOR signal decay is due to dipolar interactions of the unpaired electrons in alamethicin aggregates rather than hyperfine or hyperfine and quadrupole couplings between electrons and surrounding nuclei.[44]

Based on the results obtained, the following model for alamethicin aggregate was proposed. Two aligned tetramers containing four alamethicin molecules each form a linear system obeying the 'head-to-tail' pattern (Fig. 21 *a*). To verify the model proposed, relevant MD calculations were carried out. From experimental data it follows that the minimum peptide – peptide interaction energy is attained at a distance of 3.3 nm for those molecular conformations in which the γ-ester groups in positions 7, 8 and 19 in both peptides interact as dipoles with antiparallel orientations, thus forming seven polar clusters along the alamethicin aggregate. Figure 21 *b* shows that the histograms of the distribution over the number of different distances for the model proposed are in qualitative agreement with the experimental functions $F(r)$ for the labelled peptides A-1, A-8 and A-16 (Fig. 20 *b*).

Thus, the proposed supramolecular structure based on the PELDOR data can serve a basis for the design of peptide – membrane complexes that govern the biological function of alamethicin.

Alanine peptides. A study of peptides based on a repeating sequence $(AAAAK)_nA$ ($n = 4$, 7) was reported.[100] Various

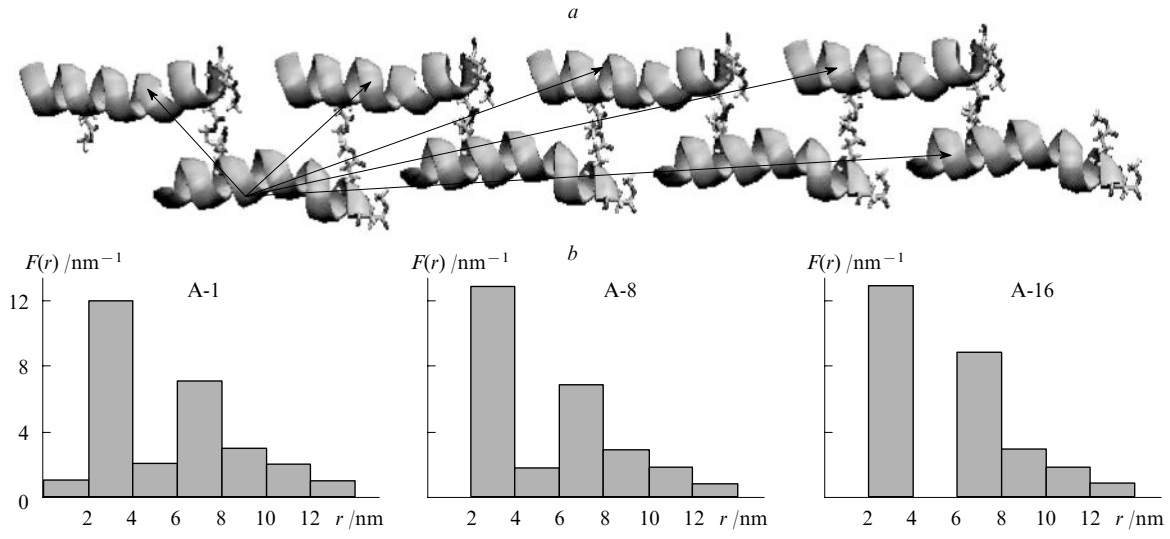


Figure 21. Structure of alamethicin aggregate.[44] Arrows point to certain possible distances between pairs of spin labels (*a*) and the distribution over the number of possible distances between pairs of spin labels (histograms) in labelled alamethicin aggregates (*b*).

alanine residues were replaced by cysteine residues to which the MTS and SAT spin labels were attached.

Dipolar couplings were studied by analysing the lineshape in the X-band EPR spectra and by the four-pulse PELDOR technique (measurements were carried out at 50 K in frozen aqueous solutions). The results obtained were compared with the results of MD calculations performed assuming the α-structure of the peptide helix. Eight peptides with $n = 4$ and one peptide with $n = 7$ were studied in detail. This allowed the authors of Ref. 100 to compare the EPR and PELDOR data in the borderline region of distance measurements (1.5–2 nm). The main conclusion drawn is that reliable results for this borderline region in the presence of conformation distance distribution can only be obtained in combined continuous wave EPR spectroscopy (lineshape analysis)/PELDOR studies. When analysing PELDOR data, a correction should be applied to allow for the durations of the pulses applied at the frequencies ν_A and ν_B and for the frequency differences between the pulses ($\Delta\nu_{AB}$).[100] The lower bound of PELDOR measurements is nearly 1.6 nm and the upper bound for continuous wave EPR measurements is in the range 1.5–1.7 nm.

The main errors in measurements in the borderline region are due to the exchange coupling and inhomogeneous EPR line broadening. It was also found that the distances determined using the SAT labels are shorter than those determined using the MTS labels, the difference going beyond the limits of measuring error. No explanation for this effect was given. By and large the distances measured by continuous wave EPR spectroscopy and PELDOR technique for the alanine peptides studied span the range from 1.07 to 4.61 nm.

c. Bionanosystems

After the development of SDSL methods and pulsed EPR techniques to study the properties and spatial organisation of spin-labelled systems (examples are given in the text above) investigations of complex nanosized biological systems became one of the most important fields of application of the PELDOR method.

In this connection mention may be made of a study on the determination of distances between amino acid residues in the sodium-proline transporter (symporter) PutP of *Escherichia coli* (*E. coli*).[101] This membrane–protein complex utilises the electrochemical gradient of Na^+ ions to drive various substrates (water, ions, sugars, amino acids, vitamins, *etc.*) across the membrane. Spin labels were attached to cysteine residues within polyoligomer loops in periplasm and cytoplasm of cell membranes (Fig. 22). Singly and doubly spin-labelled samples (mutants) were prepared and their continuous wave EPR spectra and dipolar interactions (using four-pulse PELDOR technique) studied. Analysis of the continuous wave EPR spectra of the doubly labelled mutants only showed that the spin labels are separated by distances longer than 1.8 nm. At the same time analysis of the PELDOR signal decays of the mutants allowed the distances shown in Fig. 22 to be determined. The shape of the pair distribution function for the distances between labels was assessed. The authors[101] suggested that rapid decrease in this function at $r > 2.2$ nm indicates a broad distribution of conformers in the polyoligomer loop (*i.e.*, a high flexibility of the loop regions studied).

The samples showed non-exponential PELDOR signal decays. This seems to be related to the spatial distribution of the spin labels on the outer and inner membrane surfaces (see below). The distances between the spin-labelled residues point

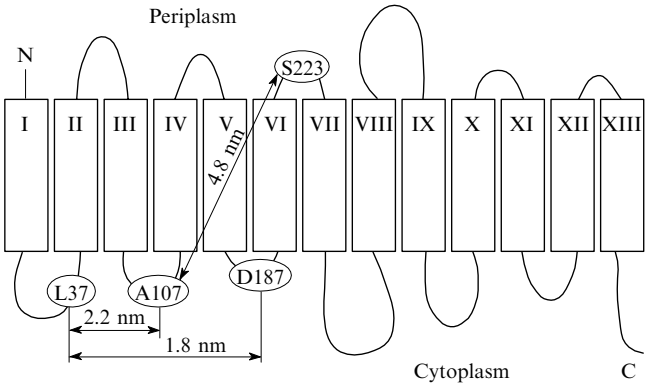


Figure 22. Structural model for *E. coli* sodium/proline transporter PutP; shown are the structural elements containing spin labels.[101] Shown are the label–label distances determined by the four-pulse PELDOR method.

to their localisation on the surface, namely, only one of the four labels is localised in the loop region in periplasm, whereas the other three spin labels are localised on the other membrane surface.[101]

More recently, the same group of researchers studied[102] the dependence of dimerisation of the Na^+/H^+-antiporter of *E. coli* on the pH value using singly spin-labelled nucleotides that can form dimers.[102] The study involved the determination of the (i) distance between the interacting nucleotides (4.4 nm) acting as dimers and (ii) distance distribution function $F(r)$ and its changes depending on the pH value of the medium. The PELDOR data were used as a basis for correction of the molecular model and mechanism of biological action of this antiporter.[102]

Interesting results were obtained in studies of weak (non-covalent) protein–protein interactions for MTS-labelled human von Willebrand factor A domain (vWF-A) from factor B contained in the complement.[103] This complex weakens the cell–cell interactions between the surface proteins and plays an important role in regulation of inner immune system. To increase the phase relaxation time, frozen solutions of vWF-A in D_2O were used. It was shown that modulation of the PELDOR signal decay is detected at times ~6 μs, which corresponds to an inter-spin distance of 6.15 ± 0.14 nm (trimolecular protein aggregate). Thus trimerisation of vWF-A in aqueous solutions can be considered established.

Considerable literature is devoted to comparison of the continuous wave and pulsed EPR techniques used for distance determination. In particular, changes in the conformations of polypeptide fragments in the course of receptor-catalysed activation of G-protein were investigated by continuous wave EPR spectroscopy and PELDOR technique.[104] The PELDOR method was used in combination with SDSL to study protein–protein interactions in cytoplasmic domain of erythrocyte membranes[105] and the structure of fibrial protein, cardiac troponin.[106]

Efficient use of three EPR techniques in different ranges of distances was reported.[107] These are the method based on measurements of the double-quantum transition intensities (used for distance determination in the range 0.7–0.8 nm), analysis of EPR linewidths (in the distance range 0.85–2.0 nm) and PELDOR technique (distance range 0.18–2.4 nm). Studies were carried out with human carboxyanhydrase II containing MTS-labelled cysteine residues.

A study of myosin, a protein participating in muscle contraction in higher organisms, was reported.[108] Spin labels were introduced into the region called gap, where, as is assumed, molecular conformations and, therefore, the distance between the spin labels ('open – closed' transition gap) change during the muscle contraction. Investigations were carried out using continuous wave EPR spectroscopy (linewidths were studied) and the PELDOR technique. The spin labels at distances 1.4 – 1.5 nm were identified by the former and those separated by 2.2 – 2.5 nm, by the latter method. It was established [108] that the average distance (2.2 – 2.5 nm) remains unchanged, within the limits of experimental error, on going from the closed to the open state of the gap, but the position of maximum of the distance distribution function changes by $\sim 3\%$. Similar changes were also found in an EPR study of the spin labels localised at a distance of about 1.5 nm. Conformational changes of these two types of labels localised in the myosin gap were also observed in the interaction between the F-actin and myosin and in phosphorylation of myosin.[24] Both these processes are associated with the functioning of muscular system.

Magnetic dipole interactions in spin-labelled b-subunits of protein complexes of F_0F_1-ATP synthetase were studied. It was shown that correct description of the dipole interactions between spin labels can be obtained using two structural models for these complexes with separated and bound subunits.[109]

Under certain conditions the concentrations of free radicals formed in the course of redox reactions and stabilised in biological systems are sufficiently high for PELDOR measurements. As a result, there is no need for introducing spin labels. The PELDOR technique was used to determine the distance between two neutral flavin radicals ($r = 2.61 \pm 0.08$ nm) in the enzyme that acts as augmenter of liver regeneration.[110] In this case the width of the EPR spectrum is about 3 mT. This makes it possible to have a frequency difference between the detection pulse and the pumping pulse as high as 78.4 MHz, which is at least comparable with the experiments with iminoxyl labels.

For one class of ribonucleotide reductases (RNR, enzymes catalysing the oxidaton of nucleotides) the role of the active complex is played by centres containing antiferromagnetic iron and tyrosyl radicals. The RNR molecule is comprised of four protein subunits, of which two contain this type of centres. The distance between radicals tyrosyl localised in two different RNR subunits of *E. coli* and mouse was determined by the PELDOR technique.[111, 112] Measurements were carried out in the X- (9 GHz) and Q-bands (34 GHz) at 30 K. The key experimental data [112] are shown in Fig. 23. The spectrum of tyrosyl radicals is rather broad (doublet with a splitting of about 2 mT, see Fig. 23 *a*) and the pump pulse and the detection pulse do not overlap ($\nu_A - \nu_B = 60$ MHz). The kinetics of PELDOR signal decay is typical of A-spin pair (see Fig. 23 *b*) and its Fourier transformation in the frequency domain gives a sharp peak at 1.39 ± 0.05 MHz, which corresponds to $r = 3.25 \pm 0.05$ nm (see Fig. 23 *c*). To ensure that modulation of the PELDOR signal decays is a result of electron – electron dipolar coupling rather than electron – nuclear interaction (ESEEM effects), the authors of this review performed measurements for RNR subunits containing one tyrosyl radical; no modulation was detected in this case. The results obtained are in good agreement with crystallographic data on the distances between tyrosyl radicals in the RNR of *E. coli*.[111] At the same time the results [112] are an important step in studies of RNR in animals, for which crystallographic data are unavailable at the moment.

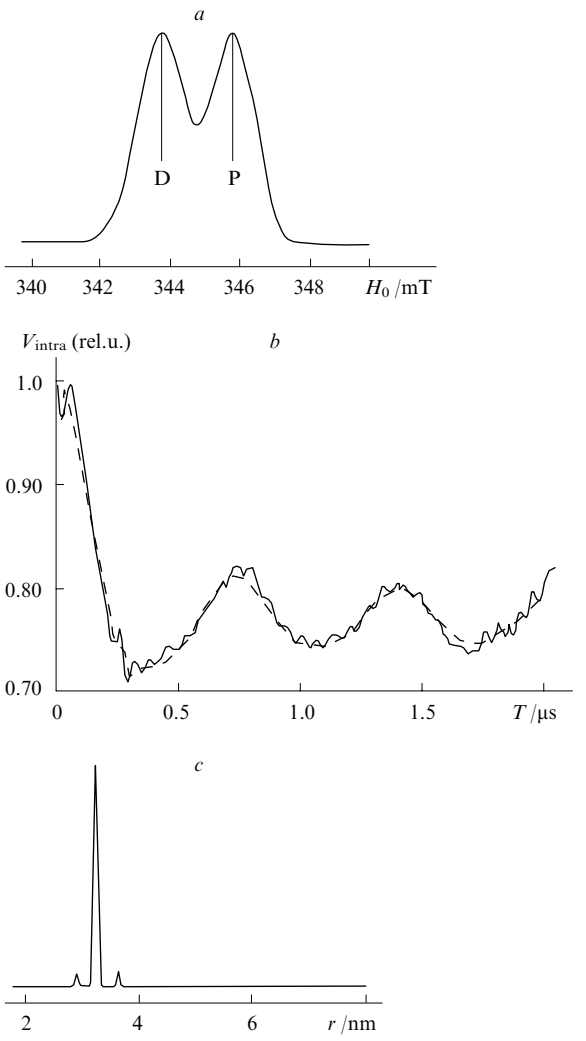


Figure 23. Results of measurements of distances between tyrosyl radicals using EPR spectroscopy.[112]
Shown are the EPR spectrum points excited by the pumping pulse (P) and echo pulse (D) (*a*), PELDOR signal decay [dashed line denotes the results of calculations using the $F(r)$ function] (*b*) and the distance distribution function $F(r)$ (*c*).

A mutant of human ubiquitin in which the Ser20 and Gly35 bases were replaced by MTS-labelled cysteine (Fig. 24) was studied [113] by the PELDOR and single-frequency double quantum coherence (DQC) [12] techniques. The aim of that study was to compare the two methods of distance determination in spin-labelled proteins. It was found that the distances measured by these methods are very similar, namely, $r = 3.55$ (PELDOR) and $r = 3.58$ nm (DQC). The distance distribution functions differ in that the function plotted using the DQC data has a peak in the region 1.5 nm, which corresponds to the proton modulation frequencies in the X-band. Comparison [113] showed that the DQC technique is more sensitive than PELDOR. However, DQC experiments (excitation of the whole EPR spectrum by a six-pulse train) can face problems due to nuclear modulation (ESEEM) and the need for meeting more severe requirements for the pulse train parameters compared to PELDOR. By and large, PELDOR appeared to be more efficient in studies of short distances (to $r \approx 1.5$ nm) while DQC was more appropriate for measuring long distances ($r > 2$ nm). Effeicient combined use of the DQC and

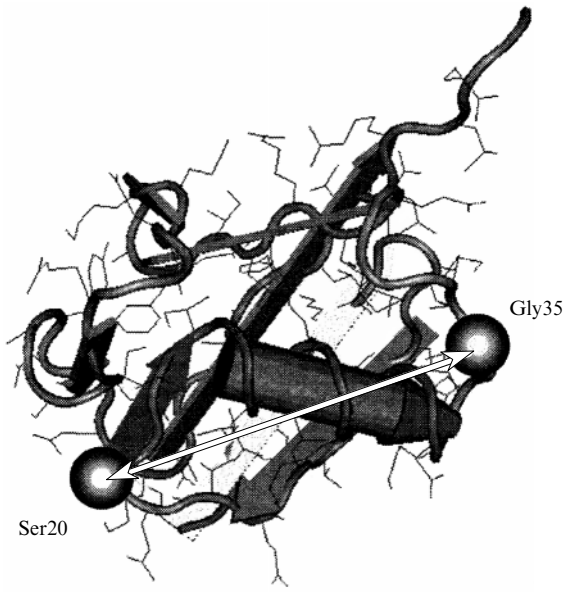


Figure 24. Structure of human ubiquitin.[113]
The distance (3.55 nm) between spin labels in the Ser20 and Gly35 bases determined by the PELDOR method is arrowed.

PELDOR techniques for distance determination in a wide range (1.4–7.0 nm) was demonstrated [114, 115] in structural studies of spin-labelled complex protein complexes and micelles.

Other examples of applications of the PELDOR technique (usually, in combination with lineshape analysis in EPR spectroscopy of spin labels) in studies of the structure and dynamics of biomacromolecules and their complexes can be found in reviews [22–24, 116, 117] and recent publications.[118–121] Analysis of the literature on the title subject shows that investigations of large biocomplexes have become one of the most important and efficient applications of pulsed EPR spectroscopy.

3. Spatial distribution of paramagnetic particles. Spin-labelled polymers and peptide–membrane complexes

PELDOR spectroscopy makes it possible not only to obtain data on distances in radical pairs or complexes, but also to study the spatial configuration of spin systems. Unfortunately, these possibilities are still of limited use among researchers abroad.

Information on the geometry of spatial distribution of paramagnetic centres can be extracted from the law that describes the kinetics of exponential PELDOR signal decay. For instance, a simple exponential decay

$$V(T) = V(0)\exp(-\alpha p_b T^q) \qquad (20)$$

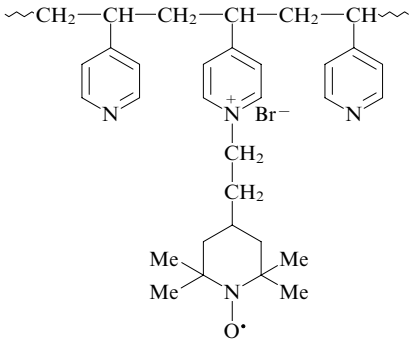
with $q = 1$ is characteristic of the volume averaging of expression (3). Averaging over any specified spatial configuration with randomly distributed particles is possible. For instance, the exponent, q, equals 2/3 for a planar case and 1/3 for linear distribution (see Refs 26 and 122). In contrast to the ESE method in the case of PELDOR the decay $V(T)$ is not masked by other relaxation mechanisms. This allows spatial effects to be studied.

An exponential decay with $q = 1$ is observed for particles uniformly distributed over the volume. Since in this case one has

$$\alpha = \Delta\omega_{1/2} = AC,$$

where C is the spin concentration, the logarithm of the signal decay rate normalised to concentration is linearly related to the change in the interval T, as shown in Fig. 25 for frozen glassy solutions of a stable 2,2,6,6-tetramethyl-4-oxopiperidin-1-yloxyl radical.[31] This situation is typical of homogeneous glassy solutions of paramagnetic centres.

An unexpected result was obtained in the kinetic studies of the decay $V(T)$ in solutions of spin-labelled polymers poly(4-vinylpyridine) (P-4VP) with different extent of labelling ($\beta = 0.06$ and 0.09, β is the ratio of the number of labels in the macromolecule to the degree of polymerisation).[123] The structure of a labelled repeating unit of the polymer is as follows:



It was found that the PELDOR signal decay is described by relation (20) with $q = 1/3$, which corresponds to a linear spatial distribution of spin labels. This was explained in the framework of a model that assumes mutual repulsion between charged groups of the polymer. Here, one can expect a linear configuration of polymer chains in contrast to globular structure of neutral groups. Linear character of the structure in these experiments was also confirmed by analysis of the concentration dependence of the exponent α in expression (20). Unlike the dependence $\alpha \sim C$ (uniform distribution of particles over the volume) the result obtained for the polymer in question was $\alpha \sim C^2$. This law is characteristic of a spatial distribution of particles for which the kinetics of the PELDOR signal decay should be calculated with allowance for the

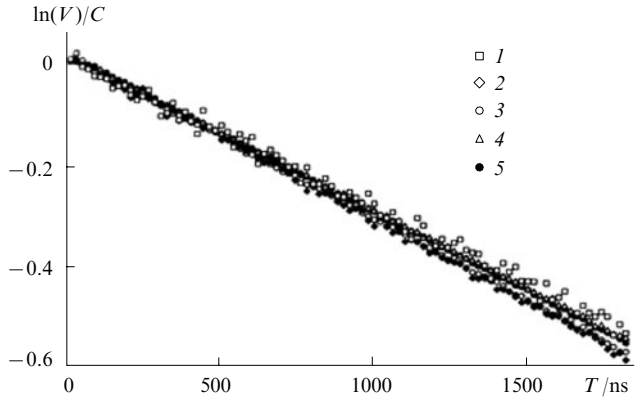


Figure 25. Experimental normalised PELDOR signal decay plotted *vs.* concentration of 2,2,6,6-tetramethyl-4-oxopiperidin-1-yloxyl radicals in frozen water–glycerol solutions (30% H_2O).[31]
Radical concentration /cm^{-1}: 1.7×10^{17} (*1*), 4×10^{17} (*2*), 6×10^{17} (*3*), 9×10^{17} (*4*) and 1.4×10^{18} (*5*).

shortest approach distance r_0 assuming that r_0 exceeds the sum of the van der Waals radii of particles.

Calculations using experimental data for P-4VP gave $r_0 = 13.5$ nm, which substantiated the hypothesis of linear structure of the polymer under the experimental conditions. Note that the laws of the kinetics of PELDOR signal decay for charged radical ions were studied in detail [31] using the classical Debye – Hückel theory and Monte Carlo calculations of the decay $V(T)$.

The spatial distribution of spin labels can even be more complex. An example is provided by the results of calculations of the kinetics of PELDOR signal decay for the spin labels localised on the cell membrane or within the membrane. Dipolar relaxation of spin labels in frozen glassy solutions of spin-labelled trichogin TO-4 in cell membranes of *Micrococcus Luteus* bacteria was studied experimentally at $T = 77$ K.[124] The results obtained were interpreted using a model which assumes localisation of paramagnetic centres either in a layer of thickness d of a sphere with the external radius $R + d$ or on the outer and inner surfaces of the sphere (Fig. 26 *a*). This geometry simulates two types of dipolar interactions between paramagnetic centres localised within membrane or on the surface of cells or vesicles. The results of calculations of the exponent q in relation (20) for $R = 500$ nm (average size of *Micrococcus Luteus* bacteria) are shown in Fig. 26 *b*. Similar calculations for other R values in the range from 250 to 1500 nm and for an ideal planar case ($R = \infty$) gave the curves that almost matched the dependences *1* and *2* in Fig. 26 *b* obtained for R = 500 nm. The horizontal straight line *3* corresponds to the experimental value $q = 0.71 \pm 0.012$ obtained in studies of the system in question. The line crosses both theoretical curves *1* and *2*. The intersection points give the d values for the corresponding model for distribution of spin labels in the membrane.

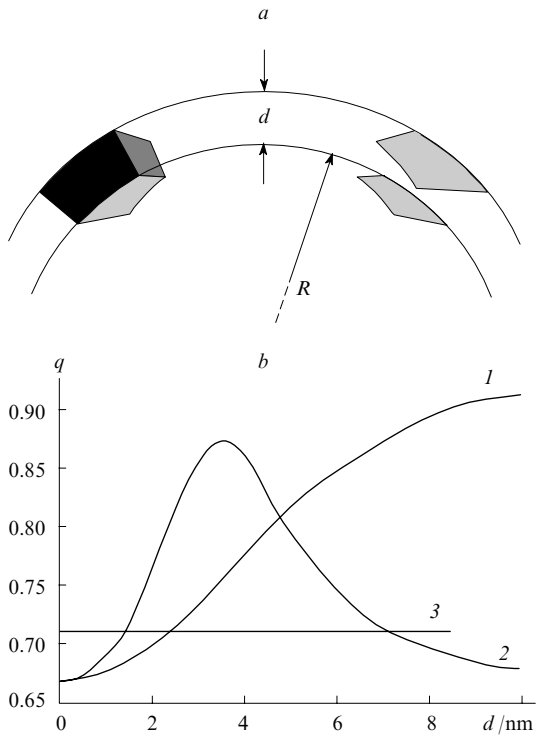


Figure 26. Scheme illustrating the calculations of the parameter q as function of arrangement of paramagnetic centres in a spherical membrane of radius R (d is the thickness of the sphere) (*a*) and calculated $q(d)$ values for paramagnetic centres located within the sphere (*1*) and on the inner and outer surfaces of the sphere (*2*) (*b*). (Line *3* corresponds to the experimental [124] value $q = 0.71$.)

The intersection of line *3* with the theoretical curve *1* at $d \approx 2.4$ nm means that experimental data do not contradict the localisation of spin labels within the layer of the specified thickness. This may indicate that the spin labels are on the outer surface of the membrane (membrane thickness is about 60 nm); here, the surface should have a loose structure such that the spin labels are actually localised within a layer 2.4 ± 0.2 nm thick. Accordig to the model considered, the intersection of the straight line *3* with curve *2* (see Fig. 26 *b*) corresponds to localisation of spin labels on both sides of the membrane. The solution corresponding to the intersection at $d = 1.5$ nm has no physical meaning, because in this case the membrane thickness ($\sim 1.5 \pm 0.2$ nm) is too small. The second intersection corresponds to a distance of 7.0 ± 0.3 nm between the surfaces on which the spin labels are localised. This numerical value is consistent with modern concepts of membrane structure.

Thus, comparison of experimental and theoretical data shows that the spin-labelled peptides studied are mainly localised near the membrane surface. Two types of peptide localisation are possible, within a loose layer about 2.4 nm thick on one surface of the membrane or on both sides of the membrane (here, the layers containing the spin labels are separated by a distance of nearly 7 nm). The average distance between spin labels was estimated at 4.5 – 10 nm depending on the model. Similar results were obtained in studies of spatial distribution of spin-labelled trichogin analogues in artificial membranes.

A PELDOR study of intramolecular and intermolecular dipole – dipole interactions between spin labels in spin-labelled trichogin analogues (TF-4, TF-1, TO-1,8) in dipalmitoylphosphatidylcholine (DPPC) multilamellar membranes frozen to 77 K was reported.[125] For the singly labelled peptides, the experimentally observed $V(T)$ decay kinetics studied at the peptide : lipid (P : L) mole ratios of 1 : 300, 1 : 250 and 1 : 82 correspond to a nonuniform spatial distribution of trichogin molecules and reflect a nearly planar character of their distribution in the multilamellar DPPC layers. For the doubly labelled trichogin analogue, the function of distance distribution between spin labels in the trichogin molecule was obtained. The function has two main maxima at distances of 1.25 and 1.75 nm. The first maximum corresponds to the α-helical structure of the trichogin analogue while the second maximum corresponds to a structure that combines a 3_{10}-helix and a more extended conformation of the trichogin analogue.

Similar results were obtained in studies of trichogins TO-4 and TO-1,8 in egg phosphatidylcholine (ePC) multilamellar membranes.[43] It was found that the addition of cholesterol to ePC causes the local concentrations of trichogin molecules to increase considerably without formation of compact aggregates.

Thus, peptide aggregation was observed neither in natural nor in artificial membranes.[43, 124, 125] Therefore, a problem of aggregation conditions posed. It was solved in a study [126] carried out by the PELDOR and ESEEM methods.[5] First of all, it was established that trichogin aggregates in the DPPC membrane are formed at high relative concentrations of the peptide. Similarly to study,[126] at P : L $< \sim 1 : 100$ the peptide molecules are not aggregated and arranged parallel to the membrane surface. An increase in the peptide mole fraction to P : L = 1 : 20 causes the formation of aggregates with $N = 2$

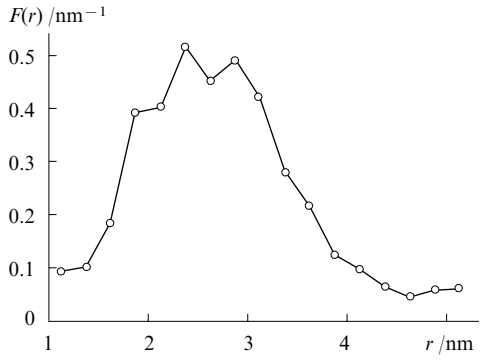


Figure 27. The distance distribution function $F(r)$ of spin-labelled trichogin TF-1 aggregates in DPPC membranes.[126]

and the corresponding distance distribution function has a maximum at 3.5 nm and a width of 1.4 nm (Fig. 27). Here, the peptide molecules are oriented normal to the membrane surface. Aggregation of alamethicin A-16 in ePC vesicles at relatively high P : L ratios was observed in a more recent study.[127]

It should be noted that the ESEEM study [126] seems to be the first one in which the peptide orientation relative to the membrane surface was studied in detail. In these experiments the supramolecular structure of the membrane–peptide system was determined using the ESEEM effect due to the interaction between the peptide spin label and protons (deuterons) of water molecules present in the surface layer of the membrane. Earlier, a test experiment aimed at determining the interaction between water and spin labels of membrane lipids localised at different distances along the lipid chain was reported for this system.[128] Based on the results obtained, the distances to the surface were determined for three spin-labelled peptides in which the spin labels were introduced near the C-terminus (TF-8), N-terminus (TO-1, TF-1) and between them (TO-4, TF-4), which eventually allowed the peptide position in the membrane to be determined.

4. Radical–ion and ion–ion pairs

Until recently only a few PELDOR studies of paramagnetic ions were reported.[129–136] They are of interest not only from the standpoint of the design of artificial supramolecular ensembles with preset properties, but also for the synthesis of metal-containing proteins and membrane complexes with paramagnetic ions. In most cases such systems possess specific paramagnetic properties that are due to the presence of metal ions. Owing to the g-factor anisotropy their EPR spectra are observed in a wider range compared to the EPR spectra of radicals. Therefore, carrying out pulsed experiment requires the allowance for mutual positions of the detection pulse and the pumping pulse in the EPR spectrum (so-called orientation selectivity in PELDOR). Usually, paramagnetic ions cause the phase relaxation time and the spin–lattice relaxation time to shorten; as a consequence, measurements should be performed at as low temperatures as possible. When the PELDOR technique is used to obtain structural information on ionic clusters, the spin states of particular metal ions in the cluster should be taken into account.

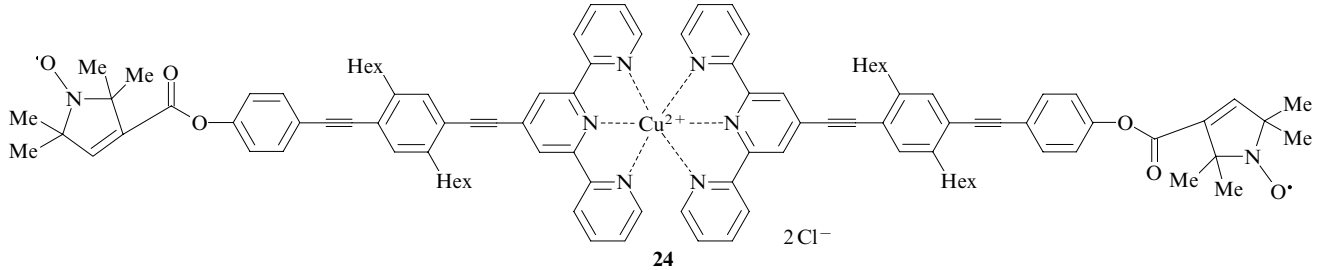
The simplest system comprises a complex of a paramagnetic ion and iminoxyl radical, *e.g.*, complex **24** of hexacoordinate Cu^{2+} ion with ligands containing two iminoxyl radicals.[129]

The X-band EPR spectrum of this complex exhibits a conventional triplet with $g \approx 2.003$ and a broad (width about 55 mT) anisotropic line of Cu^{2+} ion ($S = 1/2$) with $g_z = 2.258$. The system was excited by 32-ns pulses (measurements were carried out at 15 K) according to various modes. If the pumping pulse was centred at the maximum of the spectral line, the detection pulse excited the spins of Cu^{2+} ions at the frequencies shifted by 200 or 1465 MHz relative to the frequency at which the pumping pulse was applied. In this case analysis of the PELDOR signal decay oscillations gave the distances $r(>NO^{\bullet}\cdots Cu^{2+}) = 2.43$ and 2.46 nm, respectively. In conventional experiments involving both excitation and pumping within the contour of the EPR line of iminoxyl radical, analysis of the PELDOR modulation data gave $r(>NO^{\bullet}\cdots>NO^{\bullet}) = 5.2$ nm. The results obtained experimentally were confirmed in quantum chemical calculations.

The distance between a pair of copper ions in azurin dimer formed due to the interaction between cysteine residues on the surface of a protein complex was estimated at 2.6 nm.[130] However, it was concluded that, owing to orientation selectivity, the results obtained depend on the mutual orientation of the g-tensors of Cu^{2+} ions in the dimer and on the conditions of spectrum excitation at the frequencies ν_A and ν_B (*i.e.*, on the $\Delta\nu_{AB}$ value).

An attempt to detect orientation selectivity in a study of polyproline peptide containing (PHGGGW)Cu^{2+} terminal fragments was reported.[131] X-Band measurements carried out at four values of the magnetic field strength revealed no differences in the PELDOR signal decays predicted by theory.[27] The authors of that study believed that either the g-tensor of Cu^{2+} ions is oriented relative to the vector connecting two ions in such a manner that orientation selectivity disappears (this is predicted by theory) [27] or the effect was not detected owing to dynamic flexibility of the peptide molecule. This is still a moot question, which requires further investigations.

The distances between Cu^{2+} ions in transferrin and lactoferrin were estimated (Fe^{3+} ion pairs were replaced by Cu^{2+} ions).[132] These polypeptides bind iron ions and are their carriers. Replacement of iron ions by other ions does not



24

change the structures of the complexes.[133] Owing to the *g*-factor anisotropy and HFC both complexes have broad ($\sim$3 mT) X-band EPR lines in the region $g \approx 2.0$. The distance between Cu^{2+} ions evaluated from the PELDOR signal decay data is 4.16 ± 0.06 nm for transferrin and 4.26 ± 0.06 nm for lactoferrin. These distances are 2%–3% shorter than the corresponding distances in crystals; this can indicate a small difference between the molecular conformations in frozen solutions and crystals.[132]

The distance between $[4Fe-4S]^+$ cluster (ground-state spin $S = 1/2$) and hydroxyethylidene thiamine pyrophosphate radicals (intermediates of the catalytic cycle of oxidation involving pyruvate ferredoxin oxidoreductase) was determined by the PELDOR technique.[134] The result obtained, $r = 3.3$ nm, corresponds to magnetic dipole interaction between the B-cluster and radical (the system contains at least three types of clusters, namely, A, B and C).

The PELDOR technique was used to determine the distance between the centre of the [NiFe] cluster and the $[3Fe-4S]^+$ cluster in the structure of hydrogenase, an enzyme which catalyses heterolytic decomposition of hydrogen ($H_2 \rightleftharpoons H^+ + H^-$).[135] The molecular structure of this enzyme has been studied in detail by X-ray analysis and magnetic-resonance methods and is therefore of interest for PELDOR studies. However, the simplest analysis of the PELDOR data (three- and four-pulse PELDOR experiments at 5 K) based on the approximation of point dipoles localised at the cluster centres gave incorrect results. The authors of study [136] believed that the results obtained should be interpreted with allowance for spin–spin interactions in the cluster $[3Fe-4S]^+$. The PELDOR signal decays in these complex mononuclear systems were calculated with inclusion of the interaction between the spin states in the cluster.[136]

Interpretation of PELDOR data for systems containing paramagnetic ions or ions and ionic clusters with $S > 1/2$ is difficult. An attempt to measure the Mo···Fe distance in a cluster containing Mo^{5+} and Fe^{3+} ions in sulfite oxidase failed.[137] No PELDOR modulation was detected in the system; this was explained by a broad distribution of distances between pairs and by the presence of various conformers in the frozen aqueous buffer.

Dipole–dipole interactions between paramagnetic particles with $S > 1/2$ were analysed theoretically.[138] Analytical relations were derived for the interacting spins $S = 1$ and $S = 1/2$. In this case the effects of zero-field splitting, Zeeman energy and temperature on the lineshape of the Pake dipolar doublet can be calculated. It seems that further analysis will enable calculations of effects in PELDOR experiments for systems with any spin.

Undoubtedly, experimental and theoretical difficulties will not prevent the PELDOR technique from finding increasing application in studies of ion–ion and ion–radical systems that are of particular interest in biochemical physics and biocatalysis.

5. Radical pairs formed in photolysis

In many important physicochemical processes paramagnetic centres form pairs. For instance, solid-phase photolysis causes the formation of an electron that is trapped by an acceptor or medium at some distance from the 'parent' ion. In such systems the distance between paramagnetic centres can be described by the function $F(r)$. If the distribution function $F(r)$ is rather broad, no oscillations of PELDOR signal decay are observed. Nevertheless, information on the distribution of radical pairs can be obtained by analysing the PELDOR signal decay.

The pioneering PELDOR study [6] was devoted to investigations of pairs of hydrogen or deuterium atoms and hydroquinone radicals stabilised in glassy hydroquinone solutions in 8 M aqueous sulfuric acid or D_2SO_4. In this system paramagnetic centres are formed from hydroquinone $Ar(OH)_2$ upon photoionisation

$$Ar(OH)_2 + H_2O(H_3O^+) \longrightarrow Ar(OH)_2^{+\bullet} + H^\bullet + OH^-(H_2O).$$

The observed distance distribution is governed by two factors, (i) the free path length of an electron prior to trapping by H_3O^+ ion and (ii) diffusion path length of hydrogen atoms until trapping in the matrix. Hydrogen atoms were treated as A-spins; the pumping pulses were applied at the frequency equal to the EPR spectrum of hydroquinone radical ions $Ar(OH)_2^+$ treated as B-spins (see inset in Fig. 28). It was established that the signal decay of hydrogen atoms depends on the concentration of hydroquinone radical ions. This points to dipole–dipole interactions between hydrogen atoms and not only the 'parent' hydroquinone radicals, but also radicals that are uniformly distributed over the matrix; in other words, the signal decay can be represented as the product $V(T) = V_{intra}V_{inter}$. The dipole–dipole pair interaction, which is governed by the term V_{intra}, was determined by analysing the dependence of the $V(T)$ signal amplitude on the concentration of hydroquinone radicals. The function $F(r)$ was calculated from Eqns (11) and (12) using an approximate representation of the function $F(r)$ as a step function. The distribution function thus obtained has a maximum at 4.5 nm (see Fig. 28). Integration of the function $F(r)$ gives that for 63% of radical pairs the distances are shorter than 8.5 nm while for the remaining pairs the distances are in the range from 8.5 to 10 nm. In the latter case establishment of the actual shape of the distribution function is difficult because these radical pairs make a negligible contribution to the PELDOR signal decay.

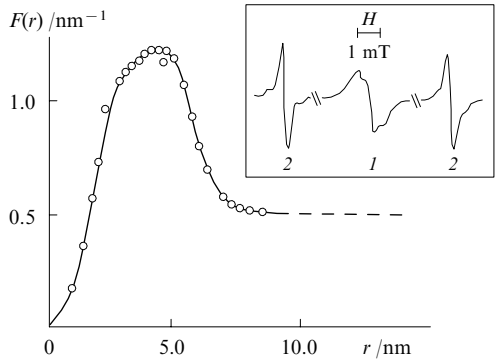


Figure 28. Pair distribution function calculated from PELDOR data for UV-irradiated frozen hydroquinone solutions.[6]
Inset: EPR spectrum of paramagnetic centres formed in this system: hydroquinone radicals, B-spins (*1*) and hydrogen atoms, A-spins (*2*).

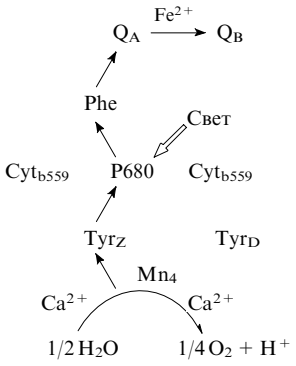
Exposure of hydrocarbon solutions of aromatic compounds to UV light at 77 K causes the formation of trapped solvent radicals. The corresponding mechanism of formation involves absorption of two photons by the aromatic molecules and energy (or charge) transfer from the aromatic molecule to the surrounding hydrocarbon molecules followed by radical decomposition.[139] A study [32] of the spatial distribution of hydrocarbon radicals trapped in these systems showed that photolysis ($\lambda > 290$ nm) of glassy naphthalene solutions in decalin at 77 K produces radicals whose EPR spectrum

exhibits six nonequidistant lines. This spectrum appears from radicals that are formed upon abstraction of a hydrogen atom from decalin molecule. Fast PELDOR signal decay at low concentrations of decalinyl radicals is followed by attainment of the limiting value V_p characteristic of the cluster distribution of radicals. The dependence of V_p on the parameter p_b determining the extent of excitation of the EPR spectrum of decalinyl radical was studied.[32] The position of the pumping pulses in the EPR spectrum was varied, but their amplitudes and durations remained constant. It was found that V_p is a linear function of p_b and the slope of the straight line remains constant in the course of photolysis, being independent of the concentration of radicals. Calculations of the parameter N from the slope of the straight line using expression (12) gave $N = 1.85 \pm 0.2$. Thus, it was established that low-temperature sensitised photolysis of decalin produces decalin radicals that are stabilised in the form of pairs. The boundary value of the distance between radicals in pairs estimated from the time $T^* = 40$ ns using expression (11) is $r = 2.5$ nm.

6. Radical pairs in photosynthetic systems

Photosynthesis is one of the most important physicochemical processes of solar energy conversion into electrochemical energy, which is necessary for functioning of living organisms. In most cases photochemical processes (energy, electron or proton transfer) involve radical ions and radicals. Information on distances between these paramagnetic centres is of considerable interest for photosynthesis research. The vast majority of studies on PELDOR applications were carried out using the photosystem II (PSII) shown in Scheme 1.

Scheme 1



A component of PSII is a primary electron donor P680, a chlorophyll *a* dimer characterised by absorption maximum at 680 nm. Light-induced excitation of P680 initiates a series of electron transfer processes in PSII. The primary acceptor in electron transfer from P680 *via* an intermediate acceptor pheophytin (Phe) is quinone Q_A and the secondary acceptor is quinone Q_B. The sequence of light-induced redox reactions in PSII is completed by water splitting and formation of oxygen. It should be noted that transfer of an electron is followed by the formation of a number of paramagnetic centres detected by EPR spectroscopy. These centres, along with the systems that simulate the structure and particular properties of the reaction centre of PSII, have been studied by various methods of chemical radiospectroscopy.[140, 141] In the case where it is possible to detect radical pairs, the PELDOR or single-frequency pulsed methods are used.

The PSII system has two redox centres based on tyrosine residues (Tyr), which act as secondary electron donors. One of them is tyrosine Z (denoted as Y_Z); at room temperature the oxidised Y_Z^+ has a short lifetime and can hardly be detected by EPR spectroscopy. The other is tyrosine D (denoted as Y_D); the oxidised Y_D^+ is stable in the dark and can be detected by EPR spectroscopy. The EPR spectrum of Y_D^+ is a narrow single line with $g \approx 2$. In addition, PSII contains a number of redox-active complexes, namely, cytochrome b559, chlorophyll Z (Chl_Z), and the manganese cluster Mn_4 with Ca^{2+} ions. This cluster is the key component in the complex of the reaction centre, which oxidises water to oxygen.

The oxygen-evolving and the Ca-depleted PSII systems were studded.[142] Depending on the oxidation state of the manganese cluster in PSII, five states ($S_0 - S_4$) of this species are distinguished. At low temperatures, the S_2 state of PSII exhibits the EPR spectrum of Y_D^+ and a well-known multiplet spectrum of the manganese cluster with a *g*-factor of 1.96 and full spectral width of about 20 mT. The S_2 state of the Ca-depleted PSII exhibits the so-called modified EPR spectrum of the manganese cluster with a larger width, larger number of lines and smaller hyperfine splitting compared to the spectrum of the oxygen-evolving PSII. In addition to the EPR spectrum of Y_D^+, Ca-depleted PSII also exhibits an EPR spectrum of unknown nature. The EPR spectrum of the S_3 state spans a much wider range compared to the spectrum of Y_D^+.

The fact that the EPR spectra of the S_3 state of the tetraatomic manganese cluster and Y_D^+ cation are different made it possible to use the PELDOR technique for measuring the dipolar coupling between these species.[142] The pumping pulse was applied to the Y_D^+ spins and the spin echo signal was formed from the S_3 state of the Mn_4 cluster. Figure 29 presents the modulated PELDOR signal decays obtained[142] for the systems mentioned above. Points denote experimental data and solid lines denote the results of calculations using the fitted parameters of dipolar coupling. The distance between the

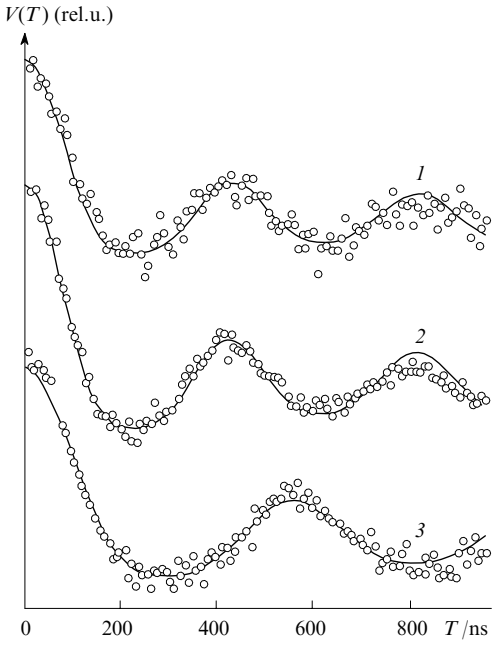


Figure 29. Modulated PELDOR signal decays of pairs of paramagnetic centres in the PSII photosystem.[142]
Oxygen-releasing system PSII containing the Mn_4 cluster in the S_2 state (*1*), Ca-depteled system PSII containing the Mn_4 cluster in the S_2 state (*2*) and Ca-depteled system PSII containing the Mn_4 cluster in the S_3 state (*3*). Points denote experimental data and solid lines denote the results of calculations.

manganese cluster (S_2 state) and Y_D^+ determined from these data is 2.7 nm (Table 2) in both systems, the oxygen-evolving PSII and the Ca-depleted PSII. The distance between the spins responsible for the EPR spectrum of the S_3 state of the Ca-depleted PSII and the tyrosine radicals Y_D^+ is 3.0 nm. Comparison of the results obtained (3.0 nm) with other data made it possible to suggest [142] the nature of the EPR spectrum of the S_3 state of PSII.

Table 2. Distances between paramagnetic centres in PSII determined by the PELDOR method.

Pair of centres	Distance /nm	Ref.
$Y_D - Mn_4(S_2)$	2.71 ± 0.02	142
$Y_D - Mn_4(S_0)$	3.4	143
$Q_A - Chl_Z$	3.40 ± 0.10	144
$Y_D - Chl_Z$	2.95 ± 0.05	145
$Q_A - Y_Z$	3.40 ± 0.10	146
$Q_A - Cyt_{b559}$	4.00 ± 0.30	147

PELDOR data for the S_0 state of the manganese cluster are available.[143] It is believed that different values of distances between the Y_D^+ cation and the Mn_4 cluster are due to different oxidation and spin states of the cluster. Structural information on paramagnetic centres in PSII obtained recently by other pulsed EPR spectroscopy techniques was also reviewed.[143]

Difficulties in the experiments with radical pairs in photosystems consist in that the EPR spectra of different centres overlap and the frequencies ν_A and ν_B should be chosen as to ensure selective pulsed microwave excitation of particular centres. This was done for the X-band EPR experiments with Y_D, Chl_Z and Q_A centres.[144, 145] The results of measurements are shown in Table 2 which also lists the results of other PELDOR distance measurements [146, 147] for PSII.

The reaction centres of photosystems are localised within specific chloroplast membrane structures called thylakoids. It is assumed that the donor fragment of PSII is localised on the opposite sides of thylakoid membrane. The orientation of the reaction centre relative to the membrane surface was studied by pulsed EPR methods (in particular, the PELDOR technique).[148] To this end, a synthetic Mylar sheet was coated with PSII and a sample oriented relative to the external magnetic field H_0 was studied. Namely, the orientation dependence of the PELDOR spectra of a radical pair comprised of tyrosine centre Y_D^+ and the manganese cluster Mn (S_2 state) was studied. It was found that the angle between the vector connecting the two centres and the normal to the surface of the thylakoid membrane is $110 \pm 2^\circ$; these are the first PELDOR orientation measurements for PSII.

Radical pairs can also artificially be produced by introducing, *e.g.*, spin labelling of the peptide chain of a protein in the reaction centre containing a stabilised radical or radical ion of the photosystem. This approach was used in the PELDOR studies [149] of the structure of the protein component of the light-harvesting complex LHCIIb, which contains chlorophyll *a*/*b* and is present in both photosystems. Spin labels were introduced pairwise into various positions in the protein structure. The distances between these positions (Fig. 30) and the distribution functions for all distances between pairs were determined. All the functions $F(r)$ related to position 3 near the N-terminus of the polypeptide (3 – 160, 3 – 52, 3 – 106) appeared to be bimodal. This indicates that the domain near

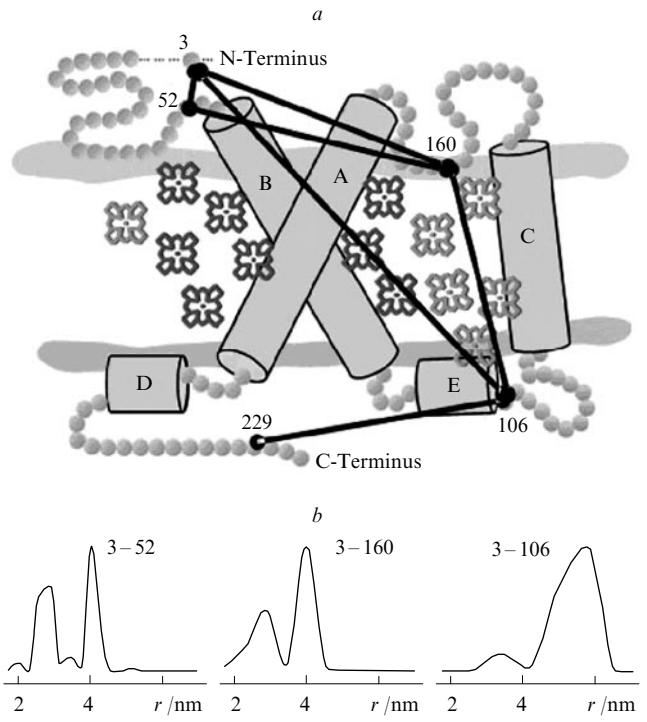


Figure 30. Distances between five spin labels in positions 3, 52, 106, 160 and 229 in the protein light-harvesting complex LHCIIb (A – E are helical domains) measured by the PELDOR method (*a*), and three out of six pair distance distribution functions between the positions 3 – 52, 3 – 160 and 3 – 106 calculated from the PELDOR data (*b*).[149]

the N-terminus, involved in light flux regulation in the photosystem, has two conformation distances. It is assumed that these two conformers correspond to two different photosystems, namely, PSI and PSII.[149]

A spin label was introduced into cysteine residue in position 156 of the subunit of a protein complex in the photosynthetic reaction centre isolated from *Rhodobacter sphaeroides R*26 bacteria.[150] The distance between the spin label and the primary acceptor $Q_A^{-\bullet}$ (semiquinone radical ion) determined by the four-pulse PELDOR technique is 3.05 ± 0.05 nm. This distance is shortened by 0.2 nm upon phototransfer of an electron and stabilisation of $Q_B^{-\bullet}$. The effect is not related to possible orientation selectivity in this system.[147] It is believed [150, 151] that the approach can be used to detect conformational changes occurring in the course of phototransfer reactions in photosystems.

Short-lived radical pairs $P_{865}^+Q_A^-$ (P_{865} is bacteriochlorophyll *a*) produced by a laser pulse in frozen solutions of reaction centres in photosynthetic bacteria *Rb. sphaeroides* [49, 51] were studied by W-band EPR spectroscopy at 95 GHz. In this spectral region the EPR spectra of the radical ions are only partially overlapped, which enables measurements with detection at the frequency ν_A and pumping at the frequency ν_B in different regions of both EPR spectra corresponding to g_{xx}, g_{yy}, g_{zz} for Q_A^- and P_{865}^+. This allows selective experiments to be carried out and not only the distance in the pair but also the orientation of the pair to be determined. One of the key questions answered by the authors of the studies cited is how does the orientation of the vector R connecting the pair $P_{865} - Q_A$ change after transfer of an electron and formation of $P_{865}^+Q_A^-$. The orientation and modulus of this vector prior to reaction is known from X-ray structural data. Based

on the results of PELDOR measurements, the modulus of the vector $\boldsymbol{R}$ is 2.84 nm and its orientation changes by 12.5°. It is important that the experimental design and procedure for calculations of structural parameters in the orientation-selective PELDOR experiments were reported in detail.[49, 51]

7. Spatial distribution of radicals upon radiolysis; radical clusters

Owing to spatial localisation of the absorption and transfer of the energy of hard radiation (α-, β- and γ-rays, nuclear fission products) the intermediate reaction products (ions, electrons, atoms, radicals) are also spatially localised within tracks and spurs. Such radical tracks were studied in detail by the ESE method (see, *e.g.*, reviews [3, 4]).

As mentioned above, analysis of the PELDOR signal decay allows a fixed number of spins in a group of paramagnetic particles to be determined as in the case of, *e.g.*, formation of aggregates having a particular structure. Of course, if a distribution over the number of spins in a group exists, the method described above gives only the effective number of spins in the group.[14, 15] The PELDOR technique was used [33, 34] to obtain information on the statistics of the number of spins in groups for γ-irradiated cyclohexane, polyethylene and a number of organic acids.

Cyclohexyl radicals in crystalline cyclohexane γ-irradiated at 77 K were studied.[33] The pattern of the PELDOR signal decay in this system is similar to that of biradicals with a broad distance distribution. A fast decay in the initial portion is followed by attainment of the limiting value V_p at times of the order of 0.5 μs. The dependence of the limiting decay V_p on the parameters p_a and p_b was studied. Unlike the available pair distribution data obtained for biradicals and radicals that appear during sensitised photolysis it was found that the average value of the parameter N depends on the probability (extent), p_a, of excitation of the spectrum by the pulses applied at the detection frequency. Figure 31 presents this dependence for cyclohexyl radicals (curve *1*) and, as a test, the results obtained for iminoxyl biradicals **12** (see Table 1). In the latter case it was found that within the limits of experimental error the parameter N_{eff} is independent of the parameter p_a and equal to 2.2 (see Fig. 31, curve *2*).

It was assumed that the dependence of N_{eff} on p_a for cyclohexyl radicals in γ-irradiated cyclohexane is due to the presence of groups containing different number of radicals. Analysis of the dependence of V_p on p_a using methods developed in Ref. 33 permitted the following conclusions about the distribution function over the number of radicals in the group. Most radicals (75% – 90%) are distributed uniformly or form pairs, while the remaining 10% – 25% of radicals form groups containing from three to several tens of radicals. The characteristic group size determined from the initial PELDOR signal decay is ~2.5 nm, which corresponds to a local concentration of about 10^{20} cm^{-3}. So high local concentrations of groups cannot be detected by the two-pulse ESE technique owing to the dead time of the ESE spectrometer. Thus, the PELDOR method makes it possible to obtain much more detailed information on spatial distribution of radicals in γ-irradiated systems compared to the ESE approach.

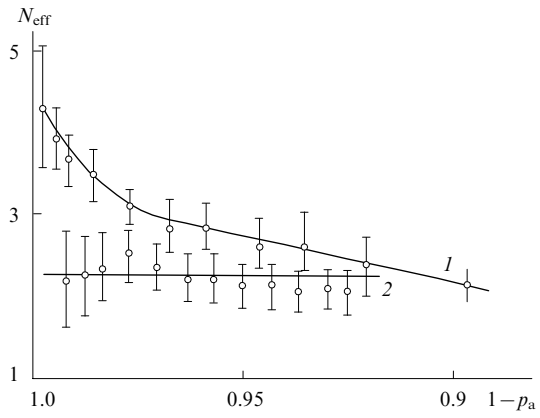


Figure 31. Effective number of particles (N_{eff}) plotted *vs.* excitation probability (p_a) of the spectrum by the pulses applied at the frequency ν_A for cyclohexyl radicals (*1*) and iminoxyl biradicals **12** (*2*).[33]

Similar results were obtained in a study [34] of alkyl radicals appeared during γ-radiolysis of polyethylene and some organic acids. As in the case of irradiated cyclohexane, the PELDOR signal decay in polyethylene is fast at short times and then reaches the limiting value V_p, which depends on p_a and p_b. By analysing these dependences one can determine N_{eff} and the first and second moments of the distribution function over the number of radicals in the group (data for polyethylene are as follows: $K_1 = 2.4$ and $K_2 \leqslant 6$). Analysis [34] showed that alkyl radicals formed in low-temperature radiolysis of polyethylene are distributed in groups with an average number of radicals of 2.4 and a characteristic group size, r, of $\leqslant 2.5$ nm.

A PELDOR study of the spatial distribution of radicals in hydrated DNA irradiated with heavy (100-MeV ^{40}Ar) ions was reported.[152] Under these conditions, two types of radicals, that is, the charged radical anions and radical cations localised on DNA bases and neutral radicals localised on carbon atoms are mainly stabilised in DNA at 77 K. The total width of the EPR spectrum was ~4 mT. The four-pulse PELDOR technique was used to study three types of samples irradiated with doses of 1.7, 15 and 50 kGy. The dependence of the PELDOR signal decay on the spectrum excitation probability p_b was measured. The p_b values were determined from relation (17) using the experimental EPR spectrum and the parameters of the microwave pulse. Experimentally, different p_b values in the range 0.179 – 0.015 were obtained by varying the amplitudes of the pumping pulses. It was found that the decay kinetics in the whole initial portion of times to 1.6 μs can be represented by the exponential function

$$V(T) \sim \exp(-kp_bCT),$$

where C is the concentration of radicals in the cluster. The kinetics of the PELDOR signal decay in the irradiated samples are plotted *vs.* p_b in Fig. 32.

Experimental results were analysed [152] using a simplest model, which assumes that DNA radicals are distributed over clusters of the same volume but the number of radicals differs from one cluster to another. In this case, irrespective of the irradiation dose, the average cluster radius is 6.8 nm and the number of radicals in it is $N = 17.7 \pm 0.7$; in turn, this means that clusters do not overlap at such doses. The results obtained also make it possible to estimate an important physical parameter of this kind of radiation, namely, the linear energy transfer (LET). The estimates appeared to be similar to the LET value measured by other physical methods. Unfortunately, the effect of the parameter p_a on the kinetics of PELDOR signal decay was not analysed;[152] this precludes evaluation of possible statistics of the distribution over the number of radicals in the cluster.

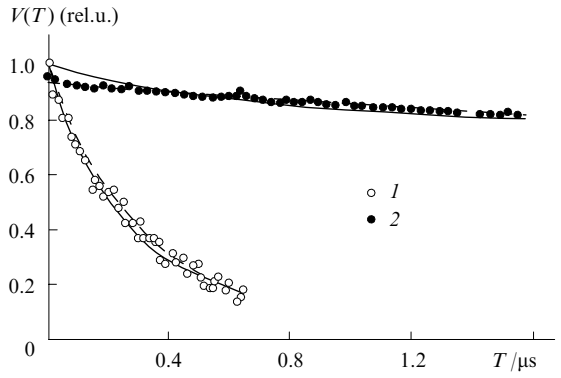


Figure 32. PELDOR signal decays at different p_b values for DNA irradiated with 100-MeV ^{40}Ar ions to a dose of 15 kGy.[152]
$p_b = 0.179$ (*1*), 0.015 (*2*).

Radical clusters were also found in polymeric systems. The cluster distribution of radicals in ionically capped poly(styrene)-poly(isoprene) diblock copolymers was studied.[19, 153, 154] Polymers (ionomers) form clusters with surface charged groups. An ionic compound, namely, a potassium salt of 4-carboxy-substituted compound TEMPO was used as a spin label. The distances between labels (label concentration was equal to two labels per cluster) on the cluster surface (2.2 nm) and the inter-cluster distance (6.6 nm) were determined from the decay kinetics of the four-pulse PELDOR signal. The former distance is independent of the polymer chain length (molecular mass) and the latter distance varies in the range 4.5 – 8.0 nm depending on the topology of the copolymer. The results obtained were explained using the data obtained by other methods and a model that describes electrostatic cluster – cluster interactions and interactions between clusters and the poly(styrene)-poly(isoprene) diblock copolymer interface.

V. Conclusion

The material presented in this review clearly demonstrates that at present pulsed EPR spectroscopy finds new fields of application for measuring distances between paramagnetic centres, determining spatial orientation of radical pairs and studying the effects of spatial distribution. These data are complementary to traditional structural parameters, such as the hyperfine coupling constants and *g*-tensor. Among pulsed methods of EPR spectroscopy, the two-frequency PELDOR technique is the most efficient. Single-frequency pulsed methods, such as the '2 + 1' (Ref. 6) or SIFTER (Ref. 13) techniques are of much more limited use. The development of single-frequency DQC technique[12] at the Advanced Centre for ESR Technology (ACERT), Cornell University, and a broad spectrum of applications of this method should also be pointed out. Recently, investigations on the structure and properties of various biomolecular structures carried out at this research centre have been a subject of a detailed review.[155] As mentioned above, the DQC technique is efficient in measuring long distances (to $r \approx 7.0 - 8.0$ nm) and shows a higher sensitivity owing to better excitation of the spectrum compared to the PELDOR technique. Unfortunately, at present the DQC and other pulsed methods are of limited use due to technical difficulties and only available in a few research laboratories.

Distances are also successfully determined (especially, for spin labels) by the most widely used methods of continuous wave EPR spectroscopy, which are based on analysis of the lineshape in the EPR spectra or on measurements of EPR signal saturation. A drawback of these etechniques is a narrow range of the available distances ($r < 2$ nm). Note also the so-called half-field technique, which is convenient for measuring short distances. Usually, the forbidden transitions between the levels $m_s = -1$ and $m_s = +1$ of a triplet spin pair are allowed for proximate spins ($r \approx 4 - 5$ Å) and lie in the magnetic fields $1/2\, H_0$ ($g \approx 4$), where H_0 is the magnetic field for the main EPR transition. The intensities of the lines due to these transitions $I_{\pm 1}$ are low compared to the intensities of the lines with $g \approx 2$; however, from a theoretical relation[156]

$$\frac{I_{\pm 1}}{I_0} \sim \frac{1}{r^6},$$

one can estimate the *r* value.

Various methods of continuous wave EPR spectroscopy and a number of pulsed EPR techniques were reviewed.[157] In Fig. 33 we summarise the potential of EPR spectroscopy in measuring distances between randomly oriented paramagnetic particles in solid samples. As can be seen, a broad range of nanometre distances can now be studied.

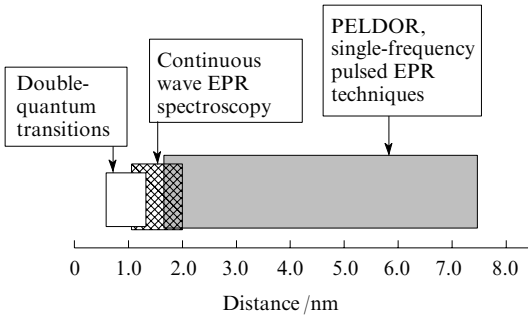


Figure 33. The scale of distances that can be determined by different EPR methods in polyoriented systems.

It should be emphasised again that at present EPR spectroscopy and especially pulsed EPR spectroscopy techniques allows not only the distances in randomly oriented systems to be measured to a good accuracy, but also self-organisation, formation of supramolecular complexes and interaction of various biologically valuable structures with membranes to be studied. Undoubtedly, high-resolution chemical EPR spectroscopy will find increasing application in chemistry and biology.

The authors of this review express their gratitude to G Jeschke, W Lubitz, O Schiemann and H Hara and to the corresponding publishing houses for kind permission to use illustrations from the published sources.

The review has been written with partial financial support from the Programme 'Leading Scientific Schools' (Project NSh-551.2008.3), the Russian Foundation for Basic Research (Project No. 06-04-48 021-a), RFBR-NWO Grant (Project Nos 06-03-91362, 0.47.017.034), the Chemistry and Materials Science Division of the Russian Academy of Sciences (in the framework of Programme 7) and the Siberian Branch of the Russian Academy of Sciences (Integratio Project No. 51).

References

1. K M Salikhov, A G Semenov, Yu D Tsvetkov *Elektronnoe Spinovoe Ekho i Ego Primenenie* (Electron Spin Echo and Its Application) (Novosibirsk: Nauka, 1976)
2. Yu D Tsvetkov *Izv. Akad. Nauk SSSR, Ser. Khim.* 90 (1976) [a]
3. K M Salikhov, Yu D Tsvetkov, in *Time Domain Electron Spin Resonance* (Eds L Kevan, R Schwartz) (New York: Wiley, 1979) p. 231
4. Yu D Tsvetkov *Usp. Khim.* **52** 1514 (1983) [*Russ. Chem. Rev.* **52** 866 (1983)]
5. S A Dikanov, Yu D Tsvetkov *Electron Spin Echo Envelope Modulation (ESEEM) Spectroscopy* (Boca Raton, FL: CRC Press, 1992)
6. A D Milov, K M Salikhov, M D Shchirov *Fiz. Tv. Tela* **23** 975 (1981) [b]
7. A B Ponomarev, A D Milov, Yu D Tsvetkov *Zh. Strukt. Khim.* **25** 51 (1984) [c]
8. D E Kaplan, E L Hahn *J. Phys. Radium* **19** 821 (1958)
9. R Graf, D E Demco, J Gottwald, S Hafner, H W Spiess *J. Chem. Phys.* **106** 885 (1997)
10. M Pannier, S Veit, A Godt, G Jeschke, H W Spiess *J. Magn. Reson.* **142** 331 (2000)
11. P P Borbat, J H Freed *Chem. Phys. Lett.* **313** 145 (1999)
12. G Jeschke, M Pannier, A Godt, H W Spiess *Chem. Phys. Lett.* **331** 243 (2000)
13. V V Kurshev, A M Raitsimring, Yu D Tsvetkov *J. Magn. Reson.* **81** 441 (1989)
14. A D Milov, A G Maryasov, Yu D Tsvetkov *Appl. Magn. Reson.* **15** 107 (1998)
15. Yu D Tsvetkov, in *Pulsed EPR: a New Field of Applications* (Eds C P Keijzers, E J Reijerse, J Schmidt) (Amsterdam: North Holland, 1989) p. 206
16. G Jeschke, M Pannier, H W Spiess, in *Biological Magnetic Resonance (Distance Measurements in Biological Systems by EPR)* (Eds G R Eaton, S S Eaton, L J Berliner) (New York: Kluwer, Plenum, 2000) Vol. 19, p. 493
17. T Prisner, M Rohrer, F MacMillan *Annu. Rev. Phys. Chem.* **52** 279 (2001)
18. Yu D Tsvetkov, in *Biological Magnetic Resonance (EPR: Instrumental Methods)* (Eds C J Bender, L J Berliner) (New York: Springer, 2004) Vol. 21, p. 385
19. G Jeschke *Macromol. Rapid Commun.* **23** 227 (2002)
20. G Jeschke *ChemPhysChem* **3** 927 (2002)
21. S A Dzuba *Usp. Khim.* **76** 752 (2007) [*Russ. Chem. Rev.* **76** 699 (2007)]
22. O Schiemann, T F Prisner *Q. Rev. Biophys.* **40** 1 (2007)
23. G Jeschke, Y Polyhach *Phys. Chem. Chem. Phys.* **9** 1895 (2007)
24. P G Fajer, L Brown, L Song, in *Biological Magnetic Resonance (ESR Spectroscopy in Membrane Biophysics)* (Eds M Hemminga, L J Berliner) (Berlin: Springer, 2006) Vol. 27, p. 95
25. A Abragam *Principles of Nuclear Magnetism* Ch. 4 (Oxford: Clarendon Press, 1961)
26. A M Raitsimring, K M Salikhov *Bull. Magn. Reson.* **7** 184 (1985)
27. A G Maryasov, Yu D Tsvetkov, J Raap *Appl. Magn. Reson.* **14** 101 (1998)
28. V N Parmon, A I Kokorin, G M Zhidomirov *Stabil'nye Biradikaly* (Stable Biradicals) (Moscow: Nauka, 1980)
29. M K Bowman, A G Maryasov, N Kim, V J DeRose *Appl. Magn. Reson.* **26** 23 (2004)
30. A D Milov, A G Maryasov, Yu D Tsvetkov, J Raap *Chem. Phys. Lett.* **303** 135 (1999)
31. A D Milov, Yu D Tsvetkov *Appl. Magn. Reson.* **18** 217 (2000)
32. A D Milov, A B Ponomarev, Yu D Tsvetkov *Chem. Phys. Lett.* **110** 67 (1984)
33. A B Ponomarev, A D Milov, Yu D Tsvetkov *Khim. Fiz.* **8** 1673 (1988) [d]
34. A B Ponomarev, A D Milov, Yu D Tsvetkov *Khim. Fiz.* **9** 498 (1990) [d]
35. G Jeschke, A Koch, U Jonas, A Godt *J. Magn. Reson.* **155** 72 (2002)
36. A D Milov, Yu D Tsvetkov, F Formaggio, S Oancea, C Toniolo, J Raap *J. Phys. Chem. B* **107** 13719 (2003)
37. G Jeschke, G Panek, A Godt, A Bender, H Paulsen *Appl. Magn. Reson.* **26** 223 (2004)
38. Y-W Chiang, P P Borbat, J H Freed *J. Magn. Reson.* **172** 279 (2005)
39. A N Tikhonov, V Y Arsenin *Solutions of Ill-Posed Problems* (New York: Wiley, 1977)
40. A D Milov, B D Naumov, Yu D Tsvetkov *Appl. Magn. Reson.* **26** 587 (2004)
41. A D Milov, D A Erilov, E S Salnikov, Yu D Tsvetkov, F Formaggio, C Toniolo, J Raap *Phys. Chem. Chem. Phys.* **7** 1794 (2005)
42. A D Milov, R I Samoilova, Yu D Tsvetkov, K Pegion, F Formadzhio, K Toniolo, Ya Raap *Dokl. Akad. Nauk* **406** 341 (2006) [e]
43. A D Milov, M I Samoilova, Yu D Tsvetkov, F Formaggio, C Toniolo, J Raap *Appl. Magn. Reson.* **29** 703 (2005)
44. A D Milov, M I Samoilova, Yu D Tsvetkov, M Jost, C Peggion, F Formaggio, M Crisma, C Toniolo, J-W Handgraaf, J Raap *Chem. Biodiversity* **4** 1275 (2007)
45. A D Milov, Yu D Tsvetkov, E Yu Gorbunova, L G Mustaeva, T V Ovchinnikova, J-W Handgraaf, J Raap *Chem. Biodiversity* **4** 1243 (2007)
46. G Jeschke, V Chechik, P Ionita, A Godt, H Zimmermann, J Bbanham, C R Timmel, D Hilger, H Jung *Appl. Magn. Reson.* **30** 473 (2006)
47. R G Larsen, D J Singel *J. Chem. Phys.* **98** 5134 (1993)
48. A G Maryasov, Yu D Tsvetkov *Appl. Magn. Reson.* **18** 583 (2000)
49. A Schnegg, A A Dubinskii, M R Fuchs, Yu A Grishin, E P Kirilina, W Lubitz, M Plato, A Savitsky, K Möbius *Appl. Magn. Reson.* **31** 59 (2007)
50. Ye Polyhach, A Godt, C Bauer, G Jeschke *J. Magn. Reson.* **185** 118 (2007)
51. A Savitsky, A A Dubinskii, M Flores, W Lubitz, K Möbius *J. Phys. Chem. B* **111** 6245 (2007)
52. V P Denysenkov, T F Prisner, J Stubbe, M Bennati *Appl. Magn. Reson.* **29** 375 (2005)
53. M M Hertel, V P Denysenkov, M Bennati, T F Prisner *Magn. Reson. Chem.* **43** S248 (2005)
54. V P Denysenkov, T F Prisner, J Stubbe, M Bennati *Proc. Natl. Acad. Sci. USA* **103** 13386 (2006)
55. A G Semenov, M D Shchirov, V L Zhidkov, V E Khmel'nitskii, E V Dvornikov *Kogerentnyi Spektrometr Elektronnogo Spinovogo Ekha. Preprint 3* (Coherent Spectrometer of Electron Spin Echo. Preprint 3) (Novosibirsk: Institute of Chemical Kinetics and Combustion, Siberian Branch of the Russian Academy of Sciences, 1980)
56. P Höfer, A Kamlowski *Bruker Spin Report* **149** 16 (2001)
57. P Höfer, R Heilig, D C Maier, I Prisecaru, D Schmalbein *Bruker Spin Report* **152** 37 (2003)
58. P Carl, R Heilig, D C Maier, P Höfer, D Schmalbein *Bruker Spin Report* **154**–**155** 35 (2004)
59. K Holczer, in *Pulsed EPR: a New Field of Application* (Eds C P Keijzers, E J Reijerse, J Schmidt) (Amsterdam: North Holland, 1989) p. 43
60. J Hyde, J C W Chien, J H Freed *J. Chem. Phys.* **48** 4211 (1968)
61. G Jeschke, H Zimmermann, A Godt *J. Magn. Reson.* **180** 137 (2006)
62. G Jeschke, A Bender, H Paulsen, H Zimmermann, A Godt *J. Magn. Reson.* **169** 1 (2004)
63. W B Mims *Rev. Sci. Instrum.* **36** 1472 (1965)
64. V A Rodionov, E G Rozantsev *Dolgozhivushchie Radikaly* (Long-Lived Radicals) (Moscow: Nauka, 1972)
65. A L Buchachenko, A M Vasserman *Stabil'nye Radikaly* (Stable Radicals) (Moscow: Khimiya, 1973)
66. L V Kulik, Yu A Grishin, S A Dzuba, I A Grigoryev, S V Klyatskaya, S F Vasilevsky, Yu D Tsvetkov *J. Magn. Reson.* **157** 61 (2002)
67. A Weber, O Schiemann, B Bode, T F Prisner *J. Magn. Reson.* **157** 277 (2002)

68. V Pfannebecker, H Klos, M Hubrich, T Volkmer, A Heuer, U Wiesner, H W Spiess *J. Phys. Chem.* **100** 13428 (1996)
69. R E Martin, M Pannier, F Diederich, V Gramlich, M Hubrich, H W Spiess *Angew. Chem., Int. Ed.* **37** 2834 (1998)
70. S Pornsuwan, G Bird, C E Schafmeister, S Saxena *J. Am. Chem. Soc.* **128** 3876 (2006)
71. B D Bode, D Margraf, J Plackmeyer, G Dürner, T F Prisner, O Schiemann *J. Am. Chem. Soc.* **129** 6736 (2007)
72. A Godt, M Schulte, H Zimmermann, G Jeschke *Angew. Chem., Int. Ed.* **45** 7560 (2006)
73. G Jeschke, A Godt *ChemPhysChem* **4** 1328 (2003)
74. *Biological Magnetic Resonance (Spin Labeling: The Next Millenim)* Vol. 14 (Ed. L J Berliner) (New York: Plenum, 1998)
75. *Biological Magnetic Resonance (EPR: Instrumental Methods)* Vol. 21 (Eds C Benderá L J Berlinger) (New York: Springer, Plenum, 2004)
76. W L Hubbell, C Altenbach, in *Membrane Protein Structure. Experimental Approaches* (Ed. S H White) (New York: Oxford University Press, 1994)
77. W L Hubbell, A Gross, R Langen, M A Lietzow *Curr. Opin. Struct. Biol.* **8** 649 (1998)
78. L J Berliner, J Grunwald, H O Hankovszky, K Hideg *Anal. Biochem.* **119** 450 (1982)
79. A Spaltenstein, B Robinson, P B Hopkins *J. Am. Chem. Soc.* **110** 1299 (1988)
80. R Rossi, A Carpita, F Bellina *Org. Prep. Proced. Int.* **27** 127 (1995)
81. K Sale, L Song, Y-S Liu, E Perozo, P Fajer *J. Am. Chem. Soc.* **127** 9334 (2005)
82. O Schiemann, N Piton, J Plackmeyer, B E Bode, T F Prisner, J W Engels *Nature Protocols* **2** 904 (2007)
83. O Schiemann, A Weber, T E Edwards, T F Prisner, S T Sigurdsson *J. Am. Chem. Soc.* **125** 3434 (2003)
84. O Schiemann, N Piton, Y Mu, G Stock, J W Engels, T F Prisner *J. Am. Chem. Soc.* **126** 5722 (2004)
85. N Piton, O Schiemann, Y Mu, G Stock, T F Prisner, J W Engels *Nucleosides, Nucleotides Nucleic Acids* **24** 771 (2005)
86. N Piton, Y Mu, G Stock, T F Prisner, O Schiemann, J W Engels *Nucleic Acids Res.* **35** 3128 (2007)
87. Q Cai, A K Kusnetzow, W L Hubbell, I S Haworth, G C Gacho, N V Eps, K Hideg, E J Chambers, P Z Qin *Nucleic Acids Res.* **34** 4722 (2006)
88. R Ward, D J Keeble, H El-Mkami, D G Norman *ChemBioChem* **8** 1957 (2007)
89. A D Milov, A G Mar'yasov, R I Samoilova, Yu D Tsvetkov, Ya Raap, V Monako, F Formadzhio, M Krisma, K Toniolo *Dokl. Akad. Nauk* **370** 265 (2000) [e]
90. V Monaco, F Formaggio, M Crisma, C Toniolo, P Hanson, G Millhauser, C George, J Deschamps, J Flippen-Anderson *Bioorg. Med. Chem.* **7** 119 (1999)
91. D J Anderson, P Hanson, J McNulty, G Millhauser, V Monaco, F Formaggio, M Crisma, C Toniolo *J. Am. Chem. Soc.* **121** 6919 (1999)
92. A D Milov, Yu D Tsvetkov, F Formaggio, M Crisma, C Toniolo, J Raap *J. Am. Chem. Soc.* **122** 3843 (2000)
93. A D Milov, Yu D Tsvetkov, F Formaggio, M Crisma, C Toniolo, J Raap *J. Am. Chem. Soc.* **123** 3784 (2001)
94. A D Milov, Yu D Tsvetkov, J Raap *Appl. Magn. Reson.* **19** 215 (2000)
95. A D Milov, Yu D Tsvetkov, F Formaggio, M Crisma, C Toniolo, J Raap *J. Peptide Sci.* **9** 690 (2003)
96. A D Milov, Yu D Tsvetkov, F Formaggio, M Krisma, C Toniolo, G L Millhauser, J Raap *J. Phys. Chem. B* **105** 11206 (2001)
97. A D Milov, Yu D Tsvetkov, F Formaggio, S Oancea, C Toniolo, J Raap *Phys. Chem. Chem. Phys.* **6** 3596 (2004)
98. A D Milov, Yu D Tsvetkov, E Yu Gorbunova, L G Mustaeva, T V Ovchinnikova, J Raap *Biopolymers* **64** 326 (2002)
99. D Marsh, in *Biological Magnetic Resonance* (Eds L J Berliner, J Reuben) (New York: Plenum, 1989) p. 255
100. J E Bahman, C M Baker, S Ceola, I J Day, G H Grant, E J J Groenen, C T Rodgers, G Jeschke, C R Timmel *J. Magn. Reson.* **191** 202 (2008)
101. G Jeschke, C Wegeher, M Nietschke, H Jung, H-J Steinhoff *Biophys. J.* **86** 2551 (2004)
102. D Hilger, H Jung, E Padan, C Wegeher, K-P Vogel, H-J Steinhoff, G Jeschke *Biophys. J.* **89** 1328 (2005)
103. J E Banham, C R Timmel, R J M Abbott, S M Lea, G Jeschke *Angew. Chem., Int. Ed.* **45** 1058 (2006)
104. W M Oldham, N Van Eps, A M Preininger, W L Hubbell, H E Hamm *Nat. Struct. Mol. Biol.* **13** 772 (2006)
105. Z Zhou, S C DeSensi, R A Stein, S Brandon, M Dixit, E J McArdle, E M Warren, H K Kroh, L K Song, C E Cobb, E J Hustedt, A H Beth *Biochemistry* **44** 15115 (2005)
106. M Nakamura, S Ueki, H Hara, T Arata *J. Mol. Biol.* **348** 127 (2005)
107. M Persson, J R Harbridge, P Hammarstrom, R Mitri, L-G Martensson, U Carlsson, G R Eaton, S S Eaton *Biophys. J.* **80** 2886 (2001)
108. P G Fajer, M Gyimesi, A Malnasi-Csizmadia, C R Bagshaw, K I Sen, L Song *J. Phys.: Condens. Matter* **19** 285208 (2007)
109. S Steigmiller, M Borsch, P Graber, M Huber *Biochim. Biophys. Acta* **1708** 143 (2005)
110. C W M Kay, C Elsässer, R Bittl, S R Farrell, C Thorpe *J. Am. Chem. Soc.* **128** 76 (2006)
111. M Bennati, A Weber, J Antonic, D L Perlstein, J Robblee, J Stubbe *J. Am. Chem. Soc.* **125** 14988 (2003)
112. D Biglino, P P Schmidt, E J Reijerse, W Lubitz *Phys. Chem. Chem. Phys.* 58 (2006)
113. H Hara, T Tenno, M Shirakawa *J. Magn. Reson.* **184** 78 (2007)
114. S-Y Park, P P Borbat, G Gonzalez-Bonet, J Bhatnagar, A M Pollard, J H Freed, A M Bilwes, B R Crane *Nat. Struct. Mol. Biol.* **13** 400 (2006)
115. P P Borbat, T F Ramlall, J H Freed, D Eliezer *J. Am. Chem. Soc.* **128** 10004 (2006)
116. H-J Steinhoff *Biol. Chem.* **385** 913 (2004)
117. P G Fajer *J. Phys.: Condens. Matter* **17** S1459 (2005)
118. L Galino, M Bonora, G E Fanucci *J. Am. Chem. Soc.* **129** 11004 (2007)
119. K I Sen, T M Logan, P G Fajer *Biochemistry* **46** 11639 (2007)
120. Z Zhou, S C DeSensi, R A Stein, S Brandon, L Song, C E Cobb, E J Hustedt, A N Beth *Biochemistry* **46** 10248 (2007)
121. O Xu, J F Ellena, M Kim, D S Cafiso *Biochemistry* **45** 10847 (2006)
122. Y E Kutsovsky, A G Maryasov, Y I Aristov, V N Parmon *React. Kinet. Catal. Lett.* **42** 19 (1990)
123. A D Milov, Yu D Tsvetkov *Appl. Magn. Reson.* **12** 495 (1997)
124. A D Milov, R I Samoilova, Yu D Tsvetkov, V A Gusev, F Formaggio, M Crisma, C Toniolo, J Raap *Appl. Magn. Reson.* **23** 81 (2002)
125. A D Milov, D A Erilov, E S Salnikov, Yu D Tsvetkov, F Formaggio, C Toniolo, J Raap *Phys. Chem. Chem. Phys.* 1794 (2005)
126. E S Salnikov, D A Erilov, A D Milov, Yu D Tsvetkov, C Peggion, F Formaggio, C Toniolo, J Raap, S A Dzuba *Biophys. J.* **91** 1532 (2006)
127. A D Milov, R I Samoilova, Yu D Tsvetkov, F Formaggio, C Toniolo, J Raap *J. Am. Chem. Soc.* **129** 9260 (2007)
128. D A Erilov, R Bartucci, R Guzzi, A A Shubin, A G Maryasov, D Marsh, S A Dzuba, L Sportelli *J. Phys. Chem. B* **109** 12003 (2005)
129. E Narr, A Godt, G Jeschke *Angew. Chem., Int. Ed.* **41** 3907 (2002)
130. I M C van Amsterdam, M Ubbink, G W Canters, M Huber *Angew. Chem., Int. Ed.* **42** 62 (2003)
131. Z Yang, J Becker, S Saxena *J. Magn. Reson.* **188** 337 (2007)
132. C W M Kay, H El-Mkami, R Cammack, R W Evans *J. Am. Chem. Soc.* **129** 4868 (2007)
133. H M Baker, C J Baker, C A Smith, E N Baker *J. Biol. Inorg. Chem.* **5** 692 (2000)

134. A V Astashkin, J Seravalli, S O Mansoorabadi, G H Reed, S W Ragsdale *J. Am. Chem. Soc.* **128** 3888 (2006)
135. C Elsässer, M Brecht, R Bittl *J. Am. Chem. Soc.* **124** 12606 (2002)
136. C Elsässer, M Brecht, R Bittl *Biochem. Soc. Trans.* **33** 15 (2005)
137. R Codd, A V Astashkin, A Pacheco, A M Raitsimring, J H Enemark *J. Biol. Inorg. Chem.* **7** 338 (2002)
138. A G Maryasov, M K Bowman, Yu D Tsvetkov *Appl. Magn. Reson.* **30** 683 (2006)
139. Kh S Bagdasar'yan *Kinet. Katal.* **8** 1073 (1967) [f]
140. *Advanced EPR. Applications in Biology and Biochemistry* (Ed. A J Hoff) (Amsterdam: Elsevier, 1989)
141. A Kawamori, H Mino, H Hara, A V Astashkin, Yu D Tsvetkov *Kwansei Gakuin Univ. Annu. Stud.* **64** 221 (1995)
142. H Hara, A Kawamori, A V Astashkin, T-A Ono *Biochim. Biophys. Acta* **1276** 140 (1996)
143. A Kawamori *Appl. Magn. Reson.* **31** 205 (2007)
144. A Kawamori, N Katsuta, H Hara *Appl. Magn. Reson.* **23** 557 (2003)
145. A Kawamori, T -A Ono, A Ishii, S Nakazawa, H Hara, T Tomo, J Minagawa, R Bittl, S A Dzuba *Photosynth. Res.* **84** 187 (2005)
146. A Kawamori, N Katsuta, H Mino, A Ishii, J Minagawa, T-A Ono *J. Biol. Phys.* **28** 413 (2002)
147. S Kuroiwa, M Tonaka, A Kawamori, K Akabori *Biochim. Biophys. Acta* **1460** 330 (2000)
148. A V Astashkin, H Hara, A Kawamori *J. Chem. Phys.* **108** 3805 (1998)
149. G Jeschke, A Bender, T Schweikardt, G Panek, H Decker, H Paulsen *J. Biol. Chem.* **280** 18623 (2005)
150. I V Borovykh, S Ceola, P Gajula, P Gast, H-J Steinhoff, M Huber *J. Magn. Reson.* **180** 178 (2006)
151. P Gajula, S Milikisyants, H-J Steinhoff, M Huber *Appl. Magn. Reson.* **31** 99 (2007)
152. M K Bowman, D Becker, M D Sevilla, J D Zimbrick *Radiat. Res.* **163** 447 (2005)
153. M Pannier, V Schädler, M Schöps, U Wiesner, G Jeschke, H W Spiess *Macromolecules* **33** 7812 (2000)
154. M Pannier, M Schöps, V Schädler, U Wiesner, G Jeschke, H W Spiess *Macromolecules* **34** 5555 (2001)
155. P P Borbat, J H Freed *EPR Newslett.* **17** 21 (2007)
156. M S de Groot, J H van der Waals *Mol. Phys.* **3** 190 (1960)
157. *Biological Magnetic Resonance (Distance Measurements in Biological Systems by EPR)* Vol. 19 (Eds G R Eaton, S S Eaton, L J Berliner) (New York, Kluwer; Plenum, 2000)

[a] — *Russ. Chem. Bull., Int. Ed. (Engl. Transl.)*
[b] — *Phys. Solid. State (Engl. Transl.)*
[c] — *J. Struct. Chem. (Engl. Transl.)*
[d] — *Russ. J. Phys. Chem., B (Engl. Transl.)*
[e] — *Dokl. Phys. Chem. (Engl. Transl.)*
[f] — *Kinet. Catal. (Engl. Transl.)*